LA-4334

LOS ALAMOS SCIENTIFIC LABORATORY
of the
University of California

LOS ALAMOS • NEW MEXICO

Polarization Measurements of 16.5-MeV and 22.1-MeV Neutrons Elastically Scattered from Liquid Tritium and Liquid Deuterium

UNITED STATES
ATOMIC ENERGY COMMISSION
CONTRACT W-7405-ENG. 36

Printed in the United States of America. Available from
Clearinghouse for Federal Scientific and Technical Information
National Bureau of Standards, U. S. Department of Commerce
Springfield, Virginia 22151
Price: Printed Copy $3.00; Microfiche $0.65

Written: November 10, 1969
Distributed: February 13, 1970

LA-4334
UC-34, PHYSICS
TID-4500

LOS ALAMOS SCIENTIFIC LABORATORY
of the
University of California
LOS ALAMOS • NEW MEXICO

Polarization Measurements of 16.5-MeV and 22.1-MeV Neutrons Elastically Scattered from Liquid Tritium and Liquid Deuterium*

by

Roger Kenneth Walter

*This report is derived from a dissertation submitted to the Department of Physics in partial fulfillment of the requirements of the degree of Doctor of Philosophy from Brigham Young University.

ABSTRACT

Cryogenic scattering samples of approximately one mole of liquid tritium and liquid deuterium were used in the measurement of $T(\vec{n},\hat{n})T$ and $D(\vec{n},\hat{n})D$ scattering. The source of 16.5-MeV, -54% polarized neutrons and of 22.1-MeV, +40% polarized neutrons was the $T(d,\vec{n})^4He$ reaction with an incident deuteron energy of 6.0 MeV. The left-right scattering asymmetries for laboratory angles from 40° to 118.5° were measured with a two-detector, time-of-flight spectrometer; and after neutron-gamma-ray discrimination was applied, the pulse height spectra were routed to an on-line computer for preliminary data analysis.

The measured asymmetry for $T(\vec{n},\hat{n})T$ at E_n = 22.1 MeV is negative at angles forward of 95° (lab) and positive at larger angles. The extrema of the n-T polarizations are -60% at 85° (lab) and +98% at 110° (lab). $T(\vec{n},\hat{n})T$ polarizations for E_n = 16.5 MeV are negative at forward angles. $D(\vec{n},\hat{n})D$ polarizations at E_n = 22.1 MeV are measured to be small and negative at forward angles and small and positive at back angles.

ACKNOWLEDGEMENTS

It required the cooperation of many persons to make this experiment a success. Especially appreciated are the efforts of advisors and co-workers, J. C. Hopkins, D. R. Dixon, J. D. Seagrave, J. T. Martin, and A. Niiler, who spent many nights at the accelerator laboratory and many days directing and guiding the author. The successful completion of this experiment is due in large part to the close collaboration of E. C. Kerr and R. H. Sherman who capably handled all of the cryogenic problems.

At the Los Alamos Van de Graaff accelerator laboratory, where the author must have set a record for number of accelerator hours per experiment, the maintenance and operating personnel were particularly helpful and patient. Also appreciated are J. Levin and M. Kellogg for assistance with on-line computer handling, and J. Elder and M. Peacock for friendly smiles and indispensable help with the grammar, the typing, and the computers. The experiment was also supported by other groups at Los Alamos Scientific Laboratory who provided shop work, radiation monitoring, electronics repair, computer programming assistance, and more.

Special appreciation is extended to Associated Western Universities for fellowship financial support while the experiment was being performed.

TABLE OF CONTENTS

	PAGE
ACKNOWLEDGEMENTS	iii
LIST OF TABLES	viii
LIST OF FIGURES	ix
CHAPTER	
I. INTRODUCTION	1
The Problem	1
The Method	2
The Results	2
Content of Following Chapters	3
II. THEORY	4
Polarization and Double Scattering	4
Scattering Amplitudes and Phase Shifts	5
III. THE EXPERIMENT	12
Production and Scattering of the Neutron Beam	12
The Van de Graaff Accelerator and Mobley Buncher	12
Time of Flight	13
The Monitor	16
Double Scattering	17
Cryogenics	17
Counting Rate	23
Detecting the Neutrons	26
Detectors and Collimators	26
Neutron-Gamma-Ray (n-γ) Discrimination	29

CHAPTER PAGE

Electronics 30

Slow side electronics 30

Fast side electronics 37

Normalization and Dead Time Corrections 38

The Measurements 40

$D(\vec{n},\hat{n})D$ and $T(\vec{n},\hat{n})T$ Asymmetries 40

$T(d,\vec{n})^4He$ Source Polarizations 41

Artificial Asymmetries and Detector Efficiencies 41

Electronic Drift 42

IV. DATA ANALYSIS 44

Computer Analyses 44

On-Line Data Reduction 44

Program FLZEIT 45

Curve Fitting 53

Corrections to the Data 56

Effective Sample Position $\langle\theta_1\rangle$ 56

Detector Interchange and Artificial Asymmetries 58

Errors 60

Relative Errors 61

Absolute Errors 62

Point source assumption 63

Electronic drift 63

Geometry 64

^3He contamination 65

CHAPTER PAGE

Inscattering 67

Multiple scattering 68

Summary 68

V. RESULTS 73

Source Polarizations 73

$T(\vec{n},\hat{n})T$ and $D(\vec{n},\hat{n})D$ Results 74

Phase Shift Analysis 77

Valuable Future Measurements 83

APPENDIX A: THE THEORY OF SCATTERING OF PARTICLES OF SPIN ½

FROM A TARGET POSSESSING THE SAME SPIN 88

Justification of Non-Relativistic Treatment 88

Reaction Kinematics 89

Reactions 90

Lab to c.m. Angle Conversion 92

Quantum Theory of Spinless Scattering 95

The Equation of Relative Motion 95

Concepts of Cross Section 98

Separation of the Wave Equation 100

Angular momentum 104

Solution of the Radial Wave Equation 105

Phase shifts 109

Matrix Formulation of Spin ½, Spin ½ Scattering 112

U, I, O Formulation of Spinless Scattering 112

Arctan $Q_\ell = \delta_\ell$ 114

CHAPTER PAGE

Extension to Include Spin Dependence 115

Cross Section in Terms of the U Matrix 123

Appearance of U for the $T(\vec{n},\hat{n})T$ Experiment 125

Polarization 126

Definition of $P(\theta)$ 126

Double Scattering 134

Data Correction Formulae 137

Artificial Asymmetry Corrections 137

Detector Efficiency Correction 138

Multiple Scattering Corrections 139

APPENDIX B 141

Program FLZEIT 141

Program DSCHNIT 172

REFERENCES 178

LIST OF TABLES

TABLE		PAGE
I.	$T(d,\vec{n})^4He$ Deuteron and Neutron Energies in MeV, $P_1(\theta_1)$ Neutron Polarizations, and Target-Sample Distances	16
II.	Results of $^4He(\vec{n},\hat{n})^4He$ Artificial Asymmetry Measurements . .	60
III.	Analysis of Asymmetries and Errors	69
IV.	$T(d,\vec{n})^4He$ Source Polarizations	74
V.	$T(\vec{n},\hat{n})T$ Polarizations $P_2(\theta_2)$	75
VI.	$D(\vec{n},\hat{n})D$ Polarizations $P_2(\theta_2)$	76
VII.	Phase Shift Fits to the 22.1-MeV n-T Data	84
AI.	Clebsch-Gordon Coefficients for Spin ½, Spin ½ Interactions	119
AII.	Non-Zero U Matrix Elements for Spin ½, Spin ½ Scattering and $\ell_{max} = 3$	127
AIII.	Multiple Scattering Corrections	140

LIST OF FIGURES

FIGURE		PAGE
1.	Double Scattering Geometry	7
2.	Target-Detector Area Geometry for the Neutron Polarization Experiment	15
3.	View of the Equipment Used to Measure $D(\vec{n},\hat{n})D$ and $T(\vec{n},\hat{n})T$ Asymmetries	19
4.	Outline Drawing of Equipment Used to Measure $D(\vec{n},\hat{n})D$ and $T(\vec{n},\hat{n})T$ Asymmetries	21
5.	Block Diagram of "Slow Side" Electronics	32
6.	Block Diagram of "Fast Side" Electronics	34
7.	A Typical Normalized Pulse Height Spectrum for A $T(\vec{n},\hat{n})T$ Foreground Run	48
8.	A Typical Normalized Pulse Height Spectrum for Scattering 22.1-MeV Neutrons from the Evacuated Dummy Cell	50
9.	The Subtracted Spectrum of $T(\vec{n},\hat{n})T$ Foreground and Dummy Cell Background Runs Illustrated in Figs. 7 and 8	52
10.	Results of the Least Squares Curve Fitting Routine as Applied to the $T(\vec{n},\hat{n})T$ Subtracted Spectra	55
11.	Geometry for the Calculation of $<\theta_1>$	57
12.	$T(\vec{n},\hat{n})T$ Polarization Data at 22.1-MeV Incident Neutron Energy	79
13.	$D(\vec{n},\hat{n})D$ Polarization Results at $E_n = 22.1$ MeV	81
14.	Phase Shift Fits to the 22.1-MeV n-T Cross Section and Polarization Data	86

FIGURE PAGE

A1. The Reaction in Laboratory Coordinates 90

A2. Elastic Scattering in Lab and c.m. Reference Frames 94

A3. P, A, R, D, C Parameters Defined 131

CHAPTER I

INTRODUCTION

I. THE PROBLEM

Previous measurements of the neutron polarization from $T(\vec{n},\hat{n})T$ elastic scattering* were limited to one set of data at 1.1-MeV incident neutron energy (Se 60) and to predictions from phase shift calculations (To 66) of cross section data (Se 60) at 1.0, 2.0, 3.5, and 6.0 MeV. Even measurements on the $^3He(\vec{p},\hat{p})^3He$ charge-conjugate system are scarce above 14 MeV (Ti 68). Part of the reason for this, of course, is the difficulty of obtaining appropriate scattering samples of $^3H(=T)$ and ^3He.

In spite of the difficulty of the experiments, however, understanding of internucleon forces depends upon the analysis of few-nucleon interactions. As a consequence, special efforts to measure scattering of single nucleons from very light nuclei are well justified. The data to be obtained from $D(\vec{n},\hat{n})D$ and $T(\vec{n},\hat{n})T$ elastic scattering promised to be of significance, and it is with these two interactions that the present work is concerned.

Differential elastic scattering cross sections for D(n,n)D at incident neutron energies between 5.6 MeV and 23 MeV and T(n,n)T between 6 MeV and 23 MeV have been measured by Hopkins, Seagrave, Kerr,

---

*The notation used here (and throughout the discussion) is borrowed from P. W. Keaton (Ke 69a). $\vec{n}$ represents a polarized neutron beam. $\hat{n}$ is the measured neutron asymmetry. $T(\vec{n},\hat{n})T$ and $T(n,\vec{n})T$ are equivalent for elastic scattering if time reversal holds (see Appendix A, Double Scattering).

and Sherman at the Los Alamos Scientific Laboratory (LASL) (Se 67, Se 69), and the present polarization measurements for the same interactions are a valuable supplement to the cross section information.

II. THE METHOD

A cryogenic system built at LASL (Se 67 and Chapter III herein) provided 23.5-cm^3 liquid scattering samples of the hydrogen isotopes, and another cryostat provided an identical sample of liquid ^4He. The ^4He was used in the determination of the source polarizations and artificial asymmetries. An accelerated, bunched beam of deuterons produced pulses of polarized neutrons from the $T(d,\vec{n})^4He$ reaction, and these neutrons were scattered from the hydrogen isotope and ^4He samples.

Detection and energy resolution of the scattered neutrons were accomplished by two 5-inch diameter liquid-scintillator, photomultiplier detector packages in a time-of-flight system, and signals remaining after neutron-gamma-ray discrimination were routed to an on-line computer for preliminary analysis.

III. THE RESULTS

The data show some very striking features, especially the $T(\vec{n},\hat{n})T$ asymmetries at 22.1-MeV incident neutron energy. The results are unique in that the n-T polarizations appear larger in magnitude than the charge-conjugate p-^3He polarizations at similar energies (Ti 68). The limited n-T data for 16.5-MeV incident neutrons are valuable for establishing the shape and sign of the polarization curve at forward angles, and the 22.1-MeV n-D polarizations confirm previous results (Ma 66). A phase-shift analysis was made for n-T scattering at 22.1 MeV, but a unique solution must await further experiments.

IV. CONTENT OF FOLLOWING CHAPTERS

Chapter II of this text outlines the theory of polarization, double scattering, and interactions between nucleons and spin ½ nuclei. In Chapter III the experimental method is examined in detail, especially the physical equipment and electronics used in performing the experiment. The procedures involved in the analysis of the data are described in Chapter IV, which also includes a section on the determination of errors and lists the measured asymmetries and errors. In the fifth chapter the final results of the measurements and phase shift analysis are tabulated and discussed. Finally at the end of the text are two appendices which treat the theory and explain the data-analysis computer programs in more detail than could be done in Chapters II and IV without sacrificing continuity.

CHAPTER II

THEORY

Only the important results of a theoretical analysis of polarization effects are outlined in this chapter in order to avoid breaking the continuity of the discussion with many pages of mathematical detail. Because it is important that a more complete analysis of the spin ½, spin ½ scattering be collected in one place, the detailed development of this theory can be found in Appendix A.

I. POLARIZATION AND DOUBLE SCATTERING

If $\vec{k}_{in}$ and $\vec{k}_{sc}$ are the wave vectors of incident and scattered beams, and the incident channel spin for collision of particles 1 and 2 is $\vec{\sigma} = \frac{1}{2}(\vec{\sigma}_1 + \vec{\sigma}_2)$, then the differential cross section for scattering through an angle θ in the presence of spin-orbit and spin-spin interaction potentials is

$$\sigma(\theta,\phi) = [I(\theta) + I(\theta)\,\vec{P}(\theta) \bullet \hat{n}] = I(\theta)[1 + P(\theta)\cos\phi] \ , \qquad \text{(II-1)}$$

where $I(\theta)$ is the spin-independent cross section, $\vec{P}(\theta)$ is a vector with a magnitude less than or equal to unity and the direction of the incident channel spin, and $\hat{n} = (\vec{k}_{in} \times \vec{k}_{sc})/(k^2 \sin\theta)$ is the normal to the plane of the scattering. ϕ is the angle between the incident channel spin and the normal to the scattering plane. In the special case of scattering of nucleons from a spinless target

$$P(\theta) = (N\uparrow - N\downarrow)/(N\uparrow + N\downarrow) \ , \qquad \text{(II-2)}$$

where N↑ and N↓ are the number of particles scattered with spins up and down with respect to the scattering plane. Hence, $\vec{P}(\theta)$ is called the polarization of the interaction.

For double scattering as shown in Fig. 1, first through angle θ_1, then again through an angle θ_2, the cross section is

$$\sigma(\theta_1,\theta_2,\phi_{12}) = I(\theta_1)\ I(\theta_2)\ [1 + P_1(\theta_1) \cdot P_2(\theta_2)]$$

$$= I(\theta_1)\ I(\theta_2)\ [1 + P_1(\theta_1)\ P_2(\theta_2)\ \cos\phi_{12}] \ , \qquad \text{(II-3)}$$

where ϕ_{12} is the angle between the two scattering planes. For the most common case when both scatterings are in the same plane, the asymmetry e is found by allowing $\phi_{12} = 0$ and $\phi_{12} = \pi$ in Eq. (II-3), so that

$$e = P_1 P_2 = (L-R)/(L+R) \ . \qquad \text{(II-4)}$$

L and R are the numbers of particles scattered through angle θ_2 to the left and right, respectively.

II. SCATTERING AMPLITUDES AND PHASE SHIFTS

The spin-independent Schrödinger wave equation is written

$$(\nabla^2 + k^2 - U_c)\ \psi(\vec{r}) = 0 \ , \qquad \text{(II-5)}$$

where the central potential $U_c = (2m/h^2)V_c(r)$, m = the reduced mass of the two-particle system, and $r = |\vec{r}_1 - \vec{r}_2|$. The differential cross section can be related to a scattering amplitude $f(\theta)$ by the equation

$$\sigma(\theta) = |f(\theta)|^2 \ , \qquad \text{(II-6)}$$

Figure 1. Double Scattering Geometry.

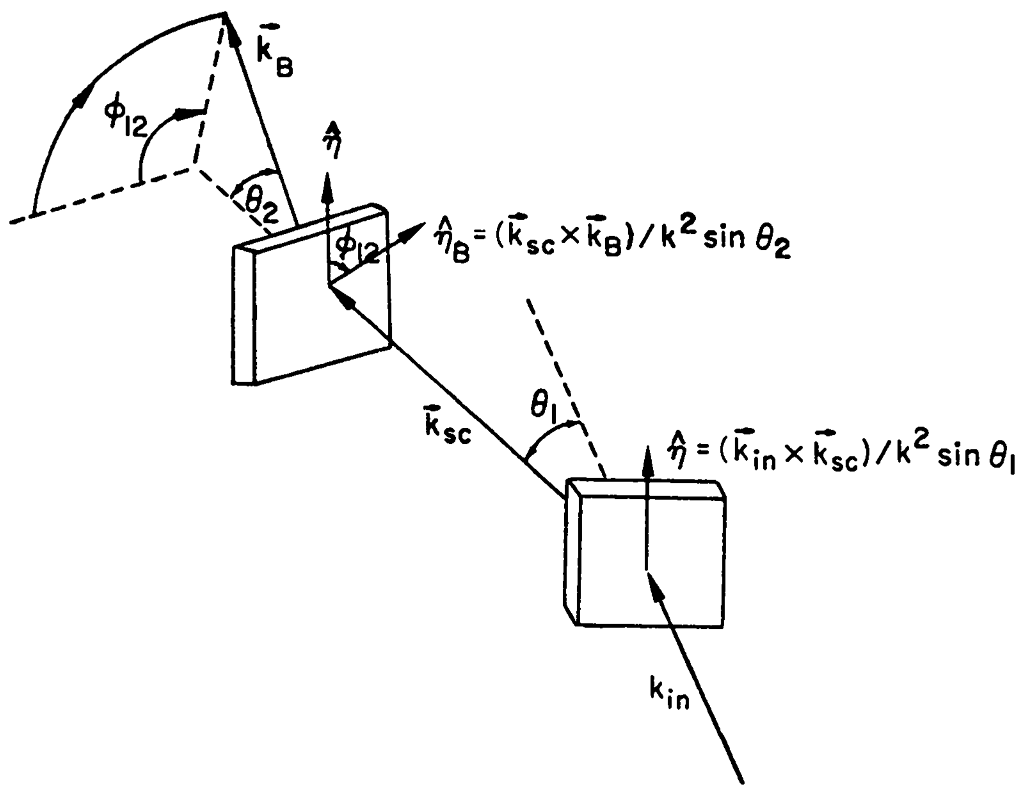

$\vec{k}_B$
ϕ_{12}
$\hat{\eta}$
θ_2
ϕ_{12}
$\hat{\eta}_B = (\vec{k}_{sc} \times \vec{k}_B)/k^2 \sin\theta_2$
θ_1
$\vec{k}_{sc}$
$\hat{\eta} = (\vec{k}_{in} \times \vec{k}_{sc})/k^2 \sin\theta_1$
k_{in}

if the wave function is considered to be a sum of incident and scattered waves. For an incident plane wave

$$\psi = \psi_{in} + \psi_{sc}$$

$$= \exp(ikz) + f(\theta)\exp(ikr)/r \qquad \text{(II-7)}$$

$$= \sum_{\ell} A_{\ell}(kr)^{-1}\sin(kr-(\ell\pi/2)+\delta_{\ell})\ P_{\ell}(\cos\theta)\ .$$

The last summation over orbital angular momentum states, ℓ, holds only for large r; and δ_{ℓ} represents a shift in phase of the scattered wave with respect to the incident plane wave. In this formulation

$$f(\theta) = \tfrac{1}{2}ik^{-1}\sum_{\ell}(2\ell+1)(1-U_{\ell})\ P_{\ell}(\cos\theta)\ , \qquad \text{(II-8)}$$

and

$$U_{\ell} = \exp(2i\delta_{\ell})\ .$$

If Q is defined

$$iQ_{\ell} = (U_{\ell}-1)(U_{\ell}+1)^{-1}$$

then

$$\delta_{\ell} = \arctan Q_{\ell}\ . \qquad \text{(II-9)}$$

If it is assumed that spin-dependent scattering can be approximated by a potential containing spin-orbit and spin-spin interaction terms, then the wave equation becomes (Appendix A and Wu 62)

$$(\nabla^2 + k^2 - W)\ \psi(\vec{r},\vec{\sigma}) = 0\ , \qquad \text{(II-10)}$$

where

$$W = (2m/\hbar^2)[V_c(r) + (\vec{\ell}\cdot\vec{S})\, V_{\ell S}(r) + TV_T(r)] \ .$$

$\vec{\ell}$, $\vec{S}$ are the orbital and spin angular momenta of the two-particle system, T is a spin-spin tensor,

$$T = \left[\frac{3(\vec{\sigma}_1\cdot\vec{r})(\vec{\sigma}_2\cdot\vec{r})}{r^2} - \vec{\sigma}_1 \cdot \vec{\sigma}_2\right] ,$$

and $\vec{\sigma}_1$, $\vec{\sigma}_2$ are the spin vectors for the incident particle and scatterer, respectively. Then the wave function is conveniently written

$$\begin{aligned} \psi(\vec{r},\vec{\sigma}) &= \psi_{in} + \psi_{sc} \\ &= \exp(ikz)\ \chi^s + \sum_{s'} f_{ss'}(\theta,\phi)\ \chi^{s'}\ \exp(ikr)/r \\ &= \sum_c C_c(I_c - \sum_{c'} U_{c'c}\, O_{c'}) \ , \end{aligned} \tag{II-11}$$

where $C_c = i\pi^{\frac{1}{2}}k^{-1}(2\ell+1)^{\frac{1}{2}}$, χ^s, $\chi^{s'}$ represent spin vectors of incident and exit channels, respectively, c, c' represent the incident and exit angular momentum quantum states (ℓ,m,J,M) and (ℓ',m',J',M'), and

$$I_c = [i^\ell \exp[-i(kr-\ell\pi/2)]\ G_m^{JM\ell}\ Y_{\ell m}(\theta,\phi)\ \chi^s]/r \ ,$$

$$O_c = [i^\ell \exp[i(kr-\ell\pi/2)]\ G_m^{JM\ell}\ Y_{\ell m}(\theta,\phi)\ \chi^s]/r \ .$$

The $G_m^{JM\ell}$ are the Clebsch-Gordon coefficients given in Appendix A in

Table AI, and the $Y_{\ell m}(\theta,\phi)$ are normalized spherical harmonics. Then

$$f(\theta,\phi,\vec{\sigma}) = \sum_{s'} f_{ss'}(\theta,\phi)\ \chi^{s'}$$

$$= \frac{i\pi^{\frac{1}{2}}}{k} \sum_{cc'} (2\ell+1)^{\frac{1}{2}}[(\frac{2\ell+1}{4\pi})^{\frac{1}{2}}\ G_c\ P_\ell(\cos\theta)\ \chi^s \qquad \text{(II-12)}$$

$$- U_{c'c}\ G_{c'}\ Y_{\ell'm'}(\theta',\phi')\ \chi^{s'}] \ ,$$

$$\sigma(\theta,\phi) = |f(\theta,\phi,\vec{\sigma})|^2 \ , \qquad \text{(II-13)}$$

and

$$P(\theta) = [\sigma(\theta,\phi) - I(\theta)]/I(\theta) \ , \qquad \text{(II-14)}$$

where

$$I(\theta) = \sum_i |f_{ii}|^2$$

= the differential cross section in the absence of mixing of quantum states between incident and exit channels.

In the spin-dependent analysis $U_{c'c}$ is a matrix relating outgoing angular momentum states to the incident states. Mixing between states occurs when allowed by conservation of total angular momentum J and parity $(-1)^\ell$. U is guaranteed unitary and symmetric by conservation of probability and time reversal properties, and is diagonal with elements $U_\ell = \exp(2i\delta_\ell)$ when no mixing occurs. Thus, if a matrix Q is defined such that in matrix notation

$$iQ = (U-1)(U+1)^{-1} \quad , \tag{II-15}$$

then the phase shifts are defined in analogy with the diagonal case as

$$\delta_{ij} = \arctan^{-1} Q_{ij} \quad . \tag{II-16}$$

In the present $T(\vec{n},\hat{n})T$ experiment for neutrons with 22-MeV incident energy, the orbital angular momentum quantum number was limited to $\ell_{max} = 3$ in which case U is a 14 by 14 matrix with 10 non-zero, off-diagonal, state-mixing elements. The explicit form of U is given in Appendix A, Table AII.

The above analysis points out the relationship between the measurable quantities, asymmetry and cross section, and the postulated nuclear interaction potentials. The connection is achieved via the scattering amplitude $f(\theta)$, the phase shifts δ_{ij}, the scattering matrix U, the wave function $\psi(\vec{r},\vec{\sigma})$, and finally the Schrödinger wave equation itself. For the description of the present experiment, the important concepts are the polarization $P(\theta)$ and the asymmetry e defined for double scattering by Eqs. (II-3) and (II-4).

CHAPTER III

THE EXPERIMENT

This chapter describes the method and the equipment involved in the measurements performed during the present experiment. How the polarized neutron beam was produced, the geometry of the problem, and the description of the cryogenic scattering samples are treated in Section I. Section II describes the detectors, collimators, and electronics; and in the last section the various measurements necessary for obtaining the desired results are discussed.

I. PRODUCTION AND SCATTERING OF THE NEUTRON BEAM

The Van de Graaff Accelerator and Mobley Buncher

The Los Alamos vertical Van de Graaff accelerator and Mobley buncher were used to produce a pulsed beam of deuterons with a repetition rate of 2 MHz and a pulse length of 1 nsec at the center of a tritium gas target. The principles of Van de Graaff electrostatic accelerator operation are described elsewhere (He 59, Va 46); Cranberg et al. have explained the details of a Mobley buncher system (Cr 61); and the features of the Los Alamos pulsed fast neutron research facility are discussed by Hopkins et al. (Ho 67).

Basically the deuteron beam is swept across an aperture near the high voltage head of the accelerator to produce a chopped 2-MHz beam of 10-nsec length pulses. The deuteron pulses pass between a pair of deflector plates located just upstream of a 90° bending, focusing magnet. An rf voltage is applied to the deflector plates in phase with the arrival of the deuteron pulse so that the pulse is fanned out, and those deuterons arriving at the magnet first are forced to travel the longest path along the outer edge of the magnet. The effect of the magnet is to focus all of the deuterons in the 10-nsec pulse on the target at the same time. Figure 2 illustrates this effect. In practice one obtains a burst of deuterons on target for approximately 1 nsec in each 500-nsec period.

Time of Flight

The target upon which the bursts of deuterons impinged in the present experiment was a 1-cm-diameter, 1-cm-long cylindrical cell filled with tritium gas at $\sim$60 psig pressure. The deuterons entered the cell from the beam tube, which is maintained at $\sim 10^{-6}$ Torr, through a 9.6-mg/cm^2 molybdenum foil window. The Van de Graaff accelerating energy was boosted to compensate for energy losses in the tritium and in the foil in order to obtain the appropriate deuteron energy at the center of the target. These energies and energy losses are tabulated in Table I. The $T(d,\vec{n})^4He$ neutron energies in the table were obtained from the reaction kinematics analysis of Appendix A, Section II. These particular energies and angles were chosen to correspond to the maximum, minimum, and zero polarization of the neutrons.

An induced "stop" pulse is picked off a cylinder at a point just before the deuteron burst enters the target. The stop pulse gives a "zero time" reference; i.e., the time at which the $T(d,\vec{n})^4He$ neutrons

Figure 2. Target-Detector Area Geometry for the
Neutron Polarization Experiment.

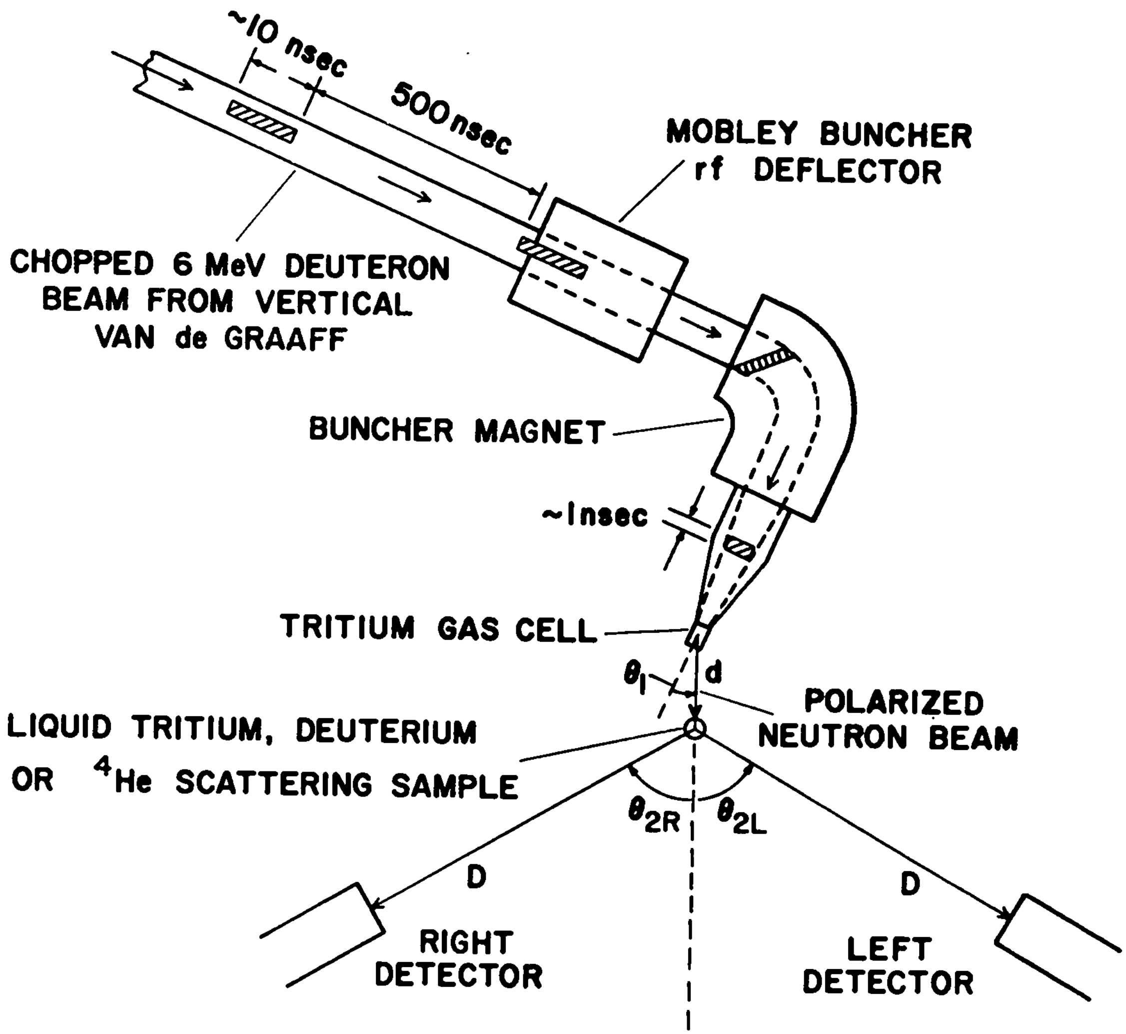

~10 nsec
500 nsec
MOBLEY BUNCHER
rf DEFLECTOR
CHOPPED 6 MeV DEUTERON
BEAM FROM VERTICAL
VAN de GRAAFF
BUNCHER MAGNET
~1nsec
TRITIUM GAS CELL
θ1
d
POLARIZED
NEUTRON BEAM
LIQUID TRITIUM, DEUTERIUM
OR 4He SCATTERING SAMPLE
θ2R
θ2L
D
D
RIGHT
DETECTOR
LEFT
DETECTOR

TABLE I

$T(d,\vec{n})^4He$ Deuteron and Neutron Energies in MeV, $P_1(\theta_1)$ Neutron Polarizations, and Target-Sample Distances.

E_d accel-erator	ΔE foil	ΔE gas	E_d target center	θ_1(lab) deg	E_n	$P_1(\theta_1)$ neutron polari-zation	d(cm) target sample distance
6.57	0.51	0.06	6.00	29.8	22.1	0.40	10.2
6.57	0.51	0.06	6.00	89.8	16.5	-0.54	7.5
3.10	0.96	0.14	2.00	29.8	17.8	0.0	10.2

were produced. The neutrons were scattered from the sample a short distance d from the target and were detected by the scintillator, photomultiplier packages at the end of a 2.55-m flight path, D. The time elapsed between the stop pulse and the arrival of the neutrons at the detectors is a measure of the scattered neutron energy. In fact, non-relativistically,

$$t(\text{nsec}) = 72.3\ D\ (\text{meters})/[E_n(\text{MeV})]^{\frac{1}{2}}\ ; \qquad \text{(III-1)}$$

and the time-of-flight system is an excellent spectrometer which separates neutrons according to their energies.

The Monitor

In addition to the detectors at θ_{2L} and θ_{2R} shown in Fig. 2, a third detector, the "neutron monitor," was located above the target at 110° to the incident beam direction. The collimator of this detector can be seen in Figs. 3 and 4. The monitor effectively counted the neutrons produced and allowed consecutive measurements to be made for the same numbers of neutrons thus compensating for fluctuations in deuteron beam intensity.

Double Scattering

The polarizations $P_1(\theta_1)$ of the neutrons produced in the $T(d,\vec{n})^4He$ reaction are given in Table I. Scattering the polarized neutrons from the liquid hydrogen isotopes produced a left-right asymmetry from which the n-D or n-T polarization $P_2(\theta_2)$ was determined by applying the double scattering equation (II-4); thus,

$$P_2(\theta_2) = e/P_1(\theta_1) = (L-R)/[(L+R)\ P_1(\theta_1)].$$

L and R, the total numbers of elastically scattered neutrons detected in the left and right detectors, respectively, were determined by scattering the neutrons from the sample and then subtracting the "background" data obtained by scattering the neutrons from an identical empty dummy cell for an equal number of monitor counts.

Cryogenics

Members of the Los Alamos Scientific Laboratory cryogenics group, especially E. C. Kerr and R. H. Sherman, built cryogenic systems for containing the liquid hydrogen isotopes and liquid ^4He scattering samples. The so-called chariot with the two cryostats for liquid deuterium and tritium can be seen in Figs. 3 and 4. The system has been described by Seagrave (Se 67).

Figure 3. View of the Equipment Used to Measure $D(\vec{n},\hat{n})D$ and $T(\vec{n},\hat{n})T$ Asymmetries. (This photograph is diagrammed and labeled in Fig. 4.)

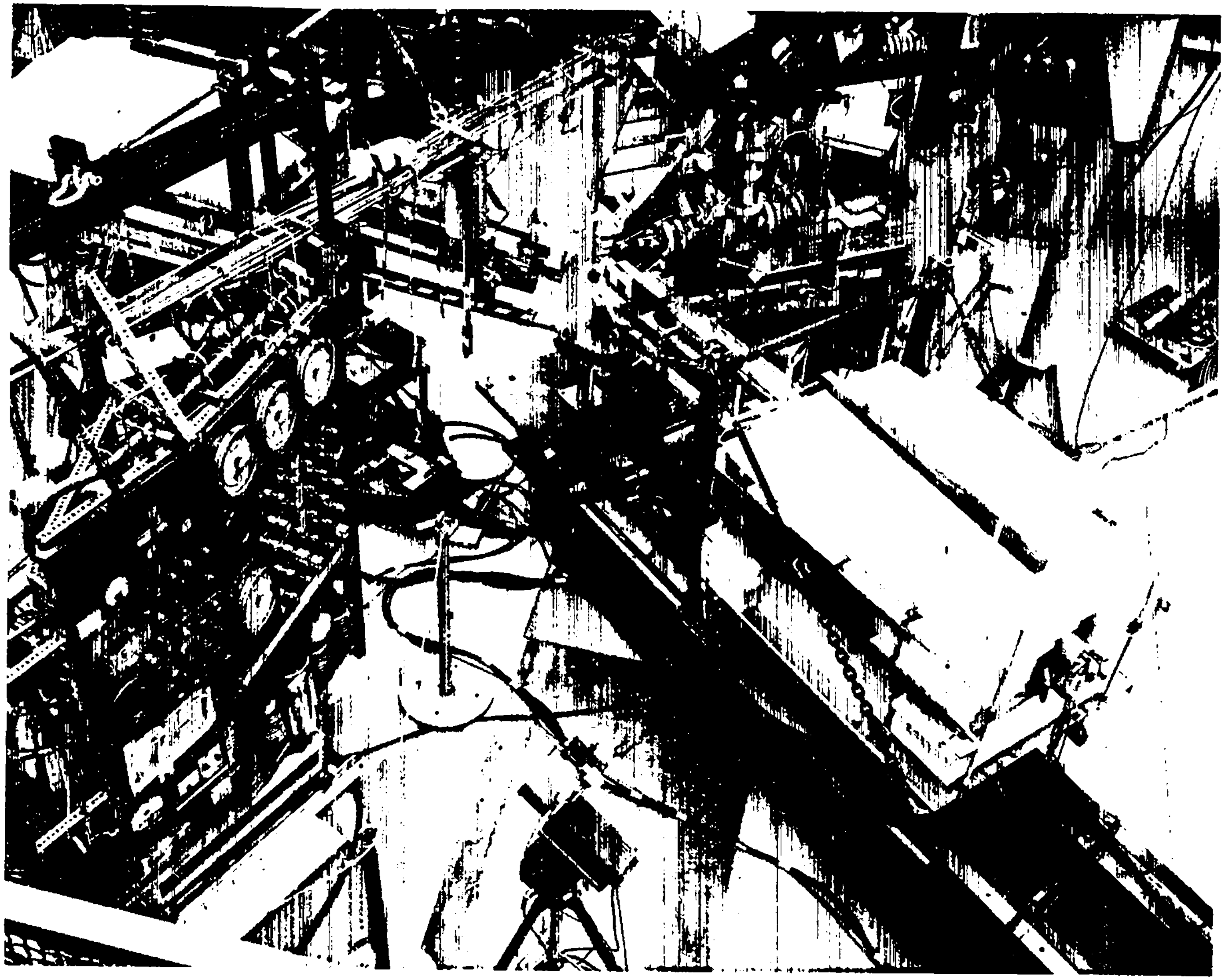

Figure 4. Outline Drawing of Equipment Used to Measure $D(\vec{n},\hat{n})D$ and $T(\vec{n},\hat{n})T$ Asymmetries.

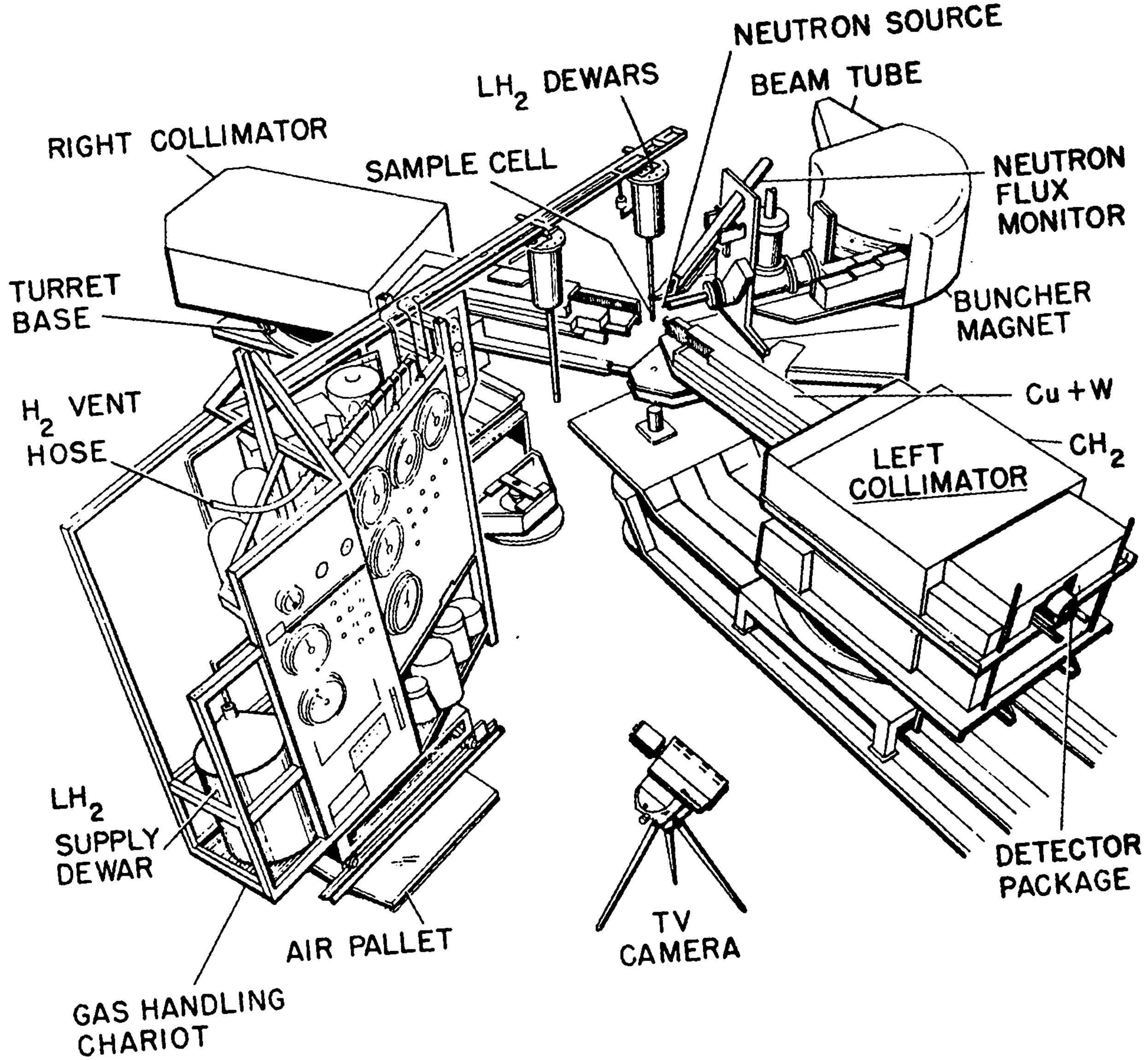
NEUTRON SOURCE
LH_2 DEWARS
BEAM TUBE
RIGHT COLLIMATOR
SAMPLE CELL
NEUTRON
FLUX
MONITOR
TURRET
BASE
BUNCHER
MAGNET
Cu + W
H_2 VENT
HOSE
CH_2
LEFT
COLLIMATOR
LH_2
SUPPLY
DEWAR
DETECTOR
PACKAGE
AIR PALLET
TV
CAMERA
GAS HANDLING
CHARIOT

Basically the cells at the tips of the cryostats are two concentric, cylindrical, stainless steel cans; the inner cell with 3-mil-thick walls contains the liquid scattering sample, and there is a vacuum jacket between the inner cell and the outer can which has 4-mil-thick walls. The inner cell dimensions are 1.34-cm radius R and 4.17-cm length; hence, the cell volume is 23.5 cm^3 or, in the case of tritium, approximately 1 mole or 60,000 curies. The tritium and deuterium were cooled and liquified by a liquid hydrogen jacket in the upper dewars.

The tritium half life for 18.6-keV β decay is 12.26 yr. This substance is extremely dangerous when released to the atmosphere since it replaces normal hydrogen in water molecules, and is easily ingested and absorbed into the human body. Thus, especially in the handling of the $\sim$30 liters at STP which were used to produce the 23.5-cm^3 liquid tritium scattering sample, it was necessary that detailed standard operating procedures be strictly followed; and radiation monitoring personnel from the LASL Health Physics Division were required in the building at all times.

A cryostat to contain liquid ^4He was also built by the cryogenics group and mounted on a separate stand. The cell was identical to that containing the hydrogen isotopes so that measurements of scattering from the different nuclei could be easily compared. Otherwise, the cryostat designs were slightly different since the precautions taken to insure a sealed system for tritium and deuterium were not necessary for ^4He. In addition, an evacuated dummy cell of identical dimensions and construction was provided to facilitate making background measurements.

Counting Rate

Before proceeding with a discussion of the detectors and electronics, it will be instructive to examine the counting rates involved in the experiment.

Normally the integrated deuteron beam current on the tritium gas target was

$$i_d \approx 3 \ \mu\text{amp} = 1.88 \times 10^{13} \text{ deuterons/sec} .$$

The number of 22.1-MeV neutrons produced in the $T(d,\vec{n})^4He$ reaction at $\theta_1 = 30°$ lab, scattered from the tritium sample, and reaching the detector per second is

$$N = I_1(\theta_1) \times f_1 \times f_{el} \times f_2(\theta_2) ,$$

where $I_1(\theta_1)$ is the intensity of neutrons from the $T(d,n)^4He$ interaction incident on the liquid tritium scattering sample,

$$I_1(\theta_1) = [i_d \ \sigma_1(\theta_1) \ n_T \ \ell \ \Omega] ;$$

f_1 is the fraction of the incident neutron beam which interacts with the tritium sample,

$f_1 = [1 - \exp(-\eta_T t \ \sigma_T)]$;

f_{el} represents the fraction of elastic scatterings,

$f_{el} = \sigma_{el}/\sigma_T$; and

f_2 is the fraction of elastic interactions which reach the detector,

$f_2 = \sigma_2(\theta_2) \ \omega/\sigma_{el}$.

Therefore,

$$N = [i_d\ \sigma_1(\theta_1)\ n_T \ell \Omega][1 - \exp(-n_T t\ \sigma_T)][\sigma_2(\theta_2)\omega/\sigma_T]\ , \qquad \text{(III-2)}$$

where

$\sigma_1(\theta_1)$ = T(d,n) differential cross section

= 12 mb/sr at θ_1 = 30° lab,

n_T = triton density in the target gas

= 2.35×10^{20} tritons/cm^3 at 60 psig, 30°C,

ℓ = effective target length = 1 cm,

Ω = solid angle subtended by the scattering sample

= 0.107 sr at d = 10.2 cm,

σ_T = total n-T cross section

= 610 mb at E_n = 22 MeV,

$\sigma_2(\theta_2)$ = T(n,n)T differential cross section

= 83 mb/sr at θ_2 = 40° lab,

= 3 mb/sr at θ_2 = 100° lab,

n_T = triton density in the liquid sample

= 5.2×10^{22} tritons/cm^3,

t = effective sample thickness = $\pi R/2$

= 2.105 cm,

ω = solid angle subtended by the 4" × 5" detector

= 0.0020 sr.

Thus, the number of elastically scattered neutrons arriving at the detector is

$N \approx$ 100 neutrons/sec at θ_2 = 40° lab

$\approx$ 4 neutrons/sec at θ_2 = 100° lab.

However, the neutron counting rate in the detector is

$$R = \varepsilon N \ ,$$

where ε is the detector efficiency,

$$\varepsilon(E) \approx [1 - \exp(-n\sigma_H x)]\ (1 - B/E),$$

n = scintillating ion density

$\approx (6 \times 10^{23}$ atoms/mole)(1 gm/cm^3)/(13 gm/mole)

$= 4.62 \times 10^{22}$ atoms/cm^3,

x = scintillator thickness = 5.1 cm,

σ_H = p(n,n)p cross section $\approx$ 1 barn, and

B = bias level $\simeq$ 2 MeV for neutrons (see "Slow side electronics," this chapter);

so that at energies $\sim$10 MeV

$$\varepsilon \simeq 0.17 \ ,$$

and

$$R \simeq 17 \text{ neutron counts/sec at } \theta_2 = 40° \text{ lab}$$
$$\simeq 1 \text{ neutron count/sec at } \theta_2 = 100° \text{ lab}.$$

Note, however, that R is only the elastic neutron counting rate and that the total counting rate per detector includes all the background and was actually measured to be $R_A \sim 200$ R counts/sec from the detector anodes and $R_D \sim 10$ R after discrimination. Thus, even without examining the data in detail one can see that the elastically scattered neutrons are only a small part of the data; and the time-of-flight system was valuable for separating the elastic neutrons, which were concentrated in $\sim$20 channels of the time spectrum, from the background, which was spread over the entire 256 channel wide spectrum.

II. DETECTING THE NEUTRONS

Detectors and Collimators

The detector packages used in the present experiment consisted of 4" × 5" × 2" liquid scintillators mounted on the face of 5-in.-diameter 58-AVP photomultiplier tubes. The scintillator glass envelopes were blown in the Los Alamos glass shop and ground optically flat by LASL group GMX-9 personnel. The glass envelopes were then sent to Nuclear Enterprises Ltd., Winnipeg (now at San Carlos, California), to be filled with a "cyclo-sol"* base liquid scintillating material, NE218; and all faces of the scintillator except, of course, the face applied to the photomultiplier tube, were coated with reflecting paint. The visible portion of the scintillators was made bubble free by means of a glass filling bubble on the face away from the photomultiplier tube and hidden from the photomultiplier tube by the reflecting paint. With a little dexterity and considerable patience all air bubbles could be transferred from the visible main envelope to the attached filling bubble, and care was used throughout the experiment not to tip the detectors in order not to reintroduce air bubbles into the visible region. NE218 exhibits a reasonable pulse height and a marked difference in pulse shape between light pulses produced by recoil protons, from incident neutrons, and recoil electrons, from incident gamma rays (Re 66). The latter property is important in neutron-gamma-ray discrimination described later in this section. The photomultiplier tubes were mounted inside high permeability metal cylinders to avoid possible changes in amplification character-

---

*"Cyclo-sol" is a product of the Shell Chemical Company.

istics due to stray magnetic fields.

The detectors were surrounded by massive shields as shown in Figs. 3 and 4. The shields for left and right detectors were essentially antisymmetric to each other. Two inches of copper and tungsten formed the inner shield around the detectors, and this shield was in turn surrounded by $\sim$2 feet of polyethylene for attenuating slow neutrons. On the sides of the detectors towards the accelerator beam tube the copper shielding was increased to more than 1-foot thickness to attenuate the high-energy neutrons originating from this area, and at the level of the detectors another 1 inch of copper was stacked around the periphery of the shields.

Cantilevered and supported by "battleship anchor chains," the copper and tungsten collimators extended from the face of the detectors to within a few centimeters of the scattering sample. The purpose of these collimators, of course, was to prevent the detector from seeing the neutron producing target and to insure that only the neutrons scattered from the sample actually entered the detectors. The collimators consisted of copper blocks 4 in. thick on the beam tube side and 2 in. thick on the opposite side. The last 10 in. of the collimator snouts nearest the tritium target were tungsten. Tests were made of the effectiveness of the shielding and collimation by using a crane on which one-ton blocks of concrete were suspended at various positions around the shielding-detector carts. It was determined from these attempts to measure the difference in background levels due to added shielding that the collimators and shielding were sufficiently heavy so that there would be no advantage in increasing their thicknesses by several feet.

It should be pointed out that the neutron monitor was also provided with a rather massive copper collimator which can be seen in the figures. The detectors with their shielding and collimators were mounted upon carts which in turn rode on rails upon two turntables. The carts were positioned so that the detectors were at a fixed distance D(= 255 cm) from the scattering sample. The pivot point of the left turntable was positioned directly under the sample, and the left detector and collimator rotated about this point. The pivot of the right turntable was of necessity placed some distance from the sample position, and the turret base of the cart was utilized to keep the right collimator pointed at the scattering sample.

Angles θ_2 of the detectors with respect to the neutron beam line were found to be most easily and accurately measured with a transit, mirror system suggested by B. Brixner at LASL. A front-surfaced mirror on a small calibrated turntable was placed at the scattering sample position and a transit was positioned some 20 feet away on the target-sample line. The zero degree mirror position was determined by looking through the transit and rotating the mirror until the image of the transit was in line with the transit cross hairs. Then the mirror was turned to half of the desired detector position angle θ_2, the collimator turntable was rotated until the transit operator was observing the center of a scale placed at the detector position, and the angle θ_2 was marked on the floor. Checks of these measurements in a variety of other ways found θ_2 to be accurate and reproducible to within 0.05°.

Neutron-Gamma-Ray (n-γ) Discrimination

The 58-AVP photomultiplier tubes were powered through modified NE5553A* pulse shape discriminator (PSD) bases. The serial numbers on these tube bases, 66 and 60, were used throughout the experiment to identify the detectors. In the scintillation counters a single pulse from the photomultiplier tube can be described as the sum of two exponential decays; the fast part of the pulse has a decay time of about 6 nsec and the slow part typically decays in 200-400 nsec. For recoil protons produced in the scintillator by neutrons the amplitude of the slow component is about 2% of the fast component, whereas for electrons produced in the scintillator by gamma rays the slow component is only about 1% as large as the fast component. The Daehnick and Sherr pulse shape discriminator circuit (Da 61) incorporated into the NE5553A tube base uses this difference in amplitude of the slow decay to produce positive output signals for neutrons and negative signals for gamma rays.

Normally the output signals of the Daehnick and Sherr circuit are amplified and routed through a discriminator in the tube base. However, D. R. Dixon (Di 68) modified the units somewhat by routing the output of the PSD circuit through an amplifier and line-driver designed by himself and LASL group P-1; the amplified PSD signals were routed outside the tube base without discrimination in order to allow external monitoring of and discrimination on the signals. The PSD circuits were carefully adjusted so that they were about 99.8%

*NE5553A pulse shape discriminator units are built by Nuclear Enterprises, San Carlos, California.

effective in rejection of all gamma rays encountered in the experiment.

Electronics

Figures 5 and 6 are block diagrams of the "slow" and "fast" electronics used in the experiment. Basically the problem to be solved by the electronics is to take three signals from each detector, discriminate against gamma rays and low energy neutrons, correct for electronic dead time, mix the signals, provide pulses to the on-line SDS 930 computer which separate the particles according to the detectors they entered, and store the time spectra in the on-line computer. The signals taken from the detectors were:

1. a linear signal with $\sim$0 to 0.1 volt amplitude, dependent upon incident particle energy, and with about a 20-μsec decay time constant;
2. the n-γ signal from the Dixon amplifier, line-driver with $\sim$0 to 0.5 volt positive amplitude for neutron produced recoil protons and a comparable negative amplitude for gamma-ray produced recoil electrons; and
3. a fast anode signal.

It will be convenient to consider the "slow" side first.

Slow side electronics. On the slow side (Fig. 5) the linear signal was first amplified and then routed through an "energy level" discriminator into a coincidence unit. The energy discrimination level was set to reject very low energy particles and was calibrated periodically

Figure 5. Block Diagram of "Slow Side" Electronics.

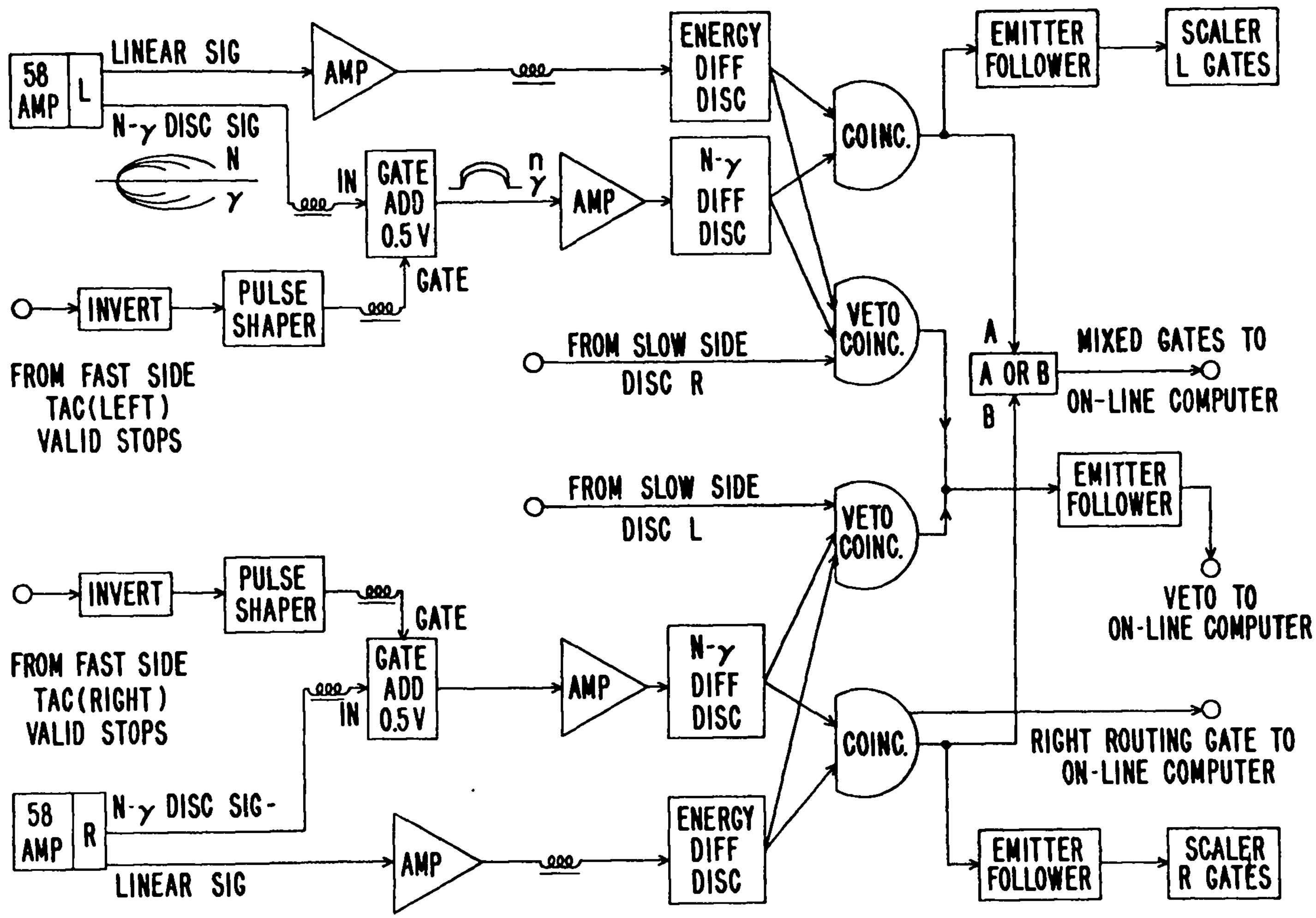

58 AMP
L
LINEAR SIG
AMP
ENERGY DIFF DISC
EMITTER FOLLOWER
SCALER L GATES
N-γ DISC SIG
N
γ
IN
GATE ADD 0.5 V
n
γ
AMP
N-γ DIFF DISC
COINC.
INVERT
PULSE SHAPER
GATE
VETO COINC.
FROM SLOW SIDE
DISC R
A
A OR B
B
MIXED GATES TO
ON-LINE COMPUTER
FROM FAST SIDE
TAC(LEFT)
VALID STOPS
FROM SLOW SIDE
DISC L
EMITTER FOLLOWER
VETO COINC.
VETO TO
ON-LINE COMPUTER
INVERT
PULSE SHAPER
GATE
GATE ADD 0.5 V
AMP
N-γ DIFF DISC
FROM FAST SIDE
TAC(RIGHT)
VALID STOPS
IN
COINC.
RIGHT ROUTING GATE TO
ON-LINE COMPUTER
58 AMP
R
N-γ DISC SIG-
AMP
ENERGY DIFF DISC
EMITTER FOLLOWER
SCALER R GATES
LINEAR SIG

Figure 6. Block Diagram of "Fast Side" Electronics.

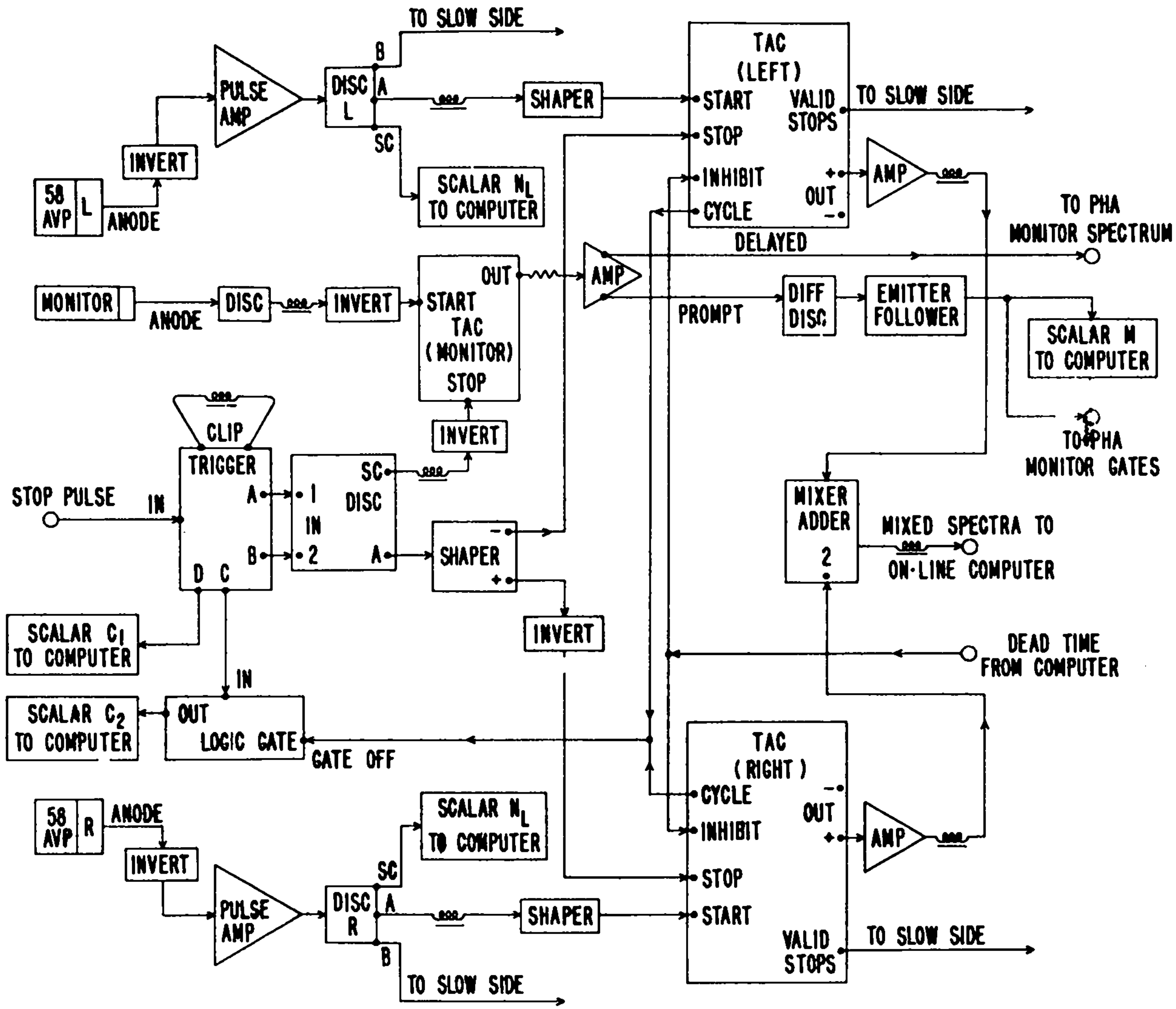
TO SLOW SIDE
58 AVP L
ANODE
INVERT
PULSE AMP
DISC L
B
A
SC
SHAPER
SCALAR N_L TO COMPUTER
TAC (LEFT)
START
STOP
INHIBIT
CYCLE
VALID STOPS
OUT
TO SLOW SIDE
AMP
TO PHA MONITOR SPECTRUM
DELAYED
PROMPT
MONITOR
ANODE
DISC
INVERT
START TAC (MONITOR) STOP
OUT
AMP
DIFF DISC
EMITTER FOLLOWER
SCALAR M TO COMPUTER
TO PHA MONITOR GATES
CLIP
TRIGGER
STOP PULSE
IN
A
B
D C
1 IN 2
SC
DISC
A
INVERT
SHAPER
INVERT
MIXER ADDER 2
MIXED SPECTRA TO ON-LINE COMPUTER
DEAD TIME FROM COMPUTER
SCALAR C_1 TO COMPUTER
IN
SCALAR C_2 TO COMPUTER
OUT
LOGIC GATE
GATE OFF
TAC (RIGHT)
CYCLE
INHIBIT
STOP
START
OUT
VALID STOPS
AMP
TO SLOW SIDE
58 AVP R
ANODE
INVERT
PULSE AMP
DISC R
SC
A
B
SCALAR N_L TO COMPUTER
SHAPER
TO SLOW SIDE

by connecting the linear input signal of the discriminator to a pulse height analyzer (PHA, not shown in the diagram). The analyzer was gated by the output of the energy discriminator. A ^{137}Cs gamma-ray emitter placed in the collimators allowed the discrimination level (PHA gate) to be set at the 0.662-MeV gamma-ray energy, which corresponds to ∿2-MeV neutron energy in the scintillator pulse heights (Cz 64).

The n-γ signal was routed into a modified gate unit which, when a complete conversion signal was obtained from the time to amplitude converter (see the description of the fast electronics below), added a 0.5-volt pedestal to the signal. It was necessary to add 0.5 volt so that the positive level of the differential discriminator could be set to reject gamma rays before the neutron signal entered the coincidence circuit. The neutron discriminator was set in the same manner as the energy discriminator except that a PuBe neutron-gamma source was used and the discrimination level (PHA gate) was set in the valley between neutrons and gammas in the PuBe spectrum. The neutron-energy coincidence signals from the two detectors were mixed and used to gate the analog-to-digital converter (ADC) at the on-line computer.

There was also a second coincidence unit in the slow side electronics which utilized the same neutron and energy signals as the ADC gate signal. However, in addition this unit required a coincidence from the anode of the opposite detector; thus, an output signal resulted from this coincidence only if there were simultaneous events in both detectors. This "veto" signal was routed to the ADC to avoid adding amplitudes of the simultaneous pulses and sending a large signal to a right detector memory location in the computer. Fortunately, these veto events were not frequent. For example, the time-integrated pulse rates for n-T scattering at $\theta_2 = 40°$ lab were:

R_A = pulse rate from the detector anode

$\simeq 3.4 \times 10^3$/sec,

R_E = pulse rate from the energy discriminator

$\simeq R_D \simeq 170$/sec, and

R_N = pulse rate from the neutron discriminator

$\simeq R_D \simeq 170$/sec.

For a double coincidence of pulses in 1-nsec bursts at 500-nsec intervals ($\tau = 1/500$), the coincidence rate is

$$R_d = \tau \left\{[(R_1/\tau)\ t_1](R_2/\tau) + [(R_2/\tau)\ t_2](R_1/\tau)\right\}$$

$$\simeq 2\ R_1R_2\ t/\tau \ ,$$

where $t_1 \simeq t_2 = t \simeq 10^{-6}$ sec is the pulse length. The veto coincidences were obtained from a triple coincidence for which the rate is

$$R_t = \tau[(R_{d1}\ t_d)(R_A/\tau) + (R_{d2}\ t_d)(R_E/\tau) + (R_{d3}\ t_d)(R_N/\tau)] \ ,$$

where $t_d \simeq t$ is the double coincidence pulse length, and the R_{di} represent the double coincidence rates ($R_{d1} = 2R_ER_Nt/\tau$, $R_{d2} = 2R_NR_At/\tau$, $R_{d3} = 2R_ER_At/\tau$). Then

$$R_t \simeq 6R_AR_ER_N\ t^2/\tau \ ,$$

so that the mixed veto coincidence rate from both detectors was

$$2R_t \simeq (12)(3.4 \times 10^3)(1.7 \times 10^2)^2(10^{-6})^2/(1/500)$$

$$= 0.6 \text{ veto pulses/sec.}$$

A third signal was sent to the ADC from the right detector N,E coincidence unit. This was the routing signal which indicated when an event had occurred in the right detector.

Fast side electronics. The fast side electronics were somewhat more complicated. The anode signal of each detector was amplified, routed through a fast discriminator with 1-nsec dead time, and used as the start signal for a time to amplitude converter (TAC). The number of pulses N from the fast discriminator were counted on a scaler.

The 2-MHz stop pulses were routed through a trigger-fan out unit. The stop pulses were counted in scaler C_1, and those pulses which arrived when neither TAC was dead were counted in scaler C_2. It may appear at this point that the circuit is backwards. The "stop" pulse as explained in Section I of this chapter was a zero-time indicator; i.e., it was the pulse picked up at the target when neutrons were produced. It would have been logical to start the TAC with this signal and to stop the converter with the anode signal from the detector indicating the arrival of a neutron. However, here again the counting rate was important. Note that the anode pulses arrive at a rate of $\sim 3.4 \times 10^3$/sec so that starting the TAC by every beam pulse would result in $\sim$600 more starts and 600 times more dead time than would result from starting the TAC by an event in the detector. To avoid this excessive dead time and, since the beam pickup was a (2000.0±0.2)-kHz pulse, the TAC's were started by a detector event and stopped by the succeeding "stop" pulse, so that the TAC output voltage decreased with increasing time of flight. Hence, in the typical data spectrum (see Figs. 7-10 in Chapter IV) time increases from right to left and the energy scale runs from left to right.

The outputs of the TAC's were mixed and routed through an ADC, which had been properly gated by the slow side electronics, to an on-line SDS 930 computer for pulse height analysis. The computer and its associated software have been described by Levin et al. (Le 69, Ga 66). The computer time scale was calibrated by sending pulses from a pulser into both start and stop sides of the TAC and delaying the start pulse input with respect to the stop pulse in 10-nsec steps. In this manner it was determined that the computer output/input signal ratio was constant over the entire running period at 2.3 channels/nsec.

The monitor electronics are also shown on the fast side. Essentially the monitor time-of-flight system was identical to that of the other detectors except that differential discrimination was performed on the monitor time spectrum rather than on energy and n-γ spectra. Monitor gates, M, were scaled.

The overall time resolution in the detectors and associated electronics was much less than 1 nsec.

Normalization and Dead Time Corrections

The purpose of scaling the quantities M, C_1, C_2, and N was for the normalization and dead time correction of the data. To calculate these effects, assume the following:

n' is the number of counts detected during a run of M' monitor counts;

n is the number of counts which would have been detected in the absence of electronic dead time;

τ_d (= 1 μsec) is the dead time introduced each time the detector anode discriminator receives a pulse;

τ_{TAC} (= 6 μsec) is the dead time introduced when the time-to-amplitude coverter receives a start signal or is inhibited by the computer;

T is the total time elapsed for a run of M' monitor counts;

τ is the total dead time during time T due to τ_{TAC} and exclusive of τ_d.

Then C_1 is the number of stop pulses and consequently is the time required for M' monitor counts (in units of 500 nsec), i.e., $C_1 = T/(5 \times 10^{-7})$; and C_2 is the time the electronics was live, i.e., $C_2 = C_1 - \tau$. The number of counts lost due to the TAC, the computer, and the associated electronics was $\sim n\tau/C_1$. Thus for $\tau << C_1$

$$n = n' + (n\tau/C_1) = n'C_1/(C_1-\tau) = n'C_1/C_2 \ . \qquad \text{(III-3)}$$

In addition there was the possibility that an anode signal could arrive just before the TAC was ready to receive it. In this case, there would be $\sim N\tau_d(\tau_d/\tau_{TAC})$ extra dead time due to the anode discriminator exclusive of the remaining electronics, so that the loss of counts due to the time the system was dead from the anode discriminators alone is $n(N\tau_d/T)(\tau_d/\tau_{TAC})$, and

$$n = n' + n\,\frac{N\tau_d}{T} \cdot \frac{\tau_d}{\tau_{TAC}} \simeq n'\,\left(1 + \frac{N\tau_d}{T}\,\frac{\tau_d}{\tau_{TAC}}\right) \ . \qquad \text{(III-4)}$$

The normalization factor by which all the data were multiplied is obtained by applying both corrections (III-3) and (III-4) and renormalizing for M monitor counts,

$$\frac{n}{n'} = \frac{M'}{M} \frac{C_1}{C_2} \left(1 + \frac{N\tau_d}{T} \cdot \frac{\tau_d}{\tau_{TAC}}\right) . \tag{III-5}$$

III. THE MEASUREMENTS

$D(\vec{n},\hat{n})D$ and $T(\vec{n},\hat{n})T$ Asymmetries

The purpose of the present experiment was to measure the polarization of n-D and n-T elastic scattering at an incident neutron energy of 22 MeV. It was assumed on the basis of earlier experiments (Pe 61) that for 6.0-MeV incident deuterons the polarization of the 22-MeV neutrons emitted by the $T(d,\vec{n})^4He$ reaction at $\theta_1 = 30°$ was maximum and known. The polarized neutrons produced in this reaction were scattered from the liquid deuterium or liquid tritium scattering cell, which was positioned a short distance d from the neutron source; the left-right asymmetry was measured for laboratory angles $40° \leq \theta_2 \leq 118.5°$. The polarization of the elastic scattering was calculated from expression (II-4),

$$P_2(\theta_2) = e/P_1(\theta_1) . \tag{III-6}$$

The 16.5-MeV neutrons from the same $T(d,\vec{n})^4He$ reaction at $\theta_1 = 90°$ lab for 6.0-MeV incident deuterons exhibit a maximum negative polarization (Pe 61), and it represented little additional effort to place the tritium scattering sample at 90° and to measure the asymmetries of 16.5-MeV n-T elastic scattering at $35° \leq \theta_2 \leq 45°$ lab. Unfortunately space and shielding limitations prevented extending this measurement over a larger range of angles.

$T(d,\vec{n})^4He$ Source Polarization

In addition to the $D(\vec{n},\hat{n})D$ and $T(\vec{n},\hat{n})T$ measurements the $T(d,\vec{n})^4He$ neutron source polarizations were measured for both 22.1- and 16.5-MeV neutron energies at $\theta_1 = 29.8°$ lab and $\theta_1 = 89.8°$ lab by placing the liquid ^4He scattering sample at d,θ_1. The polarization $P_2(\theta_2)$ for n-^4He elastic scattering is reasonably well known (Ho 66) and from measurements of the left-right asymmetry one can determine the source polarizations $P_1(\theta_1)$

$$P_1(\theta_1) = e/P_2(\theta_2) \ . \qquad \text{(III-7)}$$

Artificial Asymmetries and Detector Efficiencies

Artificial asymmetry, the asymmetry which is due to imperfect shielding and the physical configuration of the experimental equipment and which remains when the source polarization is zero, was also measured. The deuteron beam energy was reduced to 2.0 MeV at which energy the $T(d,\vec{n})^4He$ neutron polarization $P_1(\theta_1)$ is expected to be zero at $\theta_1 = 30°$ lab. The 17.8-MeV neutrons produced at this angle were scattered from the liquid ^4He sample at θ_2 = 35°, 55°, and 70° lab, and a small artificial asymmetry e_r was measured. The corrections of the data for e_r are described in Section II of Chapter IV.

Although the detectors were very well matched, it was nevertheless necessary to correct for the difference in efficiency. In lieu of measuring the detector efficiencies all measurements were performed twice with the detectors interchanged. The corrections were then applied essentially by averaging the two sets of data to cancel effects due to differences in the two detectors.

Electronic Drift

The uncertainties introduced into the measurements by the possible drift of discrimination levels, detector amplification characteristics, and various other unsuspected changes in the electronics were measured by testing the detectors in a low background area. A PuBe source, which produces 9.34×10^5 neutrons/sec and ~ 2 gamma rays per neutron, was placed at a fixed distance of approximately 1.24 m from both detectors so that the total counting rate was $\sim 2000\ \varepsilon \simeq 300$ counts/sec, comparable to the discriminated neutron-gamma counting rates in the actual experiment. A 2-MHz stop pulse was introduced by a pulser into the TAC's and random spectra were collected at the computer.

Thirteen sets of random spectra were taken over a period of six weeks during which time the detectors were subjected to a $\pm 20^\circ$F change in temperature, various electronics modules were interchanged, and experimental conditions were otherwise duplicated as closely as possible. A constant range of 100 channels was sampled and the deviation from the mean counting rate was found to be $\sim 1\%$. The error in asymmetry due to this effect is calculated in Chapter IV, Section II.

In summary, it should be apparent that, although in principle the determination of asymmetries from n-D and n-T elastic scatterings appear fairly simple, in practice the measurements were not so easily performed. Considerable care was necessary to reduce backgrounds to an acceptable level; the cryogenic system for obtaining sufficiently dense scattering samples of the liquid hydrogen isotopes was far from simple; and much attention was paid to developing a satisfactory neutron monitoring system. The scope of the measurements involved in the experiment was somewhat broader than the two elastic scatterings alone, and the experiment was only completed within a reasonable period of time due to the cooperation of the individuals directly involved and to the assistance of the accelerator maintenance, shops, electronics, and other service groups at Los Alamos Scientific Laboratory.

CHAPTER IV

DATA ANALYSIS

Analysis of the data from the experiment began with on-line preliminary data reduction by the SDS 930 computer. The time spectra were then carefully examined, renormalized, and combined by the FLZEIT program to reduce statistical errors and determine that background subtractions were performed correctly. Corrections to the data and an extensive error analysis were the last steps leading to the final asymmetries.

Artificial asymmetry results are listed in Table II in Section II of this chapter, and the results of the other asymmetry measurements are given in Table III at the end of the chapter.

I. COMPUTER ANALYSES

On-Line Data Reduction

The SDS 930 computer at the Los Alamos Van de Graaff Accelerator Laboratory was used for recording the experimental data and to perform on-line preliminary data analysis. The SDS 930 computer and its associated software are described elsewhere (Le 69, Ga 66). J. Levin (Le 68) coded a program for the time-of-flight experiments in which the computer was utilized as a 512-channel pulse height analyzer, 256 channels per detector.

The on-line program allowed the experimenter to keep a close watch on the pulse height spectra which were displayed on a scope during the experiment. In addition, options were provided for printing, plotting, and storing the data on magnetic tape at the end of each run; and properly normalized (see Normalizations and Dead Time Corrections, Chapter III) foreground-background subtractions could be made for any pair of runs. The subtraction routine also calculated standard deviations so that the experimenter could readily determine statistical accuracy and decide whether to extend the running time.

Program FLZEIT

After the data had been accumulated and the preliminary on-line analysis had been made, the data handling was transferred to the CDC 6600 computer. A FORTRAN IV data reduction code, FLZEIT, was written for this step of the analysis. A discussion of the program, including instructions on its use and the code listing, will be found in Appendix B.

Basically program FLZEIT renormalizes and calculates 1) the number of counts in channel I, NET(I), 2) the standard deviation, SD(I), 3) $\mathrm{SUM}(I) = \sum_{i=1}^{I} \mathrm{NET}(i)$, and 4) $\mathrm{SUMVAR}(I) = \sum_{i=1}^{I} (\mathrm{SD}(i))^2$ for the subtraction of any number of pairs of foreground and background runs. Printing, plotting, and storing the reduced data can be done with several options; and normalization factors can be entered from cards, used as they were calculated by the on-line computer from scaler inputs, or calculated by FLZEIT itself. The last option was valuable in checking the accuracy of the monitor by renormalizing the data for large angles θ_2 to the "hard" scattering. "Hard" scattering peaks result from the elastic scattering of neutrons from the copper and tungsten collimators and are expected to be the same for foreground and background runs. A normalization which required hard scattering to be subtracted out completely was used in place of the monitor normalization at large angles where the neutrons scattered by the collimators were well separated in energy from the neutrons scattered by the liquid samples. It should be noted that it made little difference in the final results whether the monitor or hard scattering normalizations were used so that it can be safely assumed that monitor normalizations of the data at forward angles θ_2 were also reliable.

Figures 7-9 are plots of typical time-of-flight spectra as they appear after reduction by the FLZEIT routine. Figure 7 is a normalized foreground run; Fig. 8 is the corresponding normalized background run; and Fig. 9 shows the foreground-minus-background subtraction. The time spectrum of the left detector fills channels 1 through 256, and the right detector spectrum is in channels 257 through 512. The particular set of data in the figures is $T(\vec{n},\hat{n})T$ elastic scattering at an incident neutron energy of 22.1 MeV, $\theta_1 = 29.8°$ lab, and $\theta_2 = 80°$ lab. It took about 3 hours to accumulate these foreground and background data, and statistical errors were approximately 6.5%.

The $T(\vec{n},\hat{n})T$ elastic neutron peaks in the figures are centered at channels 110 and 370 for left and right detectors, respectively; the peaks at channels 130 and 400 are hard scattering, and gamma rays which leaked through the neutron-gamma-ray discrimination are at 210 and 470. The structure at channels 30 and 305 represents a nearly constant pulse height output from the TAC's which resulted when start signals were

Figure 7. A Typical Normalized Pulse Height Spectrum for a $T(\vec{n},\hat{n})T$ Foreground Run (at 22.1-MeV incident neutron energy and $\theta_2 = 80°$ lab).

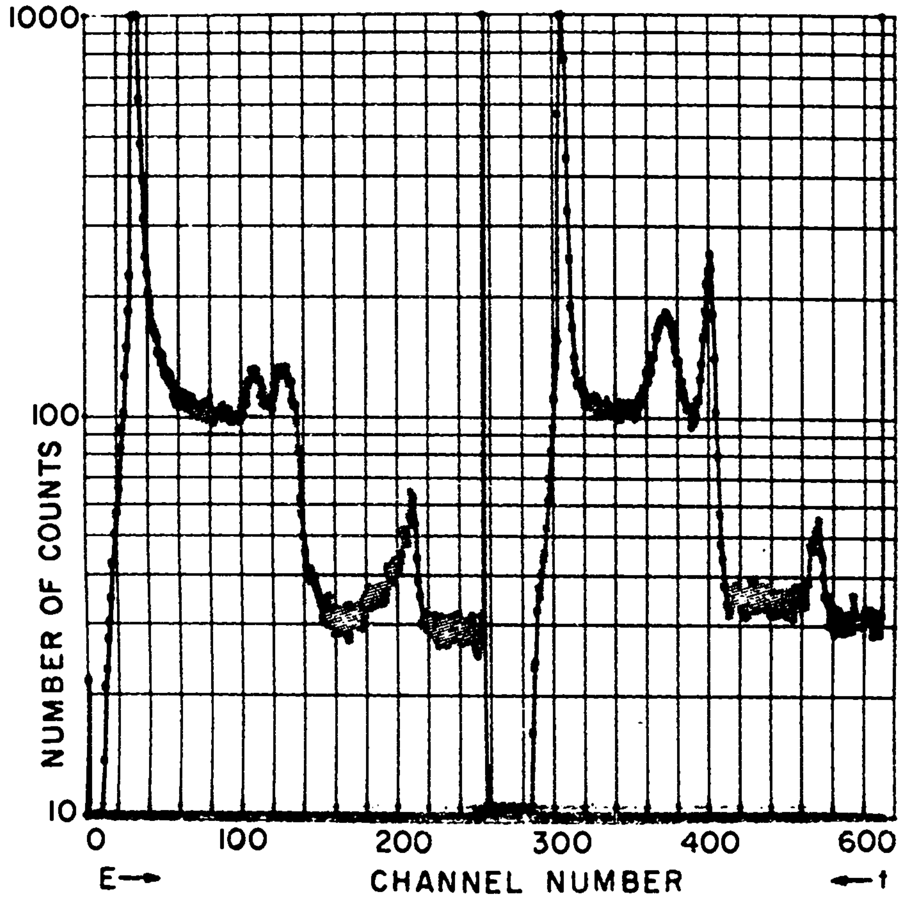
1000
100
10
NUMBER OF COUNTS
0
100
200
300
400
600
E→
CHANNEL NUMBER
←t

Figure 8. A Typical Normalized Pulse Height Spectrum for Scattering 22.1-MeV Neutrons from the Evacuated Dummy Cell (at θ_2 = 80° lab).

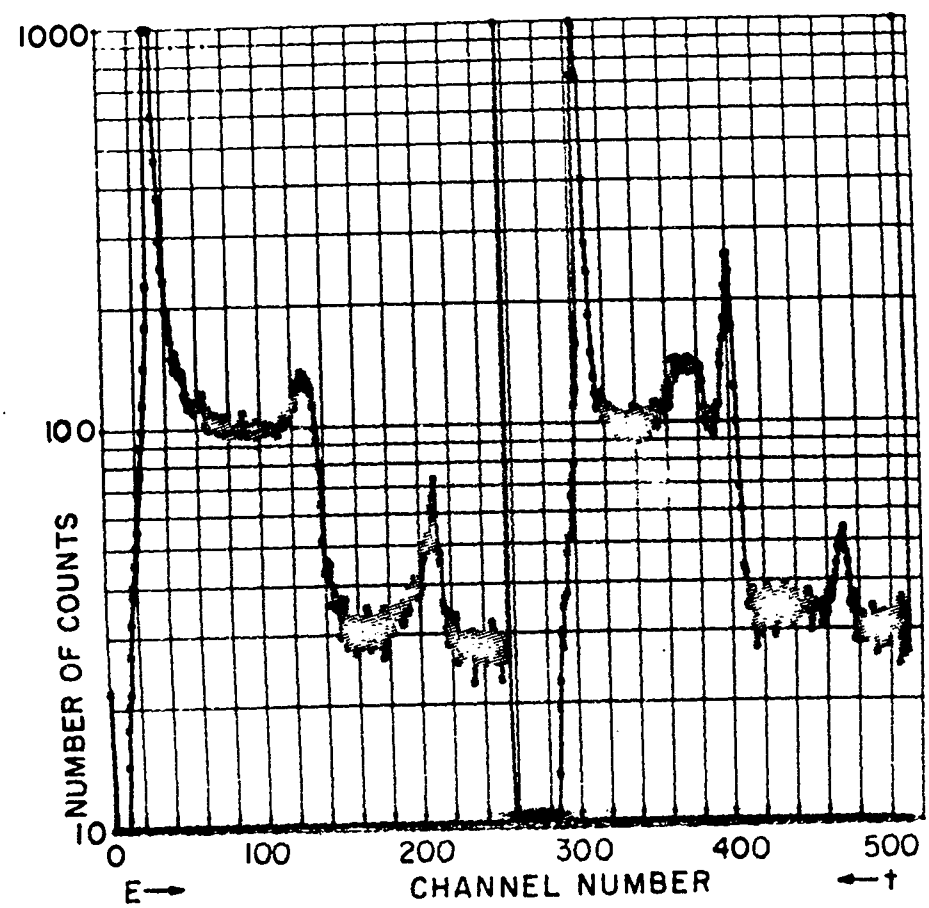

1000
100
10
NUMBER OF COUNTS
0
100
200
300
400
500
E→
CHANNEL NUMBER
←t

Figure 9. The Subtracted Spectrum of T(n,n)T Foreground and Dummy Cell Background Runs Illustrated in Figures 7 and 8.

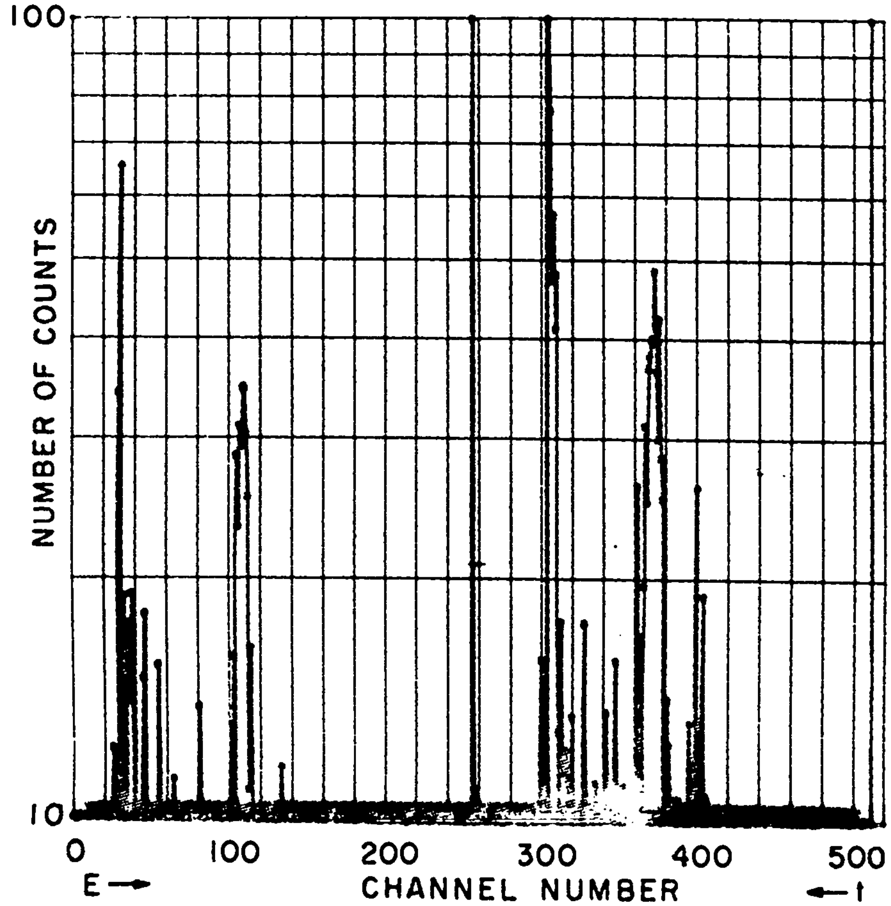
100
10
NUMBER OF COUNTS
0
100
200
300
400
500
E →
CHANNEL NUMBER
← t

detected but conversion was not completed by the arrival of a stop pulse within the required 300-nsec width. Pulses too large for the computer to handle were accumulated in channels 256 and 512; and the large background in Figs. 7 and 8 at energies lower than the elastic neutron energies resulted from the inelastic scattering of neutrons from collimators, shielding, and sample cells.

Curve Fitting

The points in Fig. 10 are a linear plot of the data shown in Fig. 9 except that the large pileup peaks have been removed. Examination of Fig. 10 clearly shows that the statistical uncertainties made it rather difficult to be objective in assigning limits to the elastic neutron peaks. For this reason a non-linear, least squares, curve fitting program written by Moore and Zeigler at LASL (Mo 60) was used to fit a skewed gaussian function to the data. The solid curve in Fig. 10 shows a fit to the data obtained for the function f(x), which is a "Gram-Charlier series of type A" in terms of the derivatives of the gaussian distribution (Ke 63);

$$(2\pi)^{\frac{1}{2}} f(x) = A_1[1 + (\mu_1 H_1/6)] \exp(-z_1^2/2)$$

$$+ A_2[1 + (\mu_2 H_2/6)] \exp(-z_2^2/2) \;, \qquad \text{(IV-1)}$$

where the subscripts 1 and 2 correspond to the left and right scattering peaks, respectively. $z = (x-x_o)/\Delta x$, x_o is the mean of the peak, and Δx is the standard deviation ($\approx$ half width at half maximum). H is the third Tchebycheff-Hermite polynomial ($H = z^3-3z$), and μ is the skewness

Figure 10. Results of the Least Squares Curve Fitting Routine as Applied to the $T(\vec{n},\hat{n})T$ Subtracted Spectra (for 22.1-MeV incident neutrons and $\theta_2 = 80^\circ$ lab. The data points are fitted with the solid curve).

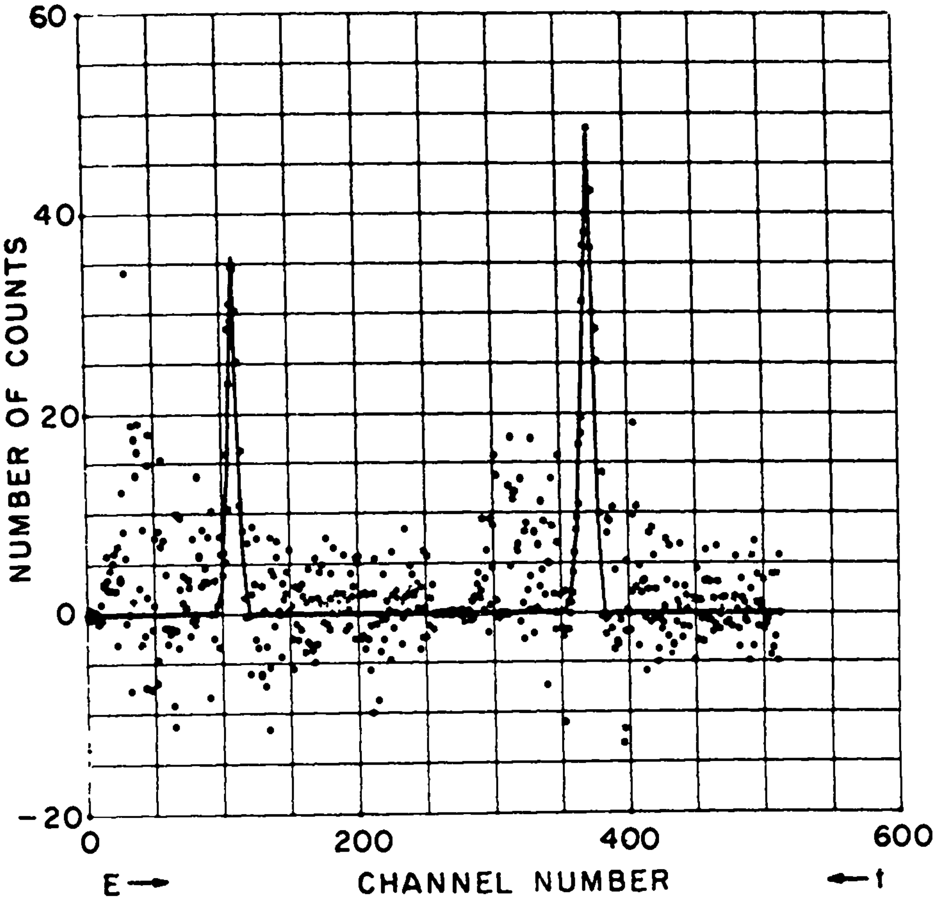

60
40
20
0
-20
NUMBER OF COUNTS
0
200
400
600
E
CHANNEL NUMBER
t

parameter

$$\mu = \int_{-\infty}^{\infty} (x-x_o)^3 \exp(-z^2/2)\, dx \ ,$$

which is the third moment about the mean of the distribution.

The parameters A, x_o, Δx, and μ for the fit were included in the output of the program. Hence, A_1 and A_2, which are the areas under the peaks and the total numbers of neutrons elastically scattered by the sample into the left and right detectors, were determined by the program. With this information the asymmetries e'_m and e''_m for the two measurements with the detectors interchanged were calculated and are tabulated in Table III at the end of this chapter;

$$e'_m = (L'-R')/(L'+R') = (A'_1-A'_2)/(A'_1+A'_2) \ , \qquad \text{(IV-2)}$$

with an identical expression for e''_m.

II. CORRECTIONS TO THE DATA

Effective Sample Position $\langle\theta_1\rangle$

Although the scattering sample was positioned so that its geometrical center was at lab angles $\theta_1 = 30.2°$ for 22-MeV incident neutrons and $\theta_1 = 90°$ for 16.4-MeV incident neutrons, the effective sample position angles were slightly smaller because of the decrease of neutron energy and flux across the sample with increasing θ_1.

The average effective angle $\langle\phi\rangle$ measured from the geometric center of the sample as shown in Fig. 11 is in general

$$\langle\phi\rangle = \int I(\phi)\ \phi\ d\phi / \int I(\phi)\ d\phi\ , \tag{IV-3}$$

where $I(\phi)$ is the effective interaction intensity. If at angle $\theta_1 + \phi$

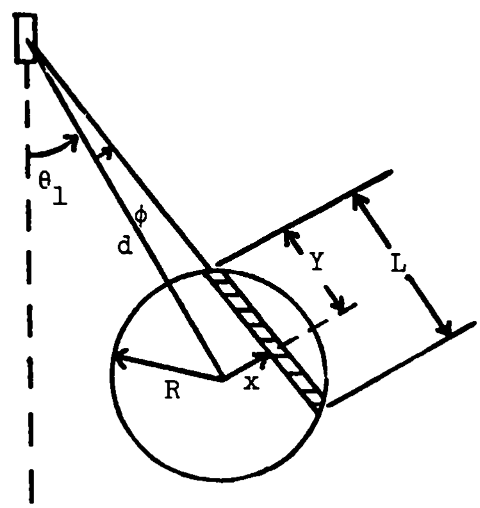

Figure 11. Geometry for the Calculation of $\langle\theta_1\rangle$.

n is the density of scattering centers in the sample and $\sigma_2(\phi)$ is the total cross section for neutrons scattered from the sample, then the interaction intensity as a function of ϕ is

$$I(\phi) = k\sigma_1(\phi)\ [1 - e^{-n\sigma_2 L}]\ , \tag{IV-4}$$

where $k\sigma_1(\phi)$ is the $T(d,n)^4He$ differential cross section for neutrons at $\theta_1 + \phi$. Also

$$L \simeq 2(R^2 - d^2\ \phi^2)^{\frac{1}{2}}\ ;$$

hence, the effective angle $\langle\theta_1\rangle$ is $\theta_1 + \langle\phi\rangle$ where

$$\langle\phi\rangle = \frac{\int_{-R/d}^{R/d} \sigma_1(\phi)\left\{1 - \exp[-2n\sigma_2(\phi)(R^2-d^2\phi^2)^{\frac{1}{2}}]\right\}\phi \, d\phi}{\int_{-R/d}^{R/d} \sigma_1(\phi)\left\{1 - \exp[-2n\sigma_2(\phi)(R^2-d^2\phi^2)^{\frac{1}{2}}]\right\} d\phi} . \qquad \text{(IV-5)}$$

A FORTRAN IV program, called DSCHNIT, was written to perform the integrals in Eq. (IV-5). This program is described in detail in Appendix B.

Using the liquid sample densities (Ke 69b), $n_H = 4.29 \times 10^{22}$ molecules/cm^3, $n_D = 5.14 \times 10^{22}$ molecules/cm^3, $n_T = 5.22 \times 10^{22}$ molecules/cm^3, and $n_{^4He} = 1.95 \times 10^{22}$ atoms/cm^3, and differential cross sections σ_1 and total cross sections σ_2 obtained from a number of sources (Bo 61, St 64, St 65, St 68, Ba 57), it was determined that for all four scattering samples at $\theta_1 = 30.2°$, $\langle\phi\rangle = -0.4°$ and the effective sample position was $\langle\theta_1\rangle = 29.8°$ lab; and at $\theta_1 = 90°$, $\langle\phi\rangle = -0.2°$ so that the effective sample position was $\langle\theta_1\rangle = 89.8°$ lab.

Detector Interchange and Artificial Asymmetries

At each angle θ_2 two asymmetries e_m' and e_m'' were measured with the detectors interchanged between measurements. The data were corrected for artificial asymmetries due to differences in detector efficiencies by averaging the measurements according to the equation derived in Appendix A, Section VI,

$$e_m = \frac{[(1+e_m')(1+e_m'')]^{\frac{1}{2}} - [(1-e_m')(1-e_m'')]^{\frac{1}{2}}}{[(1+e_m')(1+e_m'')]^{\frac{1}{2}} + [(1-e_m')(1-e_m'')]^{\frac{1}{2}}} \quad . \tag{IV-6}$$

The e_m are tabulated in Table III at the end of this chapter.

The artificial asymmetry e_r was measured in the same manner as other asymmetries except that 2.0-MeV deuterons incident on the tritium gas target produced unpolarized 17.8-MeV neutrons at $\theta_1 = 29.8°$ lab. Scattering these neutrons from liquid ^{4}He at three angles θ_2 supplied three sets of asymmetries which were averaged; and the standard deviation from the mean was calculated,

$$e_r = \overline{e}_m \ , \qquad \delta e_r = \left[\frac{\sum_i (e_{mi} - e_r)^2}{(3 - 1)}\right]^{\frac{1}{2}} \quad . \tag{IV-7}$$

The results of the artificial asymmetry measurements are given in Table II. The measured artificial asymmetry corrections were applied to the data according to the expression derived in Appendix A,

$$e = (e_m - e_r)/(1 - e_r\, e_m) \tag{IV-8}$$

$$\simeq e_m - e_r \qquad \text{for small } e_r;$$

and the values of e are tabulated in Table III at the end of the chapter.

TABLE II

Results of $^4He(\vec{n},\hat{n})^4He$ Artificial Asymmetry Measurements.

E_d = 2.0 MeV $\qquad$ θ_1 = 29.8 MeV

E_n = 17.8 MeV $\qquad$ $P_1(\theta_1)$ = 0.0

$\theta_2$lab (deg)	θ_2c.m. (deg)	$\cos\theta_2$ c.m.	e'_m	e''_m	e_m	$\lvert e_m-\bar{e}_m \rvert$
35	43.3	0.727	0.0328	-0.0535	-0.0104	0.0282
55	66.9	0.392	0.0513	-0.0036	+0.0239	0.0061
70	83.7	0.110	0.0376	0.0419	+0.0398	0.0220

$\bar{e}_m$ = 0.0178 $\qquad$ δe_r = 0.0256

Therefore,

$$e_r = 0.0178 \pm 0.0256 \ .$$

III. ERRORS

Relative errors in the data resulted from the statistical analysis of the experiment, and absolute errors were due to both the statistical and systematic uncertainties. The absolute error due to all sources i was taken to be

$$\delta e/e_m = [\sum_i (\delta e_i/e_m)^2]^{\frac{1}{2}} \ ; \qquad \text{(IV-9)}$$

and the uncertainty in the artificial asymmetry was combined with the data in the same manner,

$$\delta e = e[(\delta e/e_m)^2 + (\delta e_r/e_r)^2]^{\frac{1}{2}} . \quad \text{(IV-10)}$$

The errors in the polarization values tabulated in Chapter V were obtained from the expression

$$P_2(\theta_2) = e/P_1(\theta_1) ,$$

so that

$$\delta P_2 = P_2[(\delta e/e)^2 + (\delta P_1/P_1)^2]^{\frac{1}{2}} , \quad \text{(IV-11)}$$

with a similar equation for δP_1, the uncertainty in the measurements of the source polarization.

It was necessary in some of the error calculations to determine $\delta e/e$ when L, R, $\delta L/L$, and $\delta R/R$ were known. The expression relating these quantities follows directly from the definition of e,

$$e = (L-R)/(L+R) ;$$

$$\left|\frac{\delta e}{e}\right| = \frac{1}{e} \left[\left(\frac{\partial e}{\partial L}\right)^2 (\delta L)^2 + \left(\frac{\partial e}{\partial R}\right)^2 (\delta R)^2 + 2\,\frac{\partial e}{\partial L}\,\frac{\partial e}{\partial R}\ \text{covariance (LR)}\right]^{\frac{1}{2}} ,$$

and

$$\frac{\delta e}{e} = \frac{2LR}{(L-R)(L+R)} \left[\left(\frac{\delta L}{L}\right)^2 + \left(\frac{\delta R}{R}\right)^2\right]^{\frac{1}{2}} , \quad \text{(IV-12)}$$

if the L and R are independent and covariance (LR) = 0.

Relative Errors

The data reduction code, FLZEIT, calculated the number of counts NET(I), and the standard deviations SD(I) for each analyzer channel of the foreground minus background spectra. The statistical errors in asymmetry were then obtained directly from the FLZEIT code,

$$\delta e_{stat} = [(\delta L)^2 + (\delta R)^2]^{\frac{1}{2}}/(L+R) \ , \qquad \text{(IV-13)}$$

where

$$(\delta L)^2 = \sum_{i=a}^{b} [SD(i)]^2 \ , \qquad (\delta R)^2 = \sum_{i=c}^{d} [SD(i)]^2 \ ,$$

$$L = \sum_{i=a}^{b} NET(i), \qquad \text{and} \qquad R = \sum_{i=c}^{d} NET(i) \ .$$

a, b, c, d are the channel number limits of the data peaks. Equation (IV-13) is equivalent to Eq. (IV-12) for $L \sim R$.

Absolute Errors

Absolute uncertainties can result from several possible sources of systematic error including

1. the point neutron source assumption,
2. electronic drift,
3. geometry,
4. ^{3}He decay products in the liquid tritium sample,
5. inscattering, and
6. multiple scattering.

These sources of error are described in the following paragraphs and the results are tabulated in Table III at the end of the chapter.

Point source assumption. Other than the fact that the target is 1 cm long, the $T(d,\vec{n})^4He$ neutron source differs from a point source in two respects; first there is a ±2.5° divergence of the beam in the target; and secondly the deuteron energy decreases along the length of the target due to the energy loss in 1 cm of gas. The worst possible spread in neutron polarization is that between the neutrons emitted from the upstream end of the target (E_d = 6.06 MeV) at an angle θ_{min} less than θ_1 and the neutrons from downstream end of the target (E_d = 5.94 MeV) at an angle θ_{max} greater than θ_1. From the geometry of the problem it can be shown that for $\theta_1 = 29.8°$ the spread of angles at the target is $\theta_{min} = 26.0°$ and $\theta_{max} = 33.8°$, and for $\theta_1 = 89.8°$ the minimum and maximum angles are $\theta_{min} = 83.5°$ and $\theta_{max} = 96.1°$. Fortunately the $\theta_1 = 30°$ and $\theta_1 = 90°$ sample positions correspond to extrema in the $T(d,\vec{n})^4He$ polarizations so that the uncertainties in source polarizations resulting from the angular spread is minimized. By locating these deuteron energies and angles on the Barschall $T(d,\vec{n})^4He$ polarization contour plot (Ba 66) the uncertainties in source polarization were estimated to be

$$\delta P_1 \leq \pm 0.03 \quad \text{at} \quad \theta_1 = 29.8°$$

and

$$\delta P_1 \leq \pm 0.05 \quad \text{at} \quad \theta_1 = 89.8° \; .$$

Electronic drift. The measurements to determine electronic drift were described in Chapter III. The standard deviation from the mean counting rate in the thirteen test runs was

$$\delta L/L = \delta R/R = 0.011 \ ,$$

and the errors in asymmetries $\delta e_{elec}/e$ were calculated from Eq. (IV-12).

Geometry. There were three possible sources of systematic error arising from the geometry of the experiment. The first of these resulted from the 12.7-cm (5 in.) height of the scintillators, which caused an uncertainty of ±6.35 cm in the scattering plane at the detectors; that is ϕ in Fig. 1 could differ from zero by $\delta\phi = 6.35/255 = 0.0249$ rad. Since $\cos(\delta\phi) = 0.9997$ the uncertainty introduced by the assumption that $e = P_1(\theta_1)P_2(\theta_2)\cos\phi$ and $\phi = 0$ is

$$\delta e_\phi/e \lesssim 0.0003 \ .$$

The second source of geometric error was a $\delta D \simeq 2$ cm uncertainty in measuring the relative sample-detector distances D. The error in solid angular spread of the 10.2-cm (4 in.) × 12.7-cm (5 in.) scintillators for this δD is then

$$\frac{\delta\Omega}{\Omega} = \left(\frac{10.2}{D+\delta D} - \frac{10.2}{D-\delta D}\right)\left(\frac{12.7}{D+\delta D} - \frac{12.7}{D-\delta D}\right)/\left(\frac{10.2}{D} \times \frac{12.7}{D}\right) = 0.00025 \ ,$$

so that for this effect the error in asymmetry was also

$$\delta e_D/e \lesssim 0.0003 \ .$$

The largest sources of geometrical error were the $\delta\theta_{2d} \simeq 0.05°$ accuracy to which the detector angles were measured and the accuracy to which the position of the 10.2-cm-wide scintillator on the face of the phototube was known. The latter figure was estimated to be 0.635

cm (1/4 in.), so that $\delta\theta_{2s} \simeq [(0.635)/(255)](180/\pi) = \pm 0.14°$. Thus, the total uncertainty in the angle θ_2 at which the detector was positioned was $\delta\theta_2 = [(\delta\theta_{2d})^2 + (\delta\theta_{2s})^2]^{\frac{1}{2}} = 0.149°$. Since $\delta\theta_2$ is independent for left and right collimators, it was necessary to find $\delta L/L$ and $\delta R/R$ in terms of $\delta\theta_2$. From the theory of double scattering in Appendix A

$$L = \sigma_1(\theta_1)\ \sigma_2(\theta_2)\ (1 + e)\ , \tag{IV-14}$$

and

$$R = \sigma_1(\theta_1)\ \sigma_2(\theta_2)\ (1 - e)\ , \tag{IV-15}$$

so that

$$\left|\frac{dL}{d\theta_2}\right| = [(\frac{\partial L}{\partial \sigma_2})^2\ (\frac{d\sigma_2}{d\theta_2})^2 + (\frac{\partial L}{\partial P_2})^2\ (\frac{dP_2}{d\theta_2})^2]^{\frac{1}{2}}\ ,$$

and similarly for $|dR/d\theta_2|$. Then

$$\left|\frac{\delta L}{L}\right| = \left|\frac{\delta R}{R}\right| = [(\frac{1}{\sigma_2})^2\ (\frac{d\sigma_2}{d\theta_2})^2 + P_1^2\ (\frac{dP_2}{d\theta_2})^2]^{\frac{1}{2}}\ \delta\theta_2\ . \tag{IV-16}$$

Values for σ_2, $d\sigma_2/d\theta_2$, P_1, and $dP_2/d\theta_2$ for calculating $|\delta L/L|$ and $|\delta R/R|$ for the scatterings were obtained from a variety of source material (Se 67, Ma 66, Ho 66), and the errors in asymmetry $\delta e_{\theta_2}/e$ in Table III were calculated from Eqs. (IV-16) and (IV-12).

The total angular width (= 0.04 rad) of the scintillator is not a source of uncertainty. The effect of this width is to broaden the elastic scattering peak in the data.

<u>^{3}He contamination</u>. An analysis of the tritium from the scattering sample was performed by LASL group W-3 personnel at the completion of

the experiment and showed the following content:

$$T_2 = 96.23\%$$

$$D_2 = 0.12\%$$

$$H_2 = 0.29\%$$

$$^3He = 3.36\% .$$

If it is assumed that $L = L_T + L_{He}$ and $R = R_T + R_{He}$ then

$$e_m = (L-R)/(L+R) = (L_T-R_T+L_{He}-R_{He})/(L_T+R_T+L_{He}+R_{He}) . \qquad \text{(IV-17)}$$

the shape of the $T(\vec{n},\hat{n})T$ (Chapter V) and $^3He(\vec{n},\hat{n})^3He$ (Bü 69) polarization curves are expected to be similar, and it is possible that a difference of only a few degrees in the angle at which the curves cross the $e = 0$ axis would result in a maximum error due to the ^3He contamination caused by an extremum of the ^3He data falling at the $e = 0$ angle for the T data. In this case $L_T = R_T \equiv N$ and

$$\delta e_{He} = (L_{He} - R_{He})/(2N + L_{He} + R_{He}) . \qquad \text{(IV-18)}$$

The maximum of a set of 16-MeV $^3He(\vec{n},\hat{n})^3He$ data (Bü 69) was used to determine roughly L_{He} and $R_{He} \simeq 0.0336N$ so that for $E_n = 16.5$ MeV, $\theta_1 = 89.8°$

$$\delta e_{He} \leq 0.0028 ;$$

and for $E_n = 22.1$ MeV, $\theta_1 = 29.8°$

$$\delta e_{He} \leq 0.016 .$$

However, ^3He does not condense readily, although it does remain trapped in the liquid tritium as the tritium decays. Thus, the ^3He

impurities in the scattering sample were considerably decreased when the tritium was condensed in the cell. Since the tritium was allowed to boil at least once during the three-week period it was in the cryostat, it was again purged of part of the ^{3}He decay products. Thus, the concentration of ^{3}He impurities in the sample at any time was probably not larger than that produced by the tritium decay in the three-week running time. The amount of decay was calculated from the expression $N = N_o\ e^{-\lambda t}$ where t = 3 weeks and λ = ln2/half-life = 0.693/12.26 yr. The result, $N/N_o = 0.997$, means that the maximum concentration of ^{3}He in the cell at one time was not more than 0.3% instead of the 3% shown by the gas analysis. Thus, the errors δe_{He} calculated above are approximately a factor of 10 too large. The values of $\delta e_{He}/e$ in Table III were calculated by assuming the values $\delta e_{He} \leq 0.0003$ at 16.5-MeV neutron energy and $\delta e_{He} \leq 0.002$ at 22.1-MeV neutron energy and dividing δe_{He} by e_m.

Inscattering. One more possible source of errors in the data would be inscattering effects (scattering of the neutrons into or out of the detector by the collimators). Direct scatterings have already been treated under the name of "hard" scattering earlier in this chapter, and it was pointed out there that rather than introduce errors the hard scattering was expected to be the same for foreground and background runs and was a significant check on the monitor normalizations at large angles θ_2. The effect of a second neutron scattering in the collimator is ignored; the asymmetry has already been determined once a neutron enters a collimator so that further scattering within the collimator for which the neutron remains under the peak does not change the data.

Actually a second-order inscattering effect could be expected from an analyzing power of n-Cu scattering which would tend to scatter neutrons preferentially into or out of the collimator. However, a series of measurements made with considerably altered collimator configurations resulted in no inscattering effects which could be detected above the statistical uncertainties of the experiment.

Multiple scattering. An investigation was made of corrections for multiple scattering. A description of this analysis and the resulting corrections to the data are given at the end of Appendix A.

The $^4He(\vec{n},\hat{n})^4He$ asymmetries tabulated in Table III were used to obtain the calculated values of the $T(d,\vec{n})^4He$ neutron source polarizations $P_1(\theta_1)$ in Chapter V. The polarizations $P_2(\theta_2)$ of n-T and n-D elastic scattering were calculated from the $T(\vec{n},\hat{n})T$ asymmetries, the $D(\vec{n},\hat{n})D$ asymmetries, and the source polarizations $P_1(\theta_1)$. The errors derived in this chapter represent an upper limit on one standard deviation from the data points.

TABLE III

Analysis of Asymmetries and Errors. (L', R' and L", R" are the number of counts detected in the left and right detectors for the two detector configurations, before and after interchange.)

$e'_m = (L'-R')/(L'+R')$, $e_m \simeq (\frac{1}{2})(e'_m+e''_m)$, $e \simeq e_m - e_r$,

e_r = measured artificial asymmetry = 0.0178 ± 0.0256 ,

$\delta e/e_m = [\sum_i (\delta e_i/e_m)^2]^{\frac{1}{2}}$ for all sources of error i , $\delta e(\text{absolute}) = e[(\delta e/e_m)^2 + (\delta e_r/e_r)^2]^{\frac{1}{2}}$,

δe_{stat} = statistical (relative) uncertainties; δe_{elec} = electronic drift uncertainty; δe_{θ_2}, δe_ϕ, δe_D are geometry uncertainties; δe_{He} = uncertainty due to contamination of the liquid tritium sample, and $\delta e_\phi/e_m$ = 0.0003, $\delta e_D/e_m$ = 0.0003.

$T(\vec{n},\hat{n})T$

E_n (MeV)	$\theta_2$lab (deg)	θ_2c.m. (deg)	L' / L"	R' / R"	e'_m×100 / e''_m×100	e_m×100	$\delta e_{stat}/e_m$ / $\delta e_{elec}/e_m$	$\delta e_{\theta_2}/e_m$ / $\delta e_{He}/e_m$	$\delta e/e_m$	absolute (e±δe)×100	relative % (δe/e)×100
16.5	35	46.1	16245	16085	0.49	1.02	0.30	0.37	0.96	- 0.76±2.75	41.0
			16557	16049	1.56		0.83	0.03			
16.5	40	52.4	12276	11921	1.47	1.98	0.14	0.16	0.38	+ 0.21±2.68	130.0
			12341	11738	2.50		0.31	0.01			
16.5	45	58.7	10327	9295	5.26	5.76	0.05	0.06	0.13	+ 3.98±2.67	7.5
			10470	9236	6.26		0.10	0.01			
22.1	40	52.4	7142	7902	- 5.05	- 7.73	0.07	0.04	0.12	- 9.50±2.73	5.5
			6893	8500	-10.4		0.09	0.03			
22.1	55	70.9	4013	5127	-12.2	-12.5	0.06	0.03	0.08	-14.25±2.76	5.1
			4111	5323	-12.8		0.04	0.02			
22.1	70	88.3	1102	1527	-16.2	-16.9	0.06	0.03	0.07	-18.6 ±2.8	5.1
			957	1362	-17.5		0.03	0.01			

$T(\vec{n},\hat{n})T$ cont'd

E_n (MeV)	$\theta_2$lab (deg)	θ_2c.m. (deg)	L' / L"	R' / R"	$e'_m\times100$ / $e''_m\times100$	$e_m\times100$	$\delta e_{stat}/e_m$ / $\delta e_{elec}/e_m$	$\delta e_{\theta_2}/e_m$ / $\delta e_{He}/e_m$	$\delta e/e_m$	absolute $(e\pm\delta e)\times100$	relative % $(\delta e/e)\times100$
22.1	80	99.2	299	478	-23.0	-20.5	0.09	0.03	0.10	-22.2 ±3.3	8.6
			374	538	-18.0		0.03	0.01			
22.1	85	104.5	250	389	-21.8	-21.9	0.11	0.02	0.12	-23.6 ±3.6	11.0
			253	396	-22.0		0.02	0.01			
22.1	90	109.5	139	246	-27.8	-18.8	0.14	0.04	0.15	-20.5 ±3.8	13.0
			214	259	- 9.51		0.04	0.01			
22.1	95	114.5	157	110	17.6	16.0	0.27	0.03	0.28	+14.3 ±5.1	31.0
			191	143	14.4		0.03	0.01			
22.1	95	114.5	135	98	15.9	14.0	0.24	0.04	0.25	+12.2 ±4.3	28.0
			200	157	12.0		0.04	0.01			
								Average	at 95°	+13.3 ±3.4	21.0
22.1	100	119.2	155	171	- 4.9	23.3	0.23	0.04	0.25	+21.6 ±6.3	25.0
			82	29	48.0		0.08	0.01			
22.1	100	119.2	157	94	25.1	27.5	0.14	0.01	0.14	+25.8 ±4.7	15.0
			204	110	29.9		0.02	0.01			
								Average	at 100°	+23.7 ±3.9	14.0
22.1	105	123.8	224	107	35.3	36.1	0.10	0.01	0.10	+34.5 ±4.5	11.0
			184	85	36.8		0.01	0.01			
22.1	110¼	128.5	277	132	35.5	37.5	0.08	0.01	0.08	+36.0 ±4.0	8.5
			332	144	39.5		0.01	0.01			
22.1	118½	135.6	361	169	36.2	32.3	0.06	0.01	0.06	+30.7 ±3.3	6.3
			349	195	28.3		0.02	0.01			

$D(\vec{n},\hat{n})D$

22.1	40	58.8	8132	7844	1.80	0.16
			7987	8225	- 1.47	
22.1	40	58.8	10478	10969	- 2.29	- 1.65
			10631	10849	- 1.09	

$D(\vec{n},\hat{n})D$ cont'd

E_n (MeV)	θ_2 lab (deg)	θ_2 c.m. (deg)	L' / L"	R' / R"	$e'_m\times100$ / $e''_m\times100$	$e_m\times100$	$\delta e_{stat}/e_m$ / $\delta e_{elec}/e_m$	$\delta e_{\theta_2}/e_m$ / $\delta e_{He}/e_m$	$\delta e/e_m$	absolute $(e\pm\delta e)\times100$	relative % $(\delta e/e)\times100$
			Average at 40°			- 0.74	0.59	0.16	0.72	- 2.52±2.63	17.0
							0.38				
22.1	50.5	73.2	5695	5729	- 0.30	- 0.49	1.6	0.70	2.3	- 2.27±2.80	34.0
			5723	5801	- 0.68		1.4				
22.1	73	101.6	1147	1257	- 4.58	- 8.40					
			1224	1565	-12.2						
22.1	73	101.6	1202	1259	- 2.32	- 5.02					
			1089	1271	- 7.71						
22.1	73	101.6	1521	1771	- 7.59	- 4.88					
			1668	1742	- 2.17						
22.1	73	101.6	1510	1665	- 4.88	- 5.73					
			681	777	- 6.58						
			Average at 73°			- 6.01	0.18	0.13	0.26	- 7.78±3.01	14.0
							0.13				
22.1	105	133.9	435	498	- 6.75	5.40	0.50	0.05	0.50	+ 3.62±3.74	74.0
			556	391	17.4		0.06				

$^4He(\vec{n},\hat{n})^4He$

E_n (MeV)	θ_2 lab (deg)	θ_2 c.m. (deg)	L' / L"	R' / R"	$e'_m\times100$ / $e''_m\times100$	$e_m\times100$	$\delta e_{stat}/e_m$ / $\delta e_{elec}/e_m$	$\delta e_{\theta_2}/e_m$ / $\delta e_{He}/e_m$	$\delta e/e_m$	absolute $(e\pm\delta e)\times100$	relative % $(\delta e/e)\times100$
16.5	35	43.3	5969	4920	9.63	13.2	0.05	0.01	0.07	+11.45±2.73	5.6
			6208	4433	16.7		0.05				
16.5	45	55.3	6619	4144	23.0	19.2	0.04	0.01	0.05	+17.5 ±2.7	4.0
			6568	4826	15.3		0.03				
22.1	40	49.3	7550	9815	-13.0	-13.0					
			5093	6600	-12.9						
22.1	40	49.3	6510	10205	-22.1	-15.7					
			6460	7767	- 9.19						

$^4He(\vec{n},\hat{n})^4He$ cont'd

E_n (MeV)	$\theta_2$lab (deg)	θ_2c.m. (deg)	L' / L"	R' / R"	$e'_m\times100$ / $e''_m\times100$	$e_m\times100$	$\delta e_{stat}/e_m$ / $\delta e_{elec}/e_m$	$\delta e_{\theta_2}/e_m$ / $\delta e_{He}/e_m$	$\delta e/e_m$	absolute $(e\pm\delta e)\times100$	relative % $(\delta e/e)\times100$
			Average at 40°			-14.3	0.07	0.19	0.21	-16.0 ±3.9	6.0
							0.04				
22.1	75	89.1	616	1029	-25.1	-23.6	0.11	0.00	0.12	-25.3 ±3.8	11.0
			797	1248	-22.1		0.02				
22.1	105	119.1	388	177	37.3	38.7	0.11	0.00	0.11	+37.2 ±5.0	12.0
			546	234	40.0		0.01				

CHAPTER V

RESULTS

In this chapter the results are tabulated for the $T(d,\vec{n})^4He$ neutron source polarization measurements, for the $T(\vec{n},\hat{n})T$ polarizations at 16.5- and 22.1-MeV incident neutron energy, and for the $D(\vec{n},\hat{n})D$ polarizations at E_n = 22.1 MeV. The 22.1-MeV $T(\vec{n},\hat{n})T$ and $D(\vec{n},\hat{n})D$ polarizations are also presented in graphical form, and the results of a phase shift analysis on the 22-MeV $T(\vec{n},\hat{n})T$ data are presented.

I. SOURCE POLARIZATIONS

The $T(d,\vec{n})^4He$ source polarizations measured by $^4He(\vec{n},\hat{n})^4He$ scattering are found in Table IV. The n-^{4}He elastic scattering analyzing powers $P_2(\theta_2)$ were obtained from the Hoop and Barschall phase shift calculations (Ho 66); the source polarization $P_1(\theta_1)$ was calculated from the expression

$$P_1(\theta_1) = e/P_2(\theta_2) .$$

Note that the value of P_1 at $\theta_1 = 29.8°$ and $\theta_2 = 75°$ is quite large. This value was neglected mainly because it does not agree with other quoted values of this source polarization (Pe 61, Ba 66). However, there is a resonance in the ^{5}He system at 22.15-MeV incident neutron energy where the $^4He(\vec{n},\hat{n})^4He$ polarizations exhibit a sharp discontinuity, and it is possible that $P_2(\theta_2)$ is too small. Note, however, that the measurements in this experiment were made at a neutron

TABLE IV

$T(d,\vec{n})^4He$ Source Polarizations $P_1(\theta_1)$ for an Incident Deuteron Energy of 6.0 MeV. Neutrons were emitted at angles θ_1 with energy E_n, and the asymmetry e was measured by $^4He(\vec{n},\hat{n})^4He$ scattering into angle θ_2.

θ_1 lab (deg)	E_n (MeV)	θ_2 lab (deg)	$e\pm\delta e$(absolute)	$P_2(\theta_2)$ (Ho 66)	$P_1(\theta_1)$
29.8	22.1	40	-0.16±0.04	-0.42	+0.38
29.8	22.1	75	-0.25±0.04	-0.36	+0.69
29.8	22.1	105	+0.37±0.05	+0.86	+0.43
89.8	16.5	35	+0.11±0.03	-0.22	-0.50
89.8	16.5	45	+0.18±0.03	-0.32	-0.56

energy below the resonance energy and agree quite well with the results of Perkins and Simmons (Pe 61), so that it is probable that the $^4He(\vec{n},\hat{n})^4He$ asymmetry measurement at $\theta_2 = 75°$ is simply in error. The following values of $T(d,\vec{n})^4He$ neutron source polarization for 6.0-MeV incident deuteron energy were obtained by considering the data from Table IV, from (Pe 61), and from the error analysis in Chapter IV:

$$P_1(\theta_1 = 29.8° \text{ lab}) = 0.40 \pm 0.03$$

and

$$P_1(\theta_1 = 89.8° \text{ lab}) = -0.54 \pm 0.05 .$$

II. $T(\vec{n},\hat{n})T$ AND $D(\vec{n},\hat{n})D$ RESULTS

The n-T and n-D polarizations are tabulated in Tables V and VI for incident neutron energy E_n and scattered neutron angle θ_2. Errors were

TABLE V

$T(\vec{n},\hat{n})T$ Polarizations $P_2(\theta_2)$. E_n is the incident neutron energy. θ_2 is the scattering angle.

E_n (MeV)	θ_2 lab (deg)	θ_2 c.m. (deg)	$\cos\theta_2$ c.m.	e	$P_1(\theta_1) \pm \delta P_1$	$P_2(\theta_2)$	δP_2 absolute	$(\delta P_2/P_2)\times 100$ relative %	$P_2(\theta_2)^\dagger$
16.5	35	46.1	0.693	-0.0076	-0.54±0.05	+0.014	0.051	43.0	
16.5	40	52.4	0.610	0.0021	-0.54±0.05	-0.004	0.048	130.0	
16.5	45	58.7	0.520	0.040	-0.54±0.05	-0.074	0.050	8.1	
22.1	40	52.4	0.610	-0.095	0.40±0.03	-0.24	0.071	5.5	-0.24
22.1	55	70.9	0.327	-0.14	0.40±0.03	-0.36	0.074	5.0	-0.36
22.1	70	88.3	0.029	-0.19	0.40±0.03	-0.47	0.080	5.2	-0.47
22.1	80	99.2	-0.160	-0.22	0.40±0.03	-0.56	0.092	8.6	-0.57
22.1	85	104.5	-0.250	-0.24	0.40±0.03	-0.59	0.10	11.0	-0.60
22.1	90	109.5	-0.334	-0.20	0.40±0.03	-0.51	0.10	13.0	-0.52
22.1	95	114.5	-0.414	0.13	0.40±0.03	+0.33	0.09	21.0	+0.33
22.1	100	119.2	-0.488	0.24	0.40±0.03	+0.59	0.10	14.0	+0.68
22.1	105	123.8	-0.557	0.34	0.40±0.03	+0.86	0.13	11.0	+0.95
22.1	110¼	128.5	-0.623	0.36	0.40±0.03	+0.90	0.12	8.6	+0.98
22.1	118½	135.6	-0.714	0.31	0.40±0.03	+0.77	0.100	6.2	+0.82

† Data corrected for multiple scattering. See Multiple Scattering Corrections at the end of Appendix A.

TABLE VI

D($\vec{n}$,$\hat{n}$)D Polarizations $P_2(\theta_2)$. E_n is the incident neutron energy. θ_2 is the scattering angle.

E_n (MeV)	$\theta_2$lab (deg)	θ_2c.m. (deg)	cos θ_2 c.m.	e	$P_1(\theta_1)\pm\delta P_1$	$P_2(\theta_2)$	δP_2 absolute	$(\delta P_2/P_2)\times 100$ relative %
22.1	40	58.8	0.518	-0.025	0.40±0.03	-0.063	0.066	17
22.1	50.5	73.2	0.288	-0.023	0.40±0.03	-0.057	0.070	35
22.1	73	101.6	-0.201	-0.078	0.40±0.03	-0.195	0.077	14
22.1	105	133.9	-0.694	+0.036	0.40±0.03	+0.091	0.094	74

calculated from the following expressions:

$$\delta P_2(\text{absolute}) = P_2[(\delta e/e \text{ absolute})^2 + (\delta P_1/P_1)^2]^{\frac{1}{2}} \tag{V-1}$$

and

$$\delta P_2(\text{relative}) = P_2[\delta e/e \text{ (relative)}] \; . \tag{V-2}$$

See the analysis at the end of Appendix A for multiple scattering corrections.

The $T(\vec{n},\hat{n})T$ polarizations for 22.1-MeV incident neutron energy are plotted in Fig. 12. Tivol's $^3He(\vec{p},\hat{p})^3He$ polarizations (Ti 68) at 21.3-MeV incident proton energy are also sketched in this figure for comparison of the main features. In the present experiment the $T(\vec{n},\hat{n})T$ results are unique in exhibiting larger polarization than the $^3He(\vec{p},\hat{p})^3He$ results. In all previous experiments of charge-conjugate reactions or scatterings at nearby energies, neutron polarizations are approximately equal to, or significantly less than, the corresponding proton polarizations.

The $D(\vec{n},\hat{n})D$ polarizations are presented in Fig. 13 and compared with earlier measurements of this polarization (Ma 66).

III. PHASE SHIFT ANALYSIS

In Appendix A it is shown that spin ½, spin ½ scattering can be described by a collision matrix U for which the phase shifts δ_{ij} are defined in analogy with the case in which no mixing of states occurs by

$$\delta_{ij} = \arctan Q_{ij} \; , \tag{V-3}$$

Figure 12. $T(\vec{n},\hat{n})T$ Polarization Data at 22.1-MeV Incident Neutron Energy. Error flags indicate the relative errors.

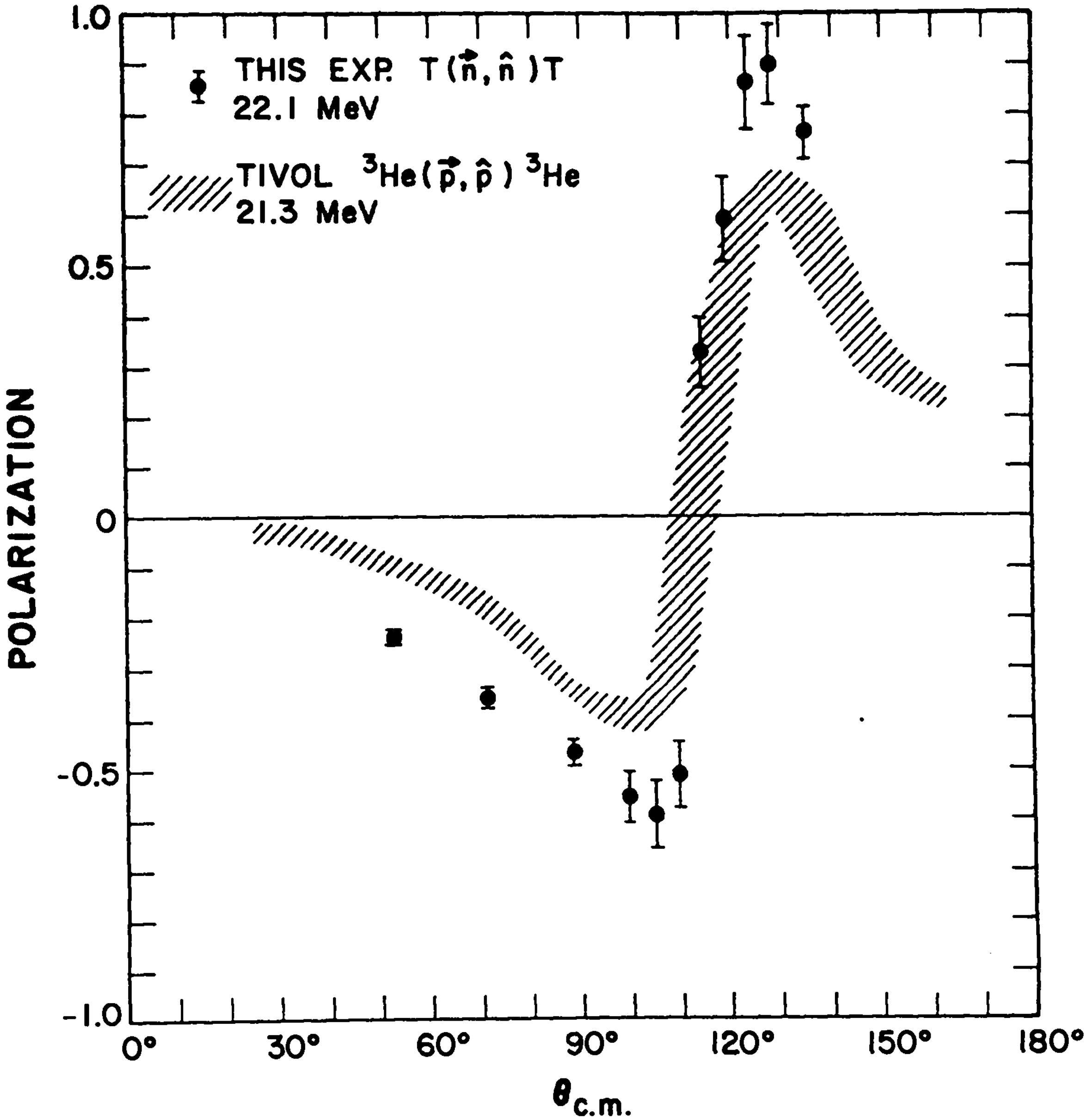

THIS EXP. T($\vec{n}$, $\hat{n}$)T
22.1 MeV
TIVOL ^{3}He($\vec{p}$, $\hat{p}$)^{3}He
21.3 MeV
POLARIZATION
1.0
0.5
0
-0.5
-1.0
0°
30°
60°
90°
120°
150°
180°
$\theta_{c.m.}$

Figure 13. $D(\vec{n},\hat{n})D$ Polarization Results at E_n = 22.1 MeV compared with results of Malanify et al. at 22.7 MeV (Ma 66). Error flags indicate absolute errors.

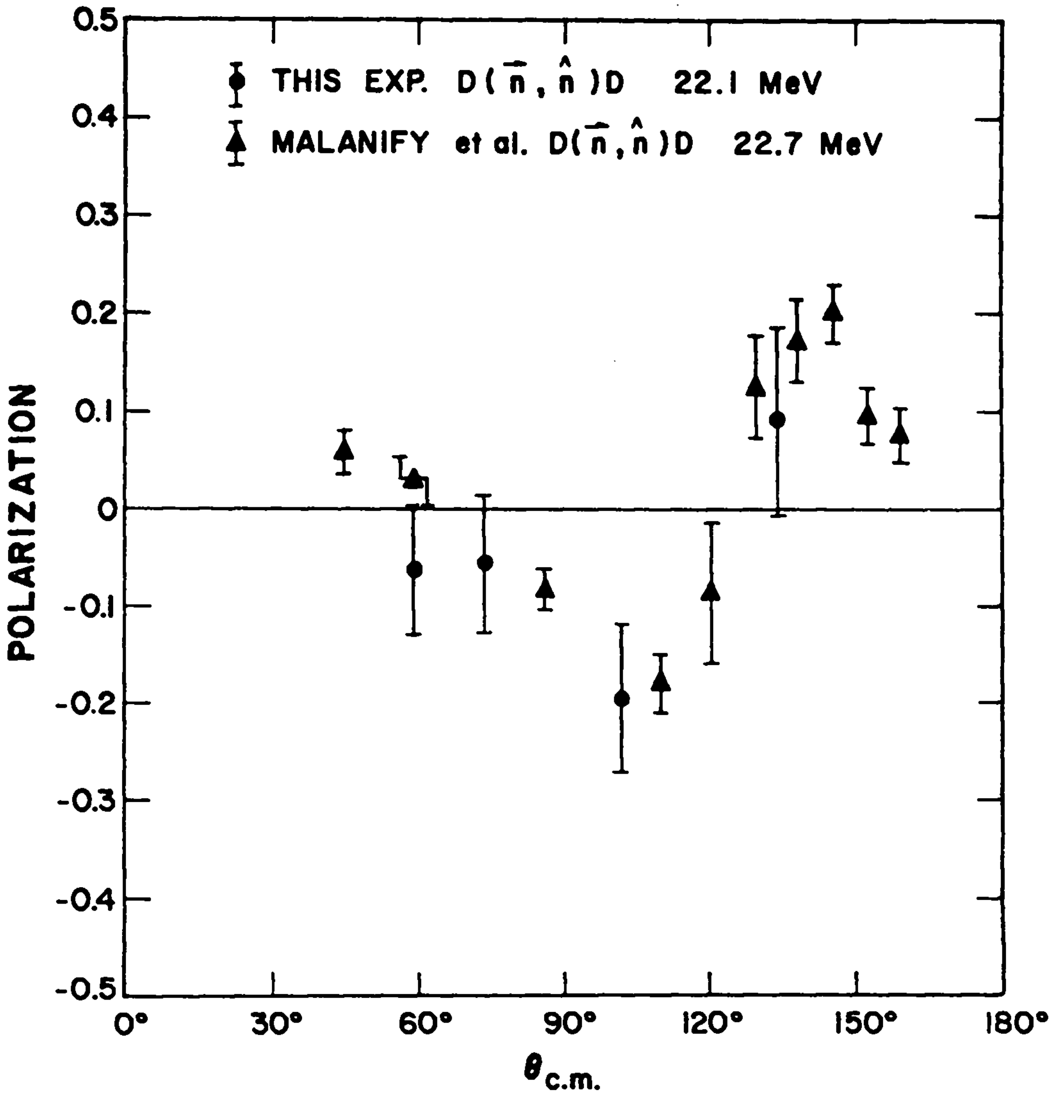

0.5
0.4
0.3
0.2
0.1
0
-0.1
-0.2
-0.3
-0.4
-0.5
POLARIZATION
THIS EXP. D(n, n̂)D 22.1 MeV
MALANIFY et al. D(n, n̂)D 22.7 MeV
0°
30°
60°
90°
120°
150°
180°
$\theta_{c.m.}$

where in matrix notation

$$iQ = (U-1)(U+1)^{-1} . \qquad (V-4)$$

Dodder has prepared an Energy Independent Reaction Matrix Analysis Code (Do 69) which has been modified for the CDC 6600 computer at LASL. The code was used to find a least squares fit of the scattering matrix elements for $\ell_{max} = 3$ to the cross section (Se 67) and polarization data of $T(\vec{n},\hat{n})T$ elastic scattering.

Initial guesses of the phase shifts δ_{ij} were obtained from Eqs. (V-3) and (V-4) by calculating the U matrix elements from Tivol's phase shifts for 19.5-MeV $^3He(\vec{p},\hat{p})^3He$ scattering (Ti 68). A typical example of the transformation equations from Tivol's mixing parameters ε and phase shifts $\delta^J_{\ell S}$ to the U matrix elements is the following conversion to U_{11}, U_{17}, and U_{77}:

$$U_{11} = \cos^2(\varepsilon_{SD}) \exp(2i\delta^1_{01}) + \sin^2(\varepsilon_{SD}) \exp(2i\delta^1_{21}) ,$$

$$U_{17} = \tfrac{1}{2}\sin(2\varepsilon_{SD})[\exp(2i\delta^1_{01}) - \exp(2i\delta^1_{21})] ,$$

and

$$U_{77} = \cos^2(\varepsilon_{SD}) \exp(2i\delta^1_{21}) + \sin^2(\varepsilon_{SD}) \exp(2i\delta^1_{01}) ,$$

where the initial and final states represented by the non-zero U_{ij} elements are given in Table AII.

Starting with the p-^{3}He phase shifts, a reasonably stable set of phase shifts (fit A) was obtained which fit the 22.1-MeV n-T data. The fit A phase shift values, changed by as much as ±50%, can be used as initial guesses in the energy independent code, and the solution will return to the fit A phase shifts. Another set of 22.1-MeV n-T phase shifts (fit B) was obtained by starting with p-^{3}He guesses but allowing the program to renormalize the polarization data assuming a ±15% error in the source polarization. The code normalized the polarizations by 40/43.4 and gave a new fit (B) for a source polarization $P_1 = 0.434$.

The phase shifts calculated from the 19.5-MeV p-^{3}He data and those for fit A and fit B are tabulated in Table VII; the predicted $T(n,n)\vec{T}$ triton polarizations for fits A and B are shown in Fig. 14a; and the differential cross section and $T(n,\vec{n})T$ neutron polarization fits are drawn in Fig. 14b. There is no apparent reason to prefer one fit over another except that the shapes of the predicted triton polarization curves in Fig. 14a are quite different from each other. Tivol (Ti 68) indicates that the ^{3}He polarization at forward angles may be negative.

IV. VALUABLE FUTURE MEASUREMENTS

It should be noted that nearly any initial guess for the 19 phase shifts in this problem will lead to a different solution, each of which fits the cross sections and neutron polarizations with about the same accuracy. Since the shape of the predicted triton polarization curve is different for different solutions, it would be useful to measure this effect. However, measurement of the triton polarizations would be an extremely difficult experiment. A more reasonable approach to the problem of determining a unique set of phase shifts is to measure the n-T neutron polarizations over a range of incident neutron energies and to attempt to find phase shift solutions which vary smoothly with

TABLE VII

Phase Shift Fits to the 22.1-MeV n-T Data and 19.5-MeV p-^{3}He phase shifts (Ti 68). $\ell_{max} = 3$

(See Table AII for definition of U_{ij} elements.)

i	j	δ_{ij}(deg) p-^{3}He	δ_{ij}(deg) n-T fit A	δ_{ij}(deg) n-T fit B
1	1	75.6	60.0	70.4
1	7	9.11	-31.6	-40.4
2	2	81.8	56.7	71.2
2	10	43.4	-27.1	-40.4
3	3	40.5	25.1	33.6
3	12	4.17	21.9	- 8.88
4	4	24.6	48.2	55.2
5	5	0.0	- 8.24	- 7.93
6	6	-12.4	10.8	20.2
6	13	1.66	16.8	- 8.45
7	7	- 5.94	-10.4	1.36
8	8	- 6.88	- 4.38	- 4.77
9	9	1.72	12.4	15.8
9	14	- 0.07	5.75	- 6.65
10	10	5.67	2.91	8.86
11	11	59.6	51.3	24.9
12	12	53.9	31.8	15.9
13	13	- 0.22	21.8	7.55
14	14	- 5.16	4.74	- 0.613
	χ^2 =		31.3	31.8
weighted variance	=		3.47	3.98

Figure 14a-b. Phase Shift Fits to the 22.1-MeV n-T Cross Section and Polarization Data. The points are the neutron polarizations measured in this experiment. The differential cross section curve matches LASL preliminary data (Se 67). $\ell_{max} = 3$.

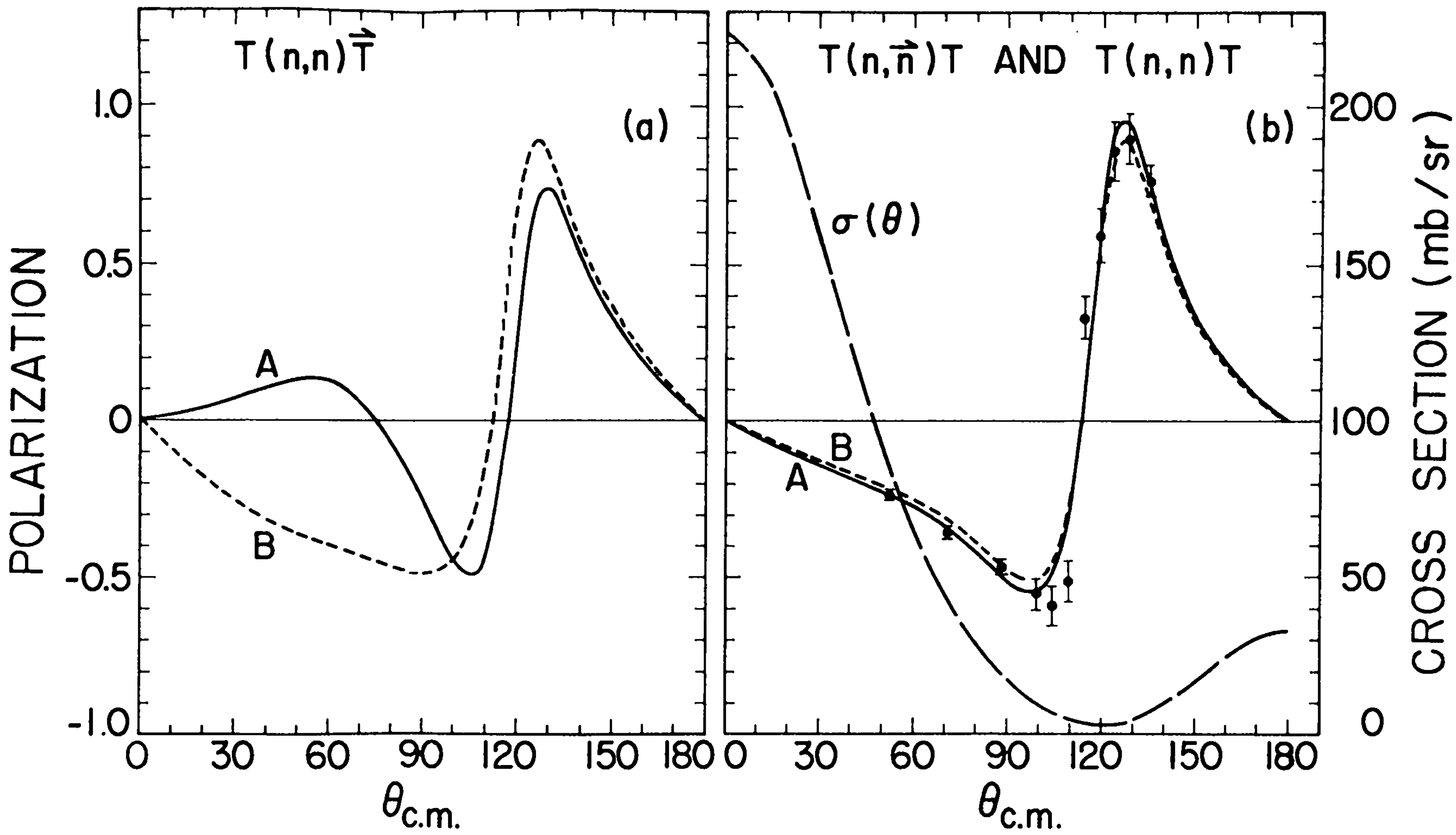

T(n,n)$\vec{\vec{T}}$
(a)
A
B
POLARIZATION
1.0
0.5
0
-0.5
-1.0
0
30
60
90
120
150
180
$\theta_{c.m.}$
T(n,$\vec{n}$)T AND T(n,n)T
(b)
σ(θ)
A
B
CROSS SECTION (mb/sr)
200
150
100
50
0
0
30
60
90
120
150
180
$\theta_{c.m.}$

energy.

The cryostats, detectors, collimators, and turntables used in this experiment are being moved to the Los Alamos tandem accelerator area where pulsed neutron beams of $\sim$4 to 30 MeV energy can be produced. With the addition of an $\sim$100 kgauss, superconducting, spin-precession solenoid which will be placed between the neutron producing target and the scattering sample, it is expected that measurements of the $T(\vec{n},\hat{n})T$ and $D(\vec{n},\hat{n})D$ interactions can be extended over a wide range of energies. These measurements must be made before one can hope to find a unique solution to the phase shift problem and thereby determine the form of the nuclear interaction potentials.

APPENDIX A

THE THEORY OF SCATTERING OF PARTICLES OF SPIN 1/2 FROM A TARGET POSSESSING THE SAME SPIN

In the following pages the theory outlined in the text will be developed in detail under the following subheadings:

I. Justification of Non-Relativistic Treatment

II. Reaction Kinematics

III. Quantum Theory of Spinless Scattering

IV. Matrix Formulation of Spin ½, Spin ½ Scattering

V. Polarization

VI. Data Correction Formulae

I. JUSTIFICATION OF NON-RELATIVISTIC TREATMENT

The momentum equation

$$|P_{rel}| = [T^2 + 2m_o c^2 T]^{\frac{1}{2}}/c \qquad \text{(A1)}$$

results from the relativistic energy momentum relationships

$$E^2 = c^2 p^2 + m_o^2 c^4$$

and

$$E = T + m_o c^2 .$$

Classically, of course,

$$|P_{cl}| = \sqrt{2m_o T} \ , \tag{A2}$$

so that

$$|P_{rel}|/|P_{cl}| = \sqrt{(T/2m_o c^2) + 1} \ . \tag{A3}$$

In the present experiment

$$T \leq 22 \text{ MeV}$$
$$M_n = m_o c^2 = 939 \text{ MeV}$$

and

$$|P_{rel}|/|P_{cl}| \leq 1.0058 \ .$$

Since all expressions to be considered contain p in powers ≥ 1, errors introduced into the analysis by a classical rather than a relativistic treatment will be less than 0.6%.

II. REACTION KINEMATICS

This section is a review of the methods for obtaining the transformation from laboratory (lab) to center of mass (c.m.) angles and for calculating reaction energies in the lab. The following constants (based on $M_{^{12}C}$ = 12.000000 amu) will be useful.

$$M_p = 1.007825 \text{ amu}$$
$$M_n = 1.008665 \text{ amu}$$
$$M_d = 2.01410 \text{ amu}$$

$$M_T = 3.016 \text{ amu}$$

$$M_{^4He} = 4.00260 \text{ amu}$$

$$Q_{T(d,n)} = 17.588 \text{ MeV}$$

$$1 \text{ amu} = 931.44 \text{ MeV} = 1.660 \times 10^{-24} \text{ gm} .$$

Reactions

The Q value of a reaction is the difference in mass between the incoming particles and the reaction products; i.e.,

$$M_1 + M_2 - (M_3 + M_4) = Q .$$

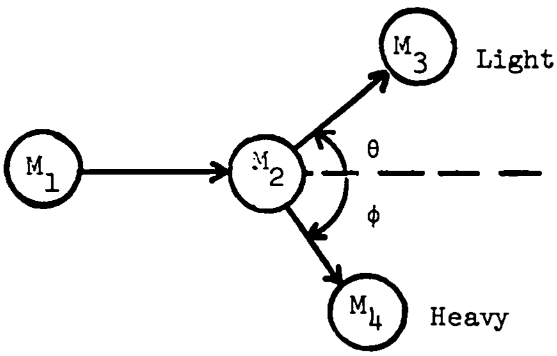

Figure A1. The Reaction in Laboratory Coordinates.

The energy-mass conservation equation is then

$$E_1 + Q = E_3 + E_4 , \qquad \text{(A4)}$$

where E_i represents the kinetic energy of the i^{th} particle. Expressions for conservation of momentum are

$$\sqrt{2M_1E_1} = \sqrt{2M_3E_3} \cos \theta + \sqrt{2M_4E_4} \cos \phi \qquad \text{(A5)}$$

and

$$0 = \sqrt{2M_3E_3} \sin \theta + \sqrt{2M_4E_4} \sin \phi \; . \tag{A6}$$

Eliminating E_4 and ϕ from Eqs. (A4-6) determines the kinetic energy of the light product, M_3, in terms of the masses, the reaction Q value, the bombarding particle energy, and the angle, θ_{lab}, at which M_3 leaves the reaction. Squaring and adding Eqs. (A5) and (A6) one obtains

$$2M_1E_1 + 2M_3E_3 - 4\sqrt{M_1E_1M_3E_3} \cos \theta = 2M_4E_4 \; ;$$

and substitution of E_4 from Eq. (A4) yields

$$2M_1E_1 + 2M_3E_3 - 4\sqrt{M_1E_1M_3E_3} \cos \theta = 2M_4E_1 + 2M_4Q - 2M_4E_3 \; ,$$

so that

$$(M_3+M_4)E_3 - 2\sqrt{M_1M_3E_1E_3} \cos \theta + (M_1-M_4)E_1 - M_4Q = 0 \; ,$$

or

$$\sqrt{E_3} = b \pm (b^2 + c)^{\frac{1}{2}} \; , \tag{A7}$$

where

$$\begin{aligned} b &= [\sqrt{M_1M_3E_1} \cos\theta]/(M_3 + M_4) \\ c &= [(M_4 - M_1)E_1 + M_4Q]/(M_3 + M_4) \; . \end{aligned} \tag{A8}$$

For the $T(d,n)^4He$ reaction $(M_4 = M_{^4He}) > (M_1 = M_n)$ and $Q > 0$; therefore, c is always positive and the positive energy solutions are

$$\boxed{\sqrt{E_3} = b + (b^2 + c)^{\frac{1}{2}}} \; .$$

Lab to c.m. Angle Conversion

Figure A2 is a diagram of the elastic scattering of M_1 and M_2 in the c.m. (Θ,Φ) and lab (θ,ϕ) reference frames where C is the center of mass and V_c is the velocity of the mass center in the lab. If V is the laboratory velocity of M_1 before collision, then $V_{1c.m.} = V-V_c$ and $V_{2c.m.} = -V_c$ before collision. By definition of the center of mass

$$\vec{P}_{1c.m.} + \vec{P}_{2c.m.} = 0 \;;$$

thus,

$$M_1(V-V_c) - M_2 V_c = 0$$

and

$$V_c/(V-V_c) = M_1/M_2 \; . \tag{A9}$$

To conserve both energy and momentum the velocities in the c.m. must remain constant throughout an elastic collision. To obtain the relationship between Θ and θ consider the triangle CEF in Fig. A2.

$$\overline{FE}/\sin(\Theta - \theta) = \overline{CF}/\sin\theta$$

$$V_c/\sin(\Theta - \theta) = (V-V_c)/\sin\theta \; ,$$

and substituting from (A9)

$$\boxed{\Theta = \theta + \sin^{-1}(M_1 \sin\theta/M_2)} \; . \tag{A10}$$

Figure A2. Elastic Scattering in Lab (θ,ϕ) and c.m. (Θ,Φ) Reference Frames.

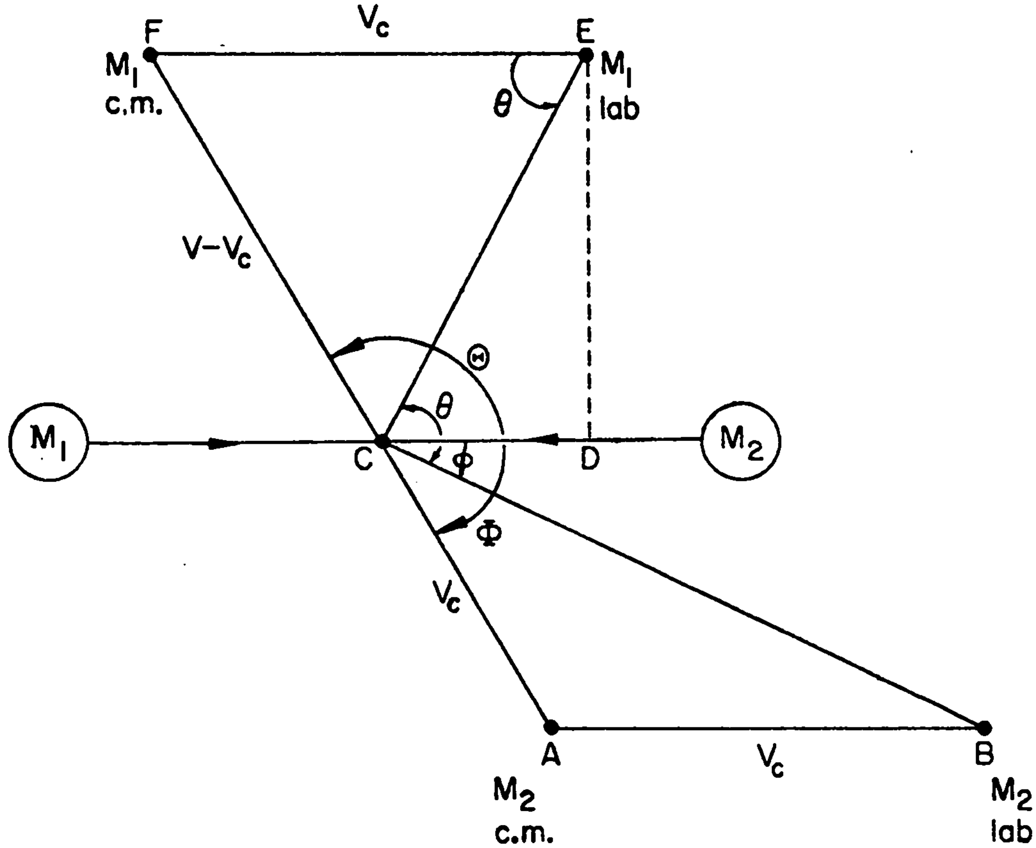

F
V_c
E
M_1
c.m.
M_1
lab
θ
$V-V_c$
Θ
θ
M_1
C
ϕ
D
M_2
Φ
V_c
A
V_c
B
M_2
c.m.
M_2
lab

III. QUANTUM THEORY OF SPINLESS SCATTERING

The Equation of Relative Motion

The problem of spin-independent nucleon-nucleus scattering is that of the motion of two particles in a potential field which depends only on the distance between the particles.

The Schrödinger wave equation for two particles of masses M_1 and M_2 can be written

$$i\hbar \frac{\partial}{\partial t} \Psi(\vec{x}_1,\vec{x}_2,t) = \left[-\frac{\hbar^2}{2M_1} \nabla_1^2 - \frac{\hbar^2}{2M_2} \nabla_2^2 + V(\vec{x}_1,\vec{x}_2,t)\right] \Psi(\vec{x}_1,\vec{x}_2,t) \ , \quad \text{(A11)}$$

where $\vec{x}_{1,2}$ represents the three space coordinates (x,y,z) of particles 1,2, respectively, $x_{1,2}$, $y_{1,2}$, $z_{1,2}$, and

$$\nabla^2_{1,2} = \frac{\partial^2}{\partial x^2_{1,2}} + \frac{\partial^2}{\partial y^2_{1,2}} + \frac{\partial^2}{\partial z^2_{1,2}} \ .$$

Assume now a central force,

$$V_c = V_c(x_1 - x_2, y_1 - y_2, z_1 - z_2) \ ,$$

and define relative coordinates $x = x_1 - x_2$, $y = y_1 - y_2$, $z = z_1 - z_2$, center of mass coordinates

$$X = (M_1 x_1 + M_2 x_2)/M$$
$$Y = (M_1 y_1 + M_2 y_2)/M$$
$$Z = (M_1 z_1 + M_2 z_2)/M \ ,$$

and the reduced mass $m = M_1 M_2/(M_1 + M_2)$, and $M = M_1 + M_2$; then

$$\frac{\partial}{\partial x_2} = - \frac{\partial}{\partial x} + \frac{M_2}{M}\frac{\partial}{\partial X} ,$$

$$\frac{\partial^2}{\partial x_2^2} = \frac{\partial^2}{\partial x^2} - \frac{2M_2}{M}\frac{\partial^2}{\partial x \partial X} + \frac{M_2^2}{M^2}\frac{\partial^2}{\partial X^2} , \tag{A12}$$

and

$$\frac{\partial^2}{\partial x_1^2} = \frac{\partial^2}{\partial x^2} + \frac{2M_1}{M}\frac{\partial^2}{\partial x \partial X} + \frac{M_1^2}{M^2}\frac{\partial^2}{\partial X^2} , \tag{A13}$$

so that

$$\frac{1}{M_1}\nabla_1^2 + \frac{1}{M_2}\nabla_2^2 = (\frac{1}{M_1} + \frac{1}{M_2}) (\frac{\partial^2}{\partial x^2} + \frac{\partial^2}{\partial y^2} + \frac{\partial^2}{\partial z^2})$$

$$+ (\frac{2}{M} - \frac{2}{M})(\frac{\partial^2}{\partial x \partial X} + \frac{\partial^2}{\partial y \partial Y} + \frac{\partial^2}{\partial z \partial Z}) + (\frac{M_2}{M^2} + \frac{M_1}{M^2})(\frac{\partial^2}{\partial X^2} + \frac{\partial^2}{\partial Y^2} + \frac{\partial^2}{\partial Z^2}) .$$

Now

$$\frac{1}{M_2} + \frac{1}{M_1} = \frac{M_1 + M_2}{M_1 M_2} = \frac{1}{m}$$

and

$$(M_1 + M_2)/M^2 = 1/M ;$$

thus, the Schrödinger wave equation for the interaction of two particles becomes

$$i\hbar \frac{\partial \Psi}{\partial t} = \left[- \frac{\hbar^2}{2M}\nabla_X^2 - \frac{\hbar^2}{2m}\nabla_x^2 + V_c(x,y,z)\right]\Psi . \tag{A14}$$

The wave equation can be separated by allowing

$$\Psi(\vec{x},\vec{X},t) = f(t)\ \psi(\vec{x})\ \chi(\vec{X}) \ .$$

In that case

$$\frac{i\hbar}{f}\frac{df}{dt} = \frac{1}{\psi\chi}\left(-\frac{\hbar^2}{2M}\nabla_X^2 - \frac{\hbar^2}{2m}\nabla_x^2 + V(\vec{x})\right)\psi\chi = W \ ,$$

and

$$df/f = -\ i\ W\ dt/\hbar \ ,$$

so that

$$f = C\ \exp[-iWt/\hbar] \ . \tag{A15}$$

Also

$$\frac{1}{\chi}\left(-\frac{\hbar^2}{2M}\nabla_X^2\ \chi(\vec{X})\right) + \frac{1}{\psi}\left(-\frac{\hbar^2}{2m}\nabla_x^2\ \psi(\vec{x}) + V_c(\vec{x})\ \psi(\vec{x})\right) = W \ .$$

Since χ and ψ are independent, one can define $W = E + E'$ where

$$(-\hbar^2/2M)\ \nabla_X^2\ \chi = E'\chi \tag{A16}$$

is the equation for the motion of a free particle of mass $M = M_1 + M_2$ and

$$[(-\hbar^2/2m)\ \nabla_x^2 + V_c]\psi = E\psi \tag{A17}$$

is the equation of motion of a particle of reduced mass, m, in a potential field V_c.

E and E' are energy eigenvalues of the two types of motion. Only the equation of relative motion contains the scattering potential; thus

Eq. (A17) is the important expression for describing the nucleon-nucleus interaction. In the following discussion the subscript x will be dropped from the operator ∇_x^2 in Eq. (A17) so that the relative kinetic energy operator in the two-particle system is $(-\hbar^2/2m)\nabla^2$. One purpose of the present experiment has been to throw some light on the interaction potential $V(\vec{x})$ between the neutron and triton.

Summary. The equation of motion of a two-particle system can be written as the free motion of the total mass of the system $M = M_1 + M_2$,

$$(-\hbar^2/2M)\ \nabla_X^2\ \chi(\vec{X}) = E'\chi(\vec{X}) \ ,$$

and the relative motion of a particle of reduced mass $m = M_1M_2/(M_1+M_2)$ in an interaction potential $V_c(\vec{x}_1-\vec{x}_2) = V_c(\vec{x})$, where

$$\boxed{(-\hbar^2/2m)\nabla^2\ \psi(\vec{x}) + V_c(\vec{x})\ \psi(\vec{x}) = E\psi(\vec{x})} \ .$$

The total wave function of the system is

$$\Psi(\vec{x},\vec{X},t) = \psi(\vec{x})\ \chi(\vec{X})\ \exp[-i(E+E')t/\hbar] \ . \tag{A18}$$

Concepts of Cross Section

Now consider the eigenvalue equation

$$(-\hbar^2/2m)\ \nabla^2\ \psi(\vec{x}) + V_c\psi(\vec{x}) = E\psi(\vec{x}) \ ,$$

and rewrite it

$$(\nabla^2 + k^2 - U_c)\ \psi(\vec{x}) = 0 \ , \tag{A19}$$

where

$$U_c = (2m/\hbar^2)\ V_c(\vec{x}) \tag{A20}$$

and

$$\hbar^2 k^2 = 2mE\ (\text{i.e., } \vec{p} = \hbar k)\ . \tag{A21}$$

ψ is the total wave function of the scattering problem; therefore, it must be the sum of an incident wave and a scattered wave. The assumed plane wave of incident particles can be represented by $\psi_{in}(\vec{x}) = \exp(ikz)$ so that the density of particles in the incident beam is $\psi_{in}\psi^*_{in} = 1$ per unit volume. If the incident velocity is V then the incident flux is $|\exp(ikz)|^2 V = V$ particles/unit area-unit time. It is easily seen by substitution into (A19) that e^{ikz} is a solution of the wave equation at large distances where the interaction potential is zero.

Now the differential cross section $\sigma(\theta)\ ds/r^2$ for elastic scattering into a solid angle ds/r^2 at mean angle θ is the ratio of the flux of scattered particles to the incident flux. It is common to define the scattered wave function in terms of a scattering amplitude $f(\theta)$.

$$\psi_{sc} \equiv f(\theta)\ \exp(ikr)/r\ . \tag{A22}$$

Then (particles scattered into ds)/(unit time) = $\psi_{sc}\psi^*_{sc}\ Vds = |f(\theta) \times \exp(ikr)/r|^2\ Vds$, and

$$\sigma(\theta)\left(\frac{ds}{r^2}\right) = \frac{\psi_{sc}\psi^*_{sc}\ Vds}{\psi_{in}\psi^*_{in}\ V} = \frac{|f(\theta)|^2\ V\ \frac{ds}{r^2}}{V}\ ,$$

so that for unit solid angle

$$\boxed{\sigma(\theta) = |f(\theta)|^2} \quad . \tag{A23}$$

In this manner the total wave function ,

$$\boxed{\psi(\vec{x}) = \psi_{in}(\vec{x}) + \psi_{sc}(\vec{x}) = \exp(ikz) + f(\theta)\exp(ikr)/r} \quad , \tag{A24}$$

and the measurable differential cross sections $\sigma(\theta)$ are connected by the Schrodinger equation to the interaction potential V_c.

Separation of the Wave Equation

It will be convenient in analysis of the scattering problem to have the wave function $\psi(\vec{x})$ separated into its spherical components.

It is straightforward (but lengthy) to show (Sh 59) that

$$\nabla^2 \equiv \frac{\partial^2}{\partial x^2} + \frac{\partial^2}{\partial y^2} + \frac{\partial^2}{\partial z^2} = \frac{1}{r^2}\frac{\partial}{\partial r}\left(r^2\frac{\partial}{\partial r}\right)$$

$$+ \frac{1}{r^2 \sin\theta}\frac{\partial}{\partial\theta}\left(\sin\theta\frac{\partial}{\partial\theta}\right) + \frac{1}{r^2\sin^2\theta}\frac{\partial^2}{\partial\phi^2} \quad ,$$

where

$$x = r\sin\theta\cos\phi$$

$$y = r\sin\theta\sin\phi$$

$$z = r\cos\theta \ .$$

This section still assumes that $V_c(\vec{x}) = V(x_1-x_2, y_1-y_2, z_1-z_2) \equiv V_c(r)$; thus, the wave equation can be written

$$\left[\frac{1}{r^2}\frac{\partial}{\partial r}\left(r^2\frac{\partial}{\partial r}\right) + \frac{1}{r^2\sin\theta}\frac{\partial}{\partial\theta}\left(\sin\theta\frac{\partial}{\partial\theta}\right) + \frac{1}{r^2\sin^2\theta}\frac{\partial^2}{\partial\phi^2}\right]\psi(r,\theta,\phi)$$

$$+ k^2\,\psi(r,\theta,\phi) - (2m/\hbar^2)\,V_c(r)\,\psi(r,\theta,\phi) = 0\,. \tag{A25}$$

Now let $\psi(r,\theta,\phi) = R(r)\ \Theta(\theta)\ \Phi(\phi) = R(r)\ Y(\theta,\phi)$, substitute into (A25), and divide by ψ to obtain

$$\frac{1}{R}\frac{d}{dr}\left(r^2\frac{dR}{dr}\right) + r^2(k^2 - U_c) = -\frac{1}{Y}\left[\frac{1}{\sin\theta}\frac{\partial}{\partial\theta}\left(\sin\theta\frac{\partial Y}{\partial\theta}\right) + \frac{1}{\sin^2\theta}\frac{\partial^2 Y}{\partial\phi^2}\right]$$

$$= -\frac{1}{\Theta}\frac{1}{\sin\theta}\frac{d}{d\theta}\left(\sin\theta\frac{d\Theta}{d\theta}\right) - \frac{1}{\Phi}\frac{1}{\sin^2\theta}\frac{d^2\Phi}{d\phi^2} = L\,. \tag{A26}$$

Since the left side of (A26) depends only on r and the right side is independent of r, both sides must be equal to a constant, L. Then

$$\frac{1}{r^2}\frac{d}{dr}\left(r^2\frac{dR}{dr}\right) + \left(k^2 - U_c - \frac{L}{r^2}\right)R = 0\,, \tag{A27}$$

and similarly

$$\frac{1}{\Theta}\sin\theta\frac{d}{d\theta}\left(\sin\theta\frac{d\Theta}{d\theta}\right) + L\sin^2\theta = -\frac{1}{\Phi}\frac{d^2\Phi}{d\phi^2} = \nu\,,$$

where ν is another separation constant. As a result

$$\frac{1}{\sin\theta}\frac{d}{d\theta}\left(\sin\theta\frac{d\Theta}{d\theta}\right) + \left(L - \frac{\nu}{\sin^2\theta}\right) = 0\,, \tag{A28}$$

and

$$\frac{d^2\Phi}{d\phi^2} + \nu\ \Phi = 0\ . \tag{A29}$$

The solutions of the Φ equation (A29) are

$$\Phi(\phi) = A\ \exp(i\nu^{\frac{1}{2}}\phi) + B\ \exp(-i\nu^{\frac{1}{2}}\phi) \qquad \nu \neq 0$$

and

$$\Phi(\theta) = A + B\ \phi \qquad \nu = 0\ ;$$

but $\Phi(\phi + 2\pi) = \Phi(\phi)$; therefore,

$$A\ \exp(i\nu^{\frac{1}{2}}\phi) + B\ \exp(-i\nu^{\frac{1}{2}}\phi) = A\ \exp[i\nu^{\frac{1}{2}}(\phi+2\pi)] + B\ \exp[-i\nu^{\frac{1}{2}}(\phi+2\pi)]$$

and $\nu^{\frac{1}{2}} = m$ where m is any integer or zero. Now $A + B\phi = A + B\phi + 2\pi B$ only if $B = 0$. The solutions A, $A\ \exp(im\phi)$, and $B\ \exp(-im\phi)$ are all linearly dependent; hence,

$$\Phi(\phi) = A\ \exp(im\phi)\ .$$

Let Φ be normalized to unity over the range $\phi = 0$ to $\phi = 2\pi$,

$$\int_0^{2\pi} \Phi^*(\phi)\ \Phi(\phi)\ d\phi = \int_0^{2\pi} A^2\ d\phi = 2\pi A^2 = 1\ ;$$

then

$$\Phi(\phi) = (2\pi)^{-\frac{1}{2}}\ \exp(im\phi)\ . \tag{A30}$$

To find the solutions of the Θ equation the following substitutions are made in (A28):

$$w = \cos\theta , \qquad \Theta(\theta) = P(w) ,$$

and

$$\frac{d}{d\theta} = \frac{d}{dw}\frac{dw}{d\theta} = -\sin\theta \frac{d}{dw} .$$

Then

$$\frac{d}{dw}\left[(1-w^2)\frac{dP}{dw}\right] + \left(L - \frac{m^2}{1-w^2}\right) P = 0 .$$

The domain of θ is 0 to π; hence, the domain of w is 1 to -1. Whittaker and Watson (Wh 50) show that for $L = \ell(\ell+1)$ the solutions for P(w) which are finite at $w = \pm 1$ are the associated Legendre polynomials $P_\ell^m(w)$ where

$$\int_{-1}^{1} P_\ell^m(w)\, P_{\ell'}^m(w)\, dw = \begin{cases} 0 & \ell' \neq \ell \\ \dfrac{2}{2\ell+1}\dfrac{(\ell+m)!}{(\ell-m)!} & \ell' = \ell \end{cases} . \qquad \text{(A31)}$$

A solution for Θ is then the normalized function

$$\Theta_{\ell m}(\theta) = \sqrt{\frac{2\ell+1}{2}\frac{(\ell-m)!}{(\ell+m)!}}\; P_\ell^m(\cos\theta) . \qquad \text{(A32)}$$

Note that when m = 0, $\Phi = \dfrac{1}{\sqrt{2\pi}}$; i.e., the wave function is axially symmetric and $\Theta_\ell(\theta)$ becomes the normalized Legendre polynomial $[(2\ell+1)/2]^{\frac{1}{2}} P_\ell(\cos\theta)$.

Jahnke and Emde (Ja 45) give expressions for evaluating the Legendre and associated polynomials. The normalized spherical harmonics $Y_{\ell m}(\theta,\phi)$ in Eq. (A26) are defined:

$$Y_{\ell m}(\theta,\phi) = \sqrt{\frac{2\ell+1}{4\pi}\frac{(\ell-m)!}{(\ell+m)!}}\; P_\ell^m(\cos\theta)\; \exp(im\phi)\ . \qquad \text{(A33)}$$

Therefore, a solution of the scattering Eq. (A19) in spherical coordinates is

$$\boxed{\psi(r,\theta,\phi) = \sum_{\substack{\ell=0 \\ |m|\leq\ell}}^{\infty} R_{\ell m}(r)\; P_\ell^m(\cos\theta)\; \exp(im\phi)}\ , \qquad \text{(A34)}$$

where $R_{\ell m}(r)$ satisfies the radial wave equation

$$\boxed{\frac{d^2R}{dr^2} + \frac{2}{r}\frac{dR}{dr} + [k^2 - U_c(r) - \frac{\ell(\ell+1)}{r^2}]R = 0}\ , \qquad \text{(A35)}$$

and normalizing constants have been absorbed into $R_{\ell m}(r)$.

<u>Angular momentum</u>. The quantity $[\ell(\ell+1)]^{\frac{1}{2}}\hbar$ can be associated with angular momentum, M, by noting that

$$M^2 = -\hbar^2[\frac{1}{\sin\theta}\frac{\partial}{\partial\theta}(\sin\theta\frac{\partial}{\partial\theta}) + \frac{1}{\sin^2\theta}\frac{\partial^2}{\partial\theta^2}] \qquad \text{(Sc 55)}$$

so that from Eq. (A26)

$$M^2 Y_{\ell m}(\theta,\phi) = L\hbar^2\; Y_{\ell m}(\theta,\phi) = \ell(\ell+1)\hbar^2\; Y_{\ell m}(\theta,\phi)\ .$$

Therefore, $Y_\ell^m(\theta,\phi)$ is an eigenfunction of the square of the angular momentum with eigenvalue $\ell(\ell+1)\hbar^2$. Also $M_z = -i\hbar(\partial/\partial\phi)$, and from Eq. (A33)

$$M_z\, Y_{\ell m}(\theta,\phi) = m\hbar\, Y_{\ell m}(\theta,\phi)\ .$$

Thus, $Y_{\ell m}$ is also an eigenfunction of the z component of angular momentum with eigenvalue m.

Solution of the Radial Wave Equation

Jahnke and Emde (Ja 45) give the function $y = x^a[J_p(\beta x^\gamma)\cos\delta - N_p(\beta x^\gamma)\sin\delta]$ as the solution to Bessel's equation

$$\frac{d^2y}{dx^2} + \frac{1-2a}{x}\frac{dy}{dx} + [(\beta\gamma x^{\gamma-1})^2 - \frac{p^2\gamma^2-a^2}{x^2}]\, y = 0\ ,$$

where δ is an arbitrary constant, $J_p(x)$ and $N_p(x)$ are Bessel functions of the first and second kind, respectively, and $N_p(x)(\sin p\pi) = J_p(x)(\cos p\pi) - J_{-p}(x)$.

Bessel's equation is equivalent to the radial Eq. (A35) if the following associations are made:

$$x = r$$

$$y = R(r)$$

$$\beta = [k^2 - U_c(r)]^{\frac{1}{2}}$$

$$\gamma = 1$$

$$a = -\tfrac{1}{2}$$

$$p^2 = (\ell+\tfrac{1}{2})^2$$

$$\alpha = \beta\gamma\ .$$

Thus, the solution of the radial equation for a particular ℓ value is

$$R_\ell(r) = A'_{\ell m}\, r^{-\frac{1}{2}}\, [J_{\ell+\frac{1}{2}}(\alpha r)\cos\delta_\ell - N_{\ell+\frac{1}{2}}(\alpha r)\sin\delta_\ell]\ . \tag{A36}$$

In the scattering problem one is interested in solutions for large r where incident and scattered particles are produced and detected. At large r (Ja 45)

$$R_\ell(r) \underset{r\to\infty}{=} A'_{\ell m} r^{-\frac{1}{2}} \Big\{ \cos[\alpha r-(\ell+\tfrac{1}{2}+\tfrac{1}{2})(\pi/2)] \cos \delta_\ell/[(\pi/2)\alpha r]^{\frac{1}{2}}$$

$$- \sin[\alpha r-(\ell+\tfrac{1}{2}+\tfrac{1}{2})(\pi/2)] \sin \delta_\ell/[(\pi/2)\alpha r)]^{\frac{1}{2}} \Big\}$$

$$= A'_{\ell m}[2/(\pi\alpha r^2)]^{\frac{1}{2}}[\sin(\alpha r-\ell\pi/2) \cos \delta_\ell + \cos(\alpha r-\ell\pi/2) \sin \delta_\ell]$$

$$= A'_{\ell m}[2/(\pi\alpha r^2)]^{\frac{1}{2}}\sin[\alpha r-(\ell\pi/2)+\delta_\ell] \;;$$

however, at large r $U_c(r) = 0$, $\alpha = k$, and

$$R_{\ell m}(r) \underset{r\to\infty}{=} A_{\ell m}(kr)^{-1} \sin[kr-(\ell\pi/2)+\delta_\ell] \;. \tag{A37}$$

The wave function for large r is then

$$\psi(r,\theta) = \exp(ikz) + f(\theta) \exp(ikr)/r$$

$$\boxed{\psi(r,\theta) = \sum_{\substack{\ell=0\\ |m|\le\ell}}^{\infty} A_{\ell m}(kr)^{-1}\sin[kr-(\ell\pi/2)+\delta_\ell]P_\ell^m(\cos\theta)\exp(im\phi)} \;. \tag{A38}$$

To determine the value of $A_{\ell m}$, it will first be necessary to solve the wave equation,

$$(\nabla^2 + k^2)\, \psi_{in}(r,\theta) = 0 \;, \tag{A39}$$

for the unscattered wave $\psi_{in} = \exp(ikz)$. The incident plane wave is symmetric about the z axis; hence the most general solution of Eq. (A39) is

$$\psi_{in}(r,\theta) = \sum_{\ell=0}^{\infty} B_\ell \, g_\ell(r) \, P_\ell(\cos\theta) = \exp(ikr \cos\theta) \; , \tag{A40}$$

where $g_\ell(r)$ is the solution of

$$\frac{d^2 g_\ell}{dr^2} + \frac{2}{r}\frac{dg}{dr} + \left[k^2 - \frac{\ell(\ell+1)}{r^2}\right] g_\ell(r) = 0 \; . \tag{A41}$$

To find $B_\ell g_\ell(r)$ multiply both sides of Eq. (A40) by $P_m(\cos\theta)\, d(\cos\theta)$ and integrate over the domain of $\cos\theta$

$$\int_{-1}^{1} e^{ikr\cos\theta} P_m(\cos\theta)\, d(\cos\theta) = \int_{-1}^{1} [B_\ell \, g_\ell(r) \, P_\ell(\cos\theta)$$

$$\cdot \, P_m(\cos\theta)\, d(\cos\theta)] = [2/(2\ell+1)] \, B_\ell \, g_\ell(r) \; .$$

Now integrating by parts

$$I = \int_{-1}^{1} e^{ikrt} \, P_\ell(t) \, dt = \frac{1}{ikr} \, [e^{ikrt} \, P_\ell(t)]_{-1}^{1} - \int_{-1}^{1} \frac{e^{ikrt}}{ikr} \, P_\ell'(t) \, dt \; ,$$

but $P_\ell(1) = 1$ and $P_\ell(-1) = (-1)^\ell$; therefore,

$$I = \frac{1}{ikr}\left\{e^{ikr} - (-1)^{\ell}\, e^{-ikr}\right\} - \frac{1}{ikr}\int_{-1}^{1} e^{ikrt}\, P_\ell'(t)\, dt$$

$$= \frac{1}{ikr}\left\{e^{ikr} - (-1)^{\ell}\, e^{-ikr}\right\} - \left(\frac{1}{ikr}\right)^2 \left\{e^{ikrt}\, P_\ell'(t)\right\}_{-1}^{1}$$

$$+ \frac{1}{ikr}\int_{-1}^{1} e^{ikrt}\, P_\ell''(t)\, dt\ .$$

All but the first term of I are of the order of r^{-2} or smaller and can be ignored for large r; thus,

$$\frac{2}{2\ell+1} B_\ell\, g_\ell(r) \approx \frac{1}{ikr}\left\{e^{ikr} - e^{i\ell\pi}\, e^{-ikr}\right\}$$

$$= \frac{1}{ikr}\, e^{i\ell\pi/2}\left\{e^{i(kr-\ell\pi/2)} - e^{-i(kr-\ell\pi/2)}\right\}$$

$$= 2i^{\ell}(kr)^{-1}\sin(kr-\ell\pi/2)$$

and

$$B_\ell\, g_\ell(r) \underset{r\to\infty}{=} (2\ell+1)i^{\ell}(kr)^{-1}\sin(kr-\ell\pi/2)\ , \qquad \text{(A42)}$$

so that the incident wave function is

$$\boxed{\psi_{in}(r,\theta) = \sum_{\ell=0}^{\infty} (2\ell+1)i^{\ell}(kr)^{-1}\sin(kr-\ell\pi/2)\, P_\ell(\cos\theta)\ .} \qquad \text{(A43)}$$

Phase shifts. One can now easily determine the meaning of δ_ℓ by comparing (A43) with the expression (A38) for the total wave function. δ_ℓ represents the shift in phase of the total wave with respect to the unscattered wave. Examination of Eqs. (A35) and (A41) and comparison with the expressions for ψ (A38) and ψ_{in} (A43) shows that $R_\ell(r)$ is shifted inward relative to $g_\ell(r)$ if the potential $U_c(r) = 2mV_c(r)/\hbar^2$ is negative; i.e., for an attractive field, $kr + \delta_\ell$ is a larger number than kr for a given r.

Hence, one obtains the following relationships:

$\delta_\ell > 0$ for attractive fields,

$\delta_\ell < 0$ for repulsive fields.

In order to determine the scattering amplitude $f(\theta)$ in terms of the phase shifts, it is necessary to substitute for the total and incident wave functions the expressions (A38) and (A43), respectively, so that

$$\psi = \psi_{inc} + \psi_{sc} = e^{ikz} + f(\theta)\ e^{ikr}/r$$

becomes

$$\sum_{\ell=0}^{\infty} A_\ell (kr)^{-1} \sin[kr-(\ell\pi/2)+\delta_\ell]\ P_\ell(\cos\theta)$$

$$= \left[\sum_{\ell=0}^{\infty} (2\ell+1) i^\ell (kr)^{-1} \sin(kr-\ell\pi/2)\ P_\ell(\cos\theta)\right] + f(\theta)\ \exp(ikr)/r\ ,$$

or

$$\sum_{\ell=0}^{\infty} \frac{A_\ell}{2ik} \left(e^{ikr} e^{-i\ell\pi/2} e^{i\delta_\ell} - e^{-ikr} e^{i\ell\pi/2} e^{-i\delta_\ell}\right) P_\ell(\cos\theta)$$

$$= \left[\sum_{\ell=0}^{\infty} \frac{2\ell+1}{2ik} i^\ell \left(e^{ikr} e^{-i\ell\pi/2} - e^{-ikr} e^{i\ell\pi/2}\right) P_\ell(\cos\theta)\right] + f(\theta)\, e^{ikr} .$$

The coefficients of exp(ikr) on both sides of this equation must be equal in order for the functions to be continuous in r; consequently,

$$2ikf(\theta) + \sum_{\ell=0}^{\infty} (2\ell+1)\, i^\ell\, e^{-i\ell\pi/2}\, P_\ell(\cos\theta)$$

$$= \sum_{\ell=0}^{\infty} A_\ell\, e^{i\delta_\ell}\, e^{-i\ell\pi/2}\, P_\ell(\cos\theta) \ , \qquad \text{(A44)}$$

and

$$\sum_{\ell=0}^{\infty} (2\ell+1)\, i^\ell\, e^{i\ell\pi/2}\, P_\ell(\cos\theta) = \sum_{\ell=0}^{\infty} A_\ell\, e^{i\ell\pi/2}\, e^{-i\delta_\ell}\, P_\ell(\cos\theta) \ . \qquad \text{(A45)}$$

Since the equation must hold for all ℓ,

$$(2\ell+1)\, i^\ell \exp(i\ell\pi/2) = A_\ell \exp(-i\delta_\ell) \exp(i\ell\pi/2) \ ,$$

or

$$A_\ell = (2\ell+1)\, i^\ell \exp(i\delta_\ell) \ .$$

Finally substitution of the above expression for A_ℓ into Eq. (A44) gives the result

$$2ikf(\theta) = \sum_{\ell=0}^{\infty} (2\ell+1)\ i^{\ell}\ \exp(2i\delta_{\ell})\ e^{-i\ell\pi/2}\ P_{\ell}(\cos\theta)$$

$$- \sum_{\ell=0}^{\infty} (2\ell+1)\ i^{\ell}\ e^{-i\ell\pi/2}\ P_{\ell}(\cos\theta) \ ,$$

or

$$\boxed{f(\theta) = (2ik)^{-1} \sum_{\ell=0}^{\infty} (2\ell+1)\ [\exp(2i\delta_{\ell}) - 1]\ P_{\ell}(\cos\theta)} \ , \qquad (A46)$$

from which it follows that the differential cross section is

$$\sigma(\theta) = |f(\theta)|^2 = \frac{1}{k^2} \left| \sum_{\ell=0}^{\infty} (2\ell+1)\ \exp(i\delta_{\ell})\ \sin\delta_{\ell}\ P_{\ell}(\cos\theta) \right|^2 , \qquad (A47)$$

and the total cross section becomes

$$\sigma = 2\pi \int_0^{\pi} \sigma(\theta)\ \sin\theta\ d\theta \ ,$$

$$\sigma = 4\pi k^{-2} \sum_{\ell=0}^{\infty} (2\ell+1)\ \sin^2\delta_{\ell} \ . \qquad (A48)$$

IV. MATRIX FORMULATION OF SPIN ½, SPIN ½ SCATTERING

U, I, O Formulation of Spinless Scattering

In order to extend the simple case of spinless scattering derived in the previous section to more complicated cases, it will be helpful to reconsider the above analysis from a slightly different viewpoint.

Let there be two functions

$$I_{\ell m} = [i^{\ell} e^{-i(kr-\ell\pi/2)} Y_{\ell m}(\theta,\phi)]/r \tag{A49}$$

and

$$O_{\ell m} = [i^{\ell} e^{i(kr-\ell\pi/2)} Y_{\ell m}(\theta,\phi)]/r \ , \tag{A50}$$

representing general incoming and outgoing waves, respectively, with wave number k. The incident beam is

$$\psi_{in} = \exp(ikz) = i\pi^{\frac{1}{2}}k^{-1} \sum_{\ell=0}^{\infty} (2\ell+1)^{\frac{1}{2}} (I_{\ell o} - O_{\ell o}) \ , \tag{A51}$$

from Eqs. (A33) and (A43) of the last section. Similarly, the form of a general solution of the wave equation can be written from (A33) and (A38) for large r as

$$\psi = \sum_{\substack{\ell=0 \\ |m|\le\ell}}^{\infty} \frac{iA_{\ell m}\exp(-i\delta_{\ell})}{2i^{\ell}k} \left[- \frac{i^{\ell}e^{i(kr-\ell\pi/2)}}{r} \exp(2i\delta_{\ell}) + \frac{i^{\ell}e^{-i(kr-\ell\pi/2)}}{r} \right]$$

$$\cdot \sqrt{\frac{4\pi \ (\ell+m)!}{(2\ell+1)(\ell-m)!}} \ Y_{\ell m}(\theta,\phi)$$

$$\psi = \sum_{\ell,m} C_{\ell m} \ (I_{\ell m} - U_{\ell m} \ O_{\ell m}) \ , \tag{A52}$$

where $C_{\ell m}$ has absorbed all the constants and $U_{\ell m}$ is the $\exp(2i\delta_\ell)$ phase shift factor.

Again, the general solution of the wave equation is the sum of the incident plane wave and the scattered wave so that Eq. (A52) can be written slightly differently, viz.

$$\psi = \psi_{inc} + \psi_{sc}$$

$$= \sum_{\ell,m} C_{\ell m}(I_{\ell m} - O_{\ell m}) + \sum_{\ell,m} C_{\ell m}(1 - U_{\ell m})\, O_{\ell m}$$

$$= i\pi^{\frac{1}{2}}k^{-1} \sum_{\ell} (2\ell+1)^{\frac{1}{2}} (I_{\ell o} - O_{\ell o}) + f(\theta)\, \exp(ikr)/r \;, \qquad \text{(A53)}$$

and it becomes evident that

$$C_{\ell m} = C_{\ell o} = [i\pi^{\frac{1}{2}}(2\ell+1)^{\frac{1}{2}}]/k \qquad\qquad m = 0$$

$$C_{\ell m} = 0 \qquad\qquad m \neq 0 \;;$$

that is, there is no component of the orbital angular momentum in the direction of the beam, and

$$\psi = \sum_{\ell} C_{\ell o}(I_{\ell o} - O_{\ell o}) + \sum_{\ell} C_{\ell o}(1 - U_{\ell o})\, O_{\ell o}$$

$$= \sum_{\ell} i\pi^{\frac{1}{2}}k^{-1}(2\ell+1)^{\frac{1}{2}} (I_{\ell o} - O_{\ell o}) + f(\theta)\, \exp(ikr)/r \;.$$

Thus,

$$f(\theta) = \sum_{\ell=0}^{\infty} \frac{i\pi^{\frac{1}{2}}(2\ell+1)^{\frac{1}{2}}}{k}\, i^{\ell}\, e^{-i\ell\pi/2}\, P_\ell(\cos\theta)\sqrt{\frac{2\ell+1}{4\pi}}\,(1-U_{\ell o}) \;,$$

$$\boxed{f(\theta) = \tfrac{1}{2} i k^{-1} \sum_{\ell} (2\ell+1)(1-U_{\ell o})\, P_\ell(\cos\theta)} \;, \qquad \text{(A54)}$$

and

$$\sigma(\theta) = |f(\theta)|^2$$

as before.

Comparison of forms (A54) and (A46) for $f(\theta)$ confirm again that

$$\boxed{U_{\ell o} = \exp(2i\delta_\ell)} \;.$$

<u>Arctan $Q_\ell = \delta_\ell$</u>

It is very important at this point to note that if one defines a quantity

$$iQ_\ell = (U_{\ell o} - 1)(U_{\ell o} + 1)^{-1} \;, \qquad \text{(A55)}$$

then

$$Q_\ell = \frac{(U_\ell - 1)}{i(U_\ell + 1)} = \frac{\exp(2i\delta_\ell)-1}{i\exp(2i\delta_\ell)+i} = \tan\delta_\ell \;,$$

and the phase shifts are

$$\boxed{\delta_\ell = \arctan Q_\ell} \qquad \text{(A56)}$$

Extension to Include Spin Dependence

If it is assumed that spin dependent scattering can be approximated by a potential containing spin-orbit and spin-spin interaction terms (Wu 62), namely,

$$V_T \equiv TV_T(r) \equiv \left[\frac{3(\vec{\sigma}_1 \cdot \vec{r})(\vec{\sigma}_2 \cdot \vec{r})}{r^2} - \vec{\sigma}_1 \cdot \vec{\sigma}_2\right] V_T(r) \tag{A57}$$

and

$$V_{LS} = (\vec{\ell} \cdot \vec{S})\ V_{\ell S}(r)\ , \tag{A58}$$

where

$$\vec{r} = \vec{r}_2 - \vec{r}_1 \qquad r = |\vec{r}_2 - \vec{r}_1|$$

$$\vec{\ell} = [\vec{r} \times \vec{p}] \qquad \vec{S} = \tfrac{1}{2}(\vec{\sigma}_1 + \vec{\sigma}_2)$$

$$\vec{p}_{c.m.} = M_1 M_2(\vec{p}_1 + \vec{p}_2)/M^2\ ,$$

and $\vec{\sigma}_1$, $\vec{\sigma}_2$ are the vector spin matrix operators for the two interacting particles, then the wave equation becomes

$$[\nabla^2 + k^2 - W(r,\sigma)]\ \psi_\ell(\vec{r},\vec{\sigma}) = 0$$

where

$$W(r,\sigma) = U_c(r) + TU_T(r) + (\vec{\ell} \cdot \vec{S})\ U_{\ell S}(r)$$

and

$$U(r) = (2m/\hbar^2)\ V(r)\ .$$

The wave function must now depend upon the spins of the interacting particles and can be written

$$\boxed{\psi(\vec{r},\vec{\sigma}) \equiv \psi(r,\theta,\phi)\ {}^{2S+1}\chi^{s}} \quad , \tag{A59}$$

where $\psi(r,\theta,\phi)$ is the spin independent wave function for the interaction and ${}^{2S+1}\chi^{s}$ is a matrix representing the spin part of the wave function.

$2S+1$ = multiplicity of the level,

$S = (\frac{1}{2})\ |(\vec{\sigma}_1 + \vec{\sigma}_2)| = |\vec{S}_1 + \vec{S}_2|$,

s = z component of spin angular momentum = $s_1 + s_2$,

and ℓ is no longer conserved in the interaction, but $J = |\vec{\ell} + \vec{S}|$, the total angular momentum, is conserved. Parity (symmetry or antisymmetry of the wave function) = $(-1)^{\ell}$ is also conserved; hence, it is now possible for mixing to occur between various possible ℓ and S states as long as J and parity are conserved. This restricts mixing to that between states for which the ℓ values differ by 0 or an even integer.

If for spin $\frac{1}{2}$, spin $\frac{1}{2}$ scattering the following possible spin functions are assumed:

$$\begin{aligned}
{}^{1}\chi^{0} &= \frac{1}{\sqrt{2}}\left[\binom{1}{0}_1 \binom{0}{1}_2 - \binom{1}{0}_2 \binom{0}{1}_1\right] \\
{}^{3}\chi^{1} &= \binom{1}{0}_1 \binom{1}{0}_2 \\
{}^{3}\chi^{0} &= \frac{1}{\sqrt{2}}\left[\binom{1}{0}_1 \binom{0}{1}_2 + \binom{1}{0}_2 \binom{0}{1}_1\right] \\
{}^{3}\chi^{-1} &= \binom{0}{1}_1 \binom{0}{1}_2 \ ,
\end{aligned} \tag{A60}$$

where $\binom{1}{0}_a$ and $\binom{0}{1}_a$ represent spin-up and spin-down, respectively, for particle a, then it is readily verified (Sc 55) that for the Pauli spin matrices

$$\sigma_x = \begin{pmatrix} 0 & 1 \\ 1 & 0 \end{pmatrix} , \qquad \sigma_y = \begin{pmatrix} 0 & -i \\ i & 0 \end{pmatrix} ,$$

$$\sigma_z = \begin{pmatrix} 1 & 0 \\ 0 & -1 \end{pmatrix} , \qquad \vec{\sigma} \cdot \vec{\sigma} = 3\begin{pmatrix} 1 & 0 \\ 0 & 1 \end{pmatrix} ,$$

and spin momentum vector components defined as follows

$$M_{si} = (\tfrac{1}{2})\hbar\sigma_i \qquad |M_s|^2 = (\tfrac{1}{4})\hbar^2(\vec{\sigma} \cdot \vec{\sigma}) ,$$

then $\begin{pmatrix} 1 \\ 0 \end{pmatrix}$ and $\begin{pmatrix} 0 \\ 1 \end{pmatrix}$ are eigenvectors of M_{sz} and $|M_s|^2$ with eigenvalues $\pm\hbar/2$ and $3\hbar^2/4$, respectively. Also the ${}^{2S+1}\chi^s$ functions are orthonormal and eigenfunctions of M_{sz} and $|M_s|^2$.

For the orthonormal spin functions defined in (A60) the total wave function is written

$$\psi(\vec{r},\vec{\sigma}) = \sum_{J\geq|M|}^{\infty} \sum_{\ell=J-1}^{J+1} A_{J\ell}\, \psi_\ell(r)\, F_{JM\ell}(\theta,\phi,\vec{\sigma}) , \tag{A61}$$

where

$$F_{JM\ell}(\theta,\phi,\vec{\sigma}) = \sum_m G_m^{JM\ell}\, Y_{\ell m}(\theta,\phi)\, {}^{2S+1}\chi^s , \tag{A62}$$

M = z component of J,

m = z component of ℓ,

s = z component of S,

and $G_m^{JM\ell}$, the Clebsch-Gordon coefficients, are worked out by Condon and Shortley (Co 63) and given in Table AI.

$\psi_\ell(r)$ satisfies the following equations (Wu 62):

for L = J

$$\frac{d^2\psi_\ell(r)}{dr^2} + \frac{2}{r}\frac{d\psi_\ell(r)}{dr} + [k^2 - \frac{\ell(\ell+1)}{r^2} + U_c(r) + 2U_T(r) - U_{\ell S}(r)]\psi_\ell(r)$$

$$= 0; \tag{A63}$$

for L = J-1

$$\frac{d^2u_\ell(r)}{dr^2} + \frac{2}{r}\frac{du_\ell(r)}{dr} + [k^2 - \frac{\ell(\ell+1)}{r^2} + U_c(r) = \frac{2\ell}{2\ell+3} U_T(r)$$

$$+ \ell U_{\ell S}(r)]\ u_\ell(r) = -6\ \frac{\sqrt{(\ell+1)(\ell+2)}}{2\ell+3} U_T(r)\ W_{\ell+2}(r)\ ; \tag{A64}$$

and for L = J+1

$$\frac{d^2W_\ell(r)}{dr^2} + \frac{2}{r}\frac{dW_\ell(r)}{dr} + [k^2 - \frac{\ell(\ell+1)}{r^2} + U_c(r) - \frac{2\ell+2}{2\ell-1} U_T(r)$$

$$- (\ell+1)\ U_{\ell S}(r)]\ W_\ell(r) = -6\ \frac{\sqrt{\ell(\ell-1)}}{2\ell-1} U_T(r)\ u_{\ell-2}(r)\ ; \tag{A65}$$

where

$$u_\ell(r) \equiv \psi_{\ell=J-1}(r)\ , \qquad W_\ell(r) = \psi_{\ell=J+1}(r)\ ,$$

and $U(r) = (2m/\hbar^2)\ V(r)$.

The expressions (A63-A65) for $\psi_\ell(r)$ are obtained by separating the new general wave equation

$$\boxed{[\nabla^2 + k^2 - W(r,\sigma)]\ \psi_\ell(\vec{r},\vec{\sigma}) = 0} \tag{A66}$$

TABLE AI

Clebsch-Gordon Coefficients for Spin ½, Spin ½ Interactions

J =	s = 1	s = 0	s = -1
$\ell+1$	$\sqrt{\frac{(\ell+M)(\ell+M+1)}{(2\ell+1)(2\ell+2)}}$	$\sqrt{\frac{(\ell-M+1)(\ell+M+1)}{(2\ell+1)(\ell+1)}}$	$\sqrt{\frac{(\ell-M)(\ell-M+1)}{(2\ell+1)(2\ell+2)}}$
ℓ	$-\sqrt{\frac{(\ell+M)(\ell-M+1)}{2\ell(\ell+1)}}$	$\frac{M}{\sqrt{\ell(\ell+1)}}$	$\sqrt{\frac{(\ell-M)(\ell+M+1)}{2\ell(\ell+1)}}$
$\ell-1$	$\sqrt{\frac{(\ell-M)(\ell-M+1)}{2\ell(2\ell+1)}}$	$-\sqrt{\frac{(\ell-M)(\ell+M)}{\ell(2\ell+1)}}$	$\sqrt{\frac{(\ell+M+1)(\ell+M)}{2\ell(2\ell+1)}}$

where

$$\boxed{W(r,\sigma) = U_c(r) + TU_T(r) + (\vec{\ell}\cdot\vec{S})\, U_{\ell S}(r)} \quad . \tag{A67}$$

Solution of the J = ℓ equation follows exactly as the solution of the radial equation in Section III of this appendix, and one obtains for large r

$$\psi_\ell(r) = A_\ell (kr)^{-1} \sin[kr - (\ell\pi/2) + \delta_\ell] \ . \tag{A68}$$

Solutions for $\psi_\ell(r)$ when $\ell = J - 1$ and $\ell = J + 1$ are somewhat more complicated because the radial wave equations (A64) and (A65) are coupled. Let these radial wave functions be written as the sum of incoming and outgoing waves: for

$\ell = J - 1$

$$u_{J-1}(r) = A_1(kr)^{-1}\exp[-i(kr-\tfrac{1}{2}[J-1]\pi)]-B_1(kr)^{-1}\exp[i(kr-\tfrac{1}{2}[J-1]\pi)] ,$$

and for

$$\ell = J + 1$$

$$W_{J+1}(r) = A_2(kr)^{-1}\exp[-i(kr-\tfrac{1}{2}[J+1]\pi)]-B_2(kr)^{-1}\exp[i(kr-\tfrac{1}{2}[J+1]\pi)] ,$$

so that the wave function with total angular momentum J and parity $(-1)^{J+1}$ is

$$\psi(\vec{r},\vec{\sigma}) = u_{J-1}(r)\; F_{J,M,J-1}(\theta,\phi,\vec{\sigma}) + W_{J+1}(r)\; F_{J,M,J+1}(\theta,\phi,\vec{\sigma}) .$$

Observe how this fits Eq. (A52) now generalized to matrix form

$$\boxed{\psi = \sum_c C_c(I_c - \sum_{c'} U_{c'c}\, O_{c'})} \quad , \tag{A69}$$

if

$$I_{\ell mJM} = [i^{\ell} e^{-i(kr-\ell\pi/2)}\; G_m^{JM\ell}\; Y_{\ell m}(\theta,\phi)\; {}^{2S+1}\chi^{s}]/r , \tag{A70}$$

and

$$O_{\ell mJM} = [i^{\ell} e^{i(kr-\ell\pi/2)}\; G_m^{JM\ell}\; Y_{\ell m}(\theta,\phi)\; {}^{2S+1}\chi^{s}]/r . \tag{A71}$$

U is the "collision matrix" defined by the coefficients

$$B_1 = U_{11}\, A_1 + U_{12}\, A_2$$

$$B_2 = U_{21}\, A_1 + U_{22}\, A_2 ;$$

i.e., $$B = UA ,$$
$$C_c = A_c/ki^{\ell} ,$$

and c,c' represent incoming (ℓmJM) and outgoing (ℓ'm'J'M') channels, respectively.

If no mixing of states occurs, the U matrix is diagonal $U_{12} = U_{21} = 0$ and, as in the simple case, $U_{11} = \exp(2i\delta_1)$, $U_{22} = \exp(2i\delta_2)$ and the phase shifts are related to a Q matrix; $\delta_1 = \arctan Q_{11}$, $\delta_2 = \arctan Q_{22}$, where Eq. (A55) is now a matrix equation

$$iQ = (U-1)\ (U+1)^{-1} . \tag{A72}$$

At this point the phase shifts may be generalized and defined in analogy with the diagonal case as the arctangents of the elements of the Q matrix, so that $\delta_{ij} \equiv \arctan Q_{ij}$.* Of course, in cases where the channel spin is greater than 1 the U matrix will mix more than two states and will not appear as a 2×2 matrix for a given possible combination of incoming and outgoing states. However, for the S = 1 case parity and J conservation allows mixing only between $\ell = J-1$ and $\ell = J+1$ states. It can be shown from density conservation and time-reversal properties that U is unitary and symmetric (Pr 62). These conditions eliminate any ambiguity in the definition of Q (hence δ) in Eq. (A72).

---

*For charged particle scattering Dodder's energy independent phase shift analysis code (Do 69) defines $K_{ij} = \arctan Q_{ij}$, $\delta_{ij} = K_{ij} - \frac{1}{2}\phi_\ell \delta(i,j)$ where $\delta(i,j)$ is the delta function, $\phi_o = 0$, $\phi_\ell = \phi_{\ell-1} + 2 \arctan(\eta/\ell)$, and $\eta = 0.1574 Z_1 Z_2 \sqrt{M_1(\text{amu})/E_1(\text{MeV})}$.

<u>Summary</u>. Spin ½, spin ½ scattering can be described by a collision matrix U which is unitary and symmetric and mixes combinations of ℓ = J-1 and ℓ = J+1 states. The wave function is described by the matrix equation

$$\boxed{\psi(\vec{r},\vec{\sigma}) = \sum_c C_c(I_c - \sum_{c'} U_{c'c}\, O_{c'})} \quad ,$$

where c and c' represent incoming and outgoing states, respectively, and

$$I_c = I_{\ell mJM} = [i^{\ell} e^{-i(kr-\ell\pi/2)}\, G_m^{JM\ell}\, Y_{\ell m}(\theta,\phi)\; {}^{2S+1}\chi^{s}]/r \; ,$$

$$O_c = O_{\ell mJM} = [i^{\ell} e^{i(kr-\ell\pi/2)}\, G_m^{JM\ell}\, Y_{\ell m}(\theta,\phi)\; {}^{2S+1}\chi^{s}]/r \; .$$

The phase shifts δ_{ij} are defined in analogy with the case in which U is diagonal and no mixing of states occurs; i.e.,

$$\boxed{\delta_{ij} = \arctan Q_{ij}} \quad ,$$

where

$$Q \equiv (1/i)\,(U-1)\,(U+1)^{-1} \; .$$

Consequently, for a given set of states (ℓ,m,J,M) and (ℓ',m',J',M') a set of phase shifts is related via the scattering matrix, the wave functions, and the wave equation to the postulated scattering potentials. It now remains to relate the phase shifts or equivalently the elements of the collision matrix to the measurable cross sections and the polarizations.

Cross Section in Terms of the U Matrix

Again the incident beam is represented by an incident plane wave except that now all spin combinations are possible, and as in (A51)

$$\psi_{in}(\vec{r},\vec{\sigma}) = \exp(ikz)\ {}^{2S+1}\chi^{s}$$

$$= i\pi^{\frac{1}{2}}(k^{-1}) \sum_{\ell=0}^{\infty} (2\ell+1)^{\frac{1}{2}} (I_{\ell oJM} - O_{\ell oJM}) \ . \tag{A73}$$

The total wave function can be written

$$\psi(\vec{r},\vec{\sigma}) = \psi_{in}(\vec{r},\vec{\sigma}) + \psi_{sc}(\vec{r},\vec{\sigma}) = \sum_{c} C_c (I_c - \sum_{c'} U_{c'c} O_{c'})$$

$$= \sum_{c} C_c (I_c - O_c) + \sum_{c} C_c (O_c - \sum_{c'} U_{c'c} O_{c'}) \ , \tag{A74}$$

so that again

$$C_c = C_{\ell oJM} = i\pi^{\frac{1}{2}} k^{-1} (2\ell+1)^{\frac{1}{2}} \qquad m = 0$$

$$C_c = 0 \qquad m \neq 0 \ ,$$

and

$$\psi(\vec{r},\vec{\sigma}) = \psi_{in}(\vec{r},\vec{\sigma}) + \sum_{\ell oJM} C_{\ell oJM} (O_{\ell oJM} - \sum_{c'} U_{c',\ell oJM}\, O_{c'})$$

$$= \psi_{in}(\vec{r},\vec{\sigma}) + f(\theta,\vec{\sigma}) \exp(ikr)/r \ . \tag{A75}$$

Therefore,

$$f(\theta,\phi,\vec{\sigma})(e^{ikr})/r = \sum_{\ell oJM} C_{\ell oJM}(O_{\ell oJM} - \sum_{c'} U_{c',\ell oJM}\, O_{c'})$$

$$= \sum_{\ell oJM} \frac{i\pi^{\frac{1}{2}}}{k} (2\ell+1)^{\frac{1}{2}} \Big[i^{\ell} \exp(ikr)\ \exp(-\ell\pi/2)\ G_o^{JM\ell} (\frac{2\ell+1}{4\pi})^{\frac{1}{2}}\ P_\ell(\cos\theta)$$

$$\cdot\ {}^{2S+1}\chi^{s}/r - \sum_{\ell' m' J' M'} U_{\ell' m' J' M',\ell oJM} (i^{\ell'} \exp(ikr)\ \exp(-\ell'\pi/2)\ G_{m'}^{J'M'\ell'}$$

$$\cdot\ Y_{\ell' m'}(\theta',\phi')\ {}^{2S'+1}\chi^{s'}/r) \Big]$$

$$\boxed{f(\theta,\phi,\vec{\sigma}) = \frac{i\pi^{\frac{1}{2}}}{k} \sum_{LJM,L'JM'} (2\ell+1)^{\frac{1}{2}} \Big[(\frac{2\ell+1}{4\pi})^{\frac{1}{2}}\ G_o^{JM\ell}\ P_\ell(\cos\theta)\ {}^{2S+1}\chi^{s} - U_{\ell' m' J' M',\ell oJM}\ G_{m'}^{J'M'\ell'}\ Y_{\ell' m'}(\theta',\phi')\ {}^{2S'+1}\chi^{s'} \Big]} \cdot \quad (A76)$$

The summation over m' has been dropped since ℓ, ℓ', J, M' are sufficient to determine m', and $J = J'$.

Also

$$\sigma(\theta,\phi) = |f(\theta,\phi,\vec{\sigma})|^2 , \qquad (A77)$$

and the spin matrices drop out of the differential cross section since the ${}^{2S+1}\chi^{s}$ are orthonormal functions. This should not be interpreted to mean, however, that the cross section is independent of spin since the scattering matrix U is implicitly spin dependent.

Appearance of U for the $T(\vec{n},\hat{n})T$ Experiment

Before deriving an expression for the polarization in terms of the scattering matrix or phase shifts, it will be instructive to examine the form of the collision matrix, U, for the $T(\vec{n},\hat{n})T$ experiment. One must, first of all, decide what is the maximum value of $\ell = \ell_{max}$ to be considered.

It would be expected classically that $\ell_{max} = |\vec{r}_{max} \times \vec{p}|$ where $\vec{p}$ = momentum of the neutron and r_{max} = distance of approach at which the nuclear potentials just begin to interact. A good guess for r_{max} is the sum of neutron and triton radii. Using $r = 1.4\ A^{1/3}$ fm one obtains $r_{max} \approx 3.4$ fm. For 22.1-MeV neutrons $p_{neut} \approx 10.9 \times 10^{-15}$ gm-cm/sec, and $|\vec{r}_{max} \times \vec{p}| \approx 3.5\ \hbar$.

According to this analysis $\ell_{max} = 3$ is the largest quantum mechanical orbital angular momentum for which interaction would be expected. Use of $\ell_{max} = 3$ will allow comparison with previous p-^{3}He phase shifts at 19.5 MeV (Ti 68), the only existing data with which one can reasonably compare the $T(\vec{n},\hat{n})T$ results of this experiment. Many more measurements are needed before a unique set of phase shifts which satisfies the data of the present experiment can be found (see the chapter on Results).

For $\ell_{max} = 3$ the non-zero elements U_{ij} of the collision matrix which satisfy conservation of total angular momentum J and parity $(-1)^{\ell}$ are given in Table AII. The order of elements in the matrix was arbitrarily chosen to begin with the initial states with greatest multiplicity, smallest ℓ, and largest J. Any other order maintaining a proper 2 by 2 matrix relationship between mixed states would be equally satisfactory. The importance of assigning ij position indices is in identifying the initial and final states in Table AII with the corresponding phase shifts in Table VII, Chapter V. Half of the non-zero, off-diagonal elements are missing from the tables, since $U_{ij} = U_{ji}$.

V. POLARIZATION

Definition of P(θ)

To relate the polarization to the quantities derived in Section IV, it will be useful to return to Eqs. (A75) and (A76) for the total wave function and scattering amplitude and redefine

$$\boxed{f(\theta,\phi,\vec{\sigma}) = \sum_{s'} f_{ss'}(\theta,\phi)\ {}^{2S'+1}\chi^{s'}} \quad , \tag{A78}$$

so that

$$\psi(r,\theta,\vec{\sigma}) = \psi_{inc}+\psi_{sc} = \exp(ikz)\ {}^{2S+1}\chi^{s}+\exp(ikr)\sum_{s'} f_{ss'}\ {}^{2S'+1}\chi^{s'}/r, \tag{A79}$$

where in Eqs. (A76) and (A77) the sum over JM' for given ℓ,ℓ' is equivalent to a summation over spin states S's'. One representation of a matrix for the spin ½, spin ½ scattering amplitude is (Mo 65)

TABLE AII

Non-Zero U Matrix Elements for Spin ½, Spin ½ Scattering and $\ell_{max} = 3$.

		Initial State				Final State			
i	j	S	ℓ	J	$^{2S+1}\ell_J$	S'	ℓ'	J'	$^{2S'+1}\ell'_{J'}$
1	1	1	0	1	$^3S_1$	1	0	1	$^3S_1$
1	7	1	0	1	$^3S_1$	1	2	1	$^3D_1$
2	2	1	1	2	$^3P_2$	1	1	2	$^3P_2$
2	10	1	1	2	$^3P_2$	1	3	2	$^3F_2$
3	3	1	1	1	$^3P_1$	1	1	1	$^3P_1$
3	12	1	1	1	$^3P_1$	0	1	1	$^1P_1$
4	4	1	1	0	^3P_o	1	1	0	^3P_o
5	5	1	2	3	$^3D_3$	1	2	3	$^3D_3$
6	6	1	2	2	$^3D_2$	1	2	2	$^3D_2$
6	13	1	2	2	$^3D_2$	0	2	2	$^1D_2$
7	7	1	2	1	$^3D_1$	1	2	1	$^3D_1$
8	8	1	3	4	$^3F_4$	1	3	4	$^3F_4$
9	9	1	3	3	$^3F_3$	1	3	3	$^3F_3$
9	14	1	3	3	$^3F_3$	0	3	3	$^1F_3$
10	10	1	3	2	$^3F_2$	1	3	2	$^3F_2$
11	11	0	0	0	^1S_o	0	0	0	^1S_o
12	12	0	1	1	$^1P_1$	0	1	1	$^1P_1$
13	13	0	2	2	$^1D_2$	0	2	2	$^1D_2$
14	14	0	3	3	$^1F_3$	0	3	3	$^1F_3$

$$f(\theta,\phi) = \frac{1}{2}\begin{vmatrix} 2f_{11} & \sqrt{2}f_{10} & \sqrt{2}f_{10} & 2f_{1-1} \\ \sqrt{2}f_{01} & f_{00}+f_s & f_{00}-f_s & \sqrt{2}f_{0-1} \\ \sqrt{2}f_{01} & f_{00}-f_s & f_{00}+f_s & \sqrt{2}f_{0-1} \\ 2f_{-11} & \sqrt{2}f_{-10} & \sqrt{2}f_{-10} & 2f_{-1-1} \end{vmatrix} \tag{A80}$$

f_s is the element for singlet scattering; i.e., S = 0, s = 0. Otherwise, f_{ij} is an element which scatters an incident s = i state to an outgoing s' = j state. The $f(\theta,\phi)$ matrix (A80) multiplied by the column vector

$$\chi = \begin{vmatrix} {}^1\chi^0 \\ {}^3\chi^1 \\ {}^3\chi^0 \\ {}^3\chi^{-1} \end{vmatrix} \tag{A81}$$

is one form of Eq. (A78) and is related to the U matrix via Eq. (A76).

Using this scattering amplitude matrix and the density matrix $\rho = \psi\psi^\dagger$ Mott and Massey (Mo 65) obtain the expressions

$$\sigma(\theta) = \tfrac{1}{4}\ \mathrm{tr}\ ff^\dagger \tag{A82}$$

and

$$\vec{P}(\theta) = \tfrac{1}{4}\ \mathrm{tr}\ (ff^\dagger\vec{\sigma})/\sigma(\theta) \tag{A83}$$

for the differential cross section and the polarization, respectively.

Note that for this particular case there are 10 independent terms in the scattering amplitude array, any or all of which can be complex. Hence, one must measure more than one vector polarization and scalar cross section to determine the scattering amplitude matrix. Some of the measurable quantities are

the differential cross section $\sigma(\theta,\phi)$,

the polarization of the incident particle $\vec{P}_n$,

the polarization of the scatterer $\vec{P}_T$, and

the spin correlation parameters C_{NN} and C_{KP} where N, K, P represent any of the orthogonal direction coordinates x, y, z.

These parameters along with other parameters A (triple scattering parameters), D (depolarization), and R(rotation) are explained diagramatically in Fig. (A3). A, D, R, and the C's are measured in triple scattering or polarized beam and target experiments which will not be discussed here, but which are treated by (Wo 54, Wo 56) and (Wu 62) Section J.

Analyzing power P_A is the quality of a second scatterer to analyze a polarized beam and is equivalent for elastic scattering to the polarization which would be produced by scattering an unpolarized beam from the analyzer.

A somewhat less elegant approximation may clarify the physical meaning of polarization, $P(\theta)$. If there were no spin interactions one would expect an equal probability of all equal incident and scattered states. That is, $\sigma(\theta,\phi)$ would be

$$I(\theta) = |f_s|^2 + |f_{11}|^2 + |f_{00}|^2 + |f_{-1-1}|^2 \quad . \tag{A84}$$

or

$$\boxed{I(\theta) = \sum_i |f_{ii}|^2} \quad .$$

Figure (A3). P, A, R, D, C Parameters Defined.

P = polarization — D = depolarization parameter

A = triple scattering parameter — C = spin correlation parameter

R = rotation parameter

defined in terms of incident polarization P_o, analyzer and scatterer polarizations P_A and P_S, and the number of particles scattered Up (U), Down (D), Left (L), and Right (R) with and without the presence of a spin-precessing magnetic field H. (Figure borrowed from John C. Hopkins, LASL.)

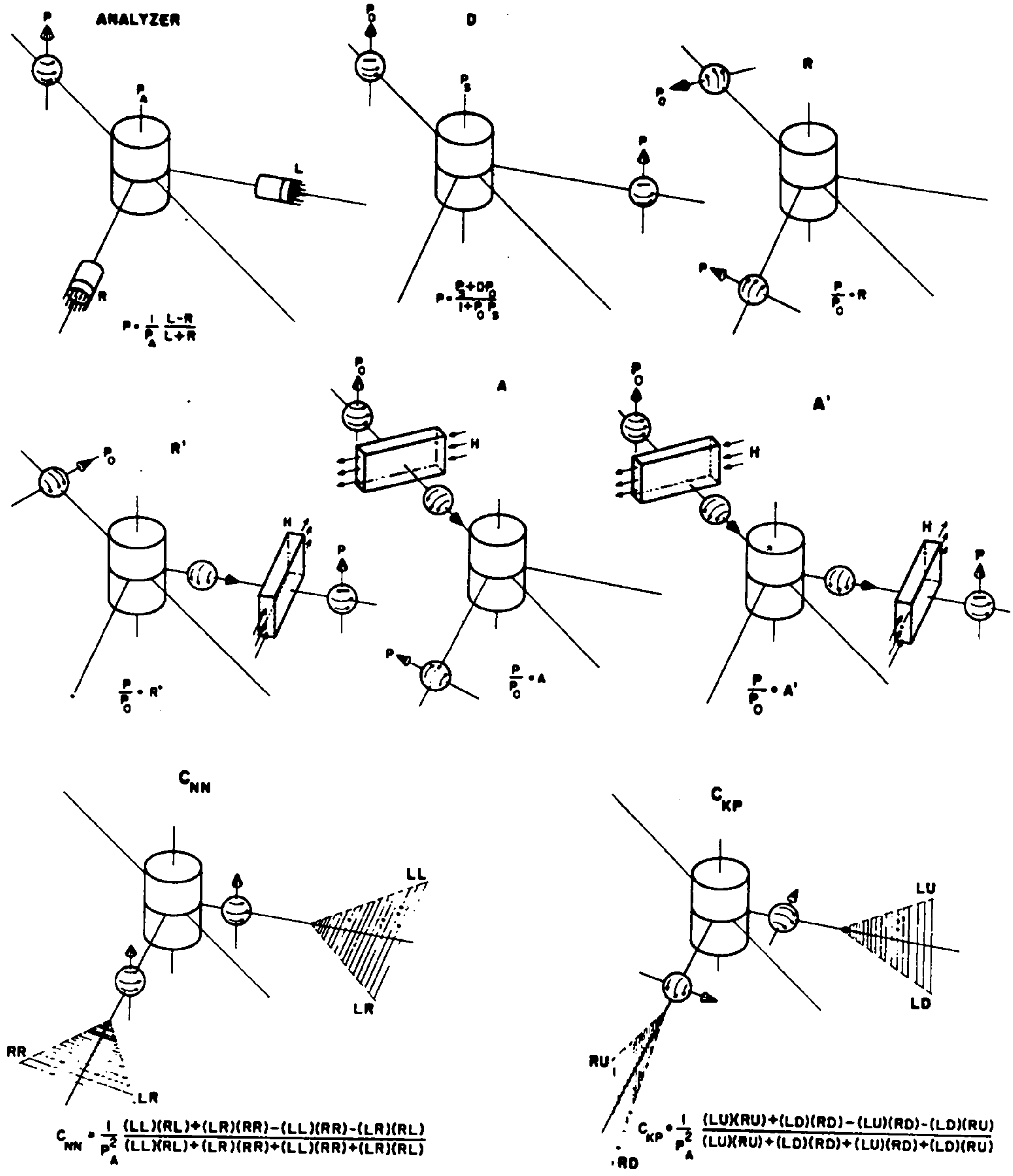

ANALYZER
D
R
R'
A
A'
C_{NN}
C_{KP}
L
R
H
LL
LR
RR
LU
LD
RU
RD
$P = \frac{1}{P_A}\frac{L-R}{L+R}$
$P = \frac{P_S + DP_O}{1 + P_O P_S}$
$\frac{P}{P_O} = R$
$\frac{P}{P_O} = R'$
$\frac{P}{P_O} = A$
$\frac{P}{P_O} = A'$
$C_{NN} = \frac{1}{P_A^2}\frac{(LL)(RL)+(LR)(RR)-(LL)(RR)-(LR)(RL)}{(LL)(RL)+(LR)(RR)+(LL)(RR)+(LR)(RL)}$
$C_{KP} = \frac{1}{P_A^2}\frac{(LU)(RU)+(LD)(RD)-(LU)(RD)-(LD)(RU)}{(LU)(RU)+(LD)(RD)+(LU)(RD)+(LD)(RU)}$

However, spin interactions do occur and account is taken of this by writing the cross section as a sum of spin independent and spin dependent terms,

$$\boxed{\sigma(\theta,\phi) = I(\theta)\,[1 + P\,\hat{\eta}\cdot\hat{\sigma}]} \quad , \tag{A85}$$

where P is a number of magnitude less than 1 yet to be defined. $\hat{\eta} = (\vec{k}\times\vec{k}')/(k^2\sin\theta)$ for elastic scattering, and $\vec{k},\vec{k}'$ are the wave vectors for the incident and scattered waves, respectively; thus, $\hat{\eta}$ is a unit vector normal to the plane of scattering. $\hat{\sigma}$ is a unit vector in the direction of the channel spin $\vec{S} = \vec{S}_1 + \vec{S}_2 = \tfrac{1}{2}(\vec{\sigma}_1 + \vec{\sigma}_2)$, $\hat{\sigma} = (\vec{\sigma}_1 + \vec{\sigma}_2)/|\vec{\sigma}_1 + \vec{\sigma}_2|$.

Now define a vector $\vec{P} = P\hat{\sigma}$ so that

$$\sigma(\theta,\phi) = I(\theta)\,[1 + P\cos\phi] \quad , \tag{A86}$$

where ϕ is now redefined as the angle between the normal to the scattering plane and the channel spin vector. If Eq. (A77) for the differential cross section can be written

$$\boxed{\sigma(\theta,\phi) = \Big|\sum_{ij} f_{ij}\Big|^2} \quad , \tag{A87}$$

then it follows from Eqs. (A84-86) that

$$P(\theta) = [\sigma(\theta,\phi) - I(\theta)]/[I(\theta)\cos\phi]$$

$$\boxed{P(\theta) = [\Big|\sum_{ij} f_{ij}\Big|^2 - \sum_i |f_{ii}|^2]/(\sum_i |f_{ii}|^2 \cos\phi)} \quad . \tag{A88}$$

One can see the significance of $P(\theta)$ by considering the special case of scattering of nucleons from spinless targets. In this case

$$\psi = \exp(ikz)\ {}^2\chi^s + \exp(ikr) \sum_{s'} f_{ss'}(\theta,\phi)\ {}^2\chi^{s'}/r$$

and $f(\theta,\phi)$ is a 2×2 matrix which can be written as a function of the unit matrix E and the Pauli spin matrices σ_i, $(\vec{\sigma} = \sigma_x\hat{i} + \sigma_y\hat{j} + \sigma_z\hat{k})$,

$$f(\theta,\phi) = g(\theta)\ E + \vec{h}(\theta) \cdot \vec{\sigma}\ . \tag{A89}$$

Assume an incident particle in spin state

$$\chi^c = \binom{a_+}{a_-} = a_+\ {}^2\chi^{\frac{1}{2}} + a_-\ {}^2\chi^{-\frac{1}{2}}\ ,$$

and choose the normal to the scattering plane and the spin direction to be the z axis ($\phi = 0$). Then the scattered wave is

$$\psi_{sc} = \frac{e^{ikr}}{r}\begin{pmatrix} g+h_z & o \\ o & g-h_z \end{pmatrix}\begin{pmatrix} a_+ \\ a_- \end{pmatrix} = \frac{e^{ikr}}{r}\begin{pmatrix} f_c^+(\theta) \\ f_c^-(\theta) \end{pmatrix}\ ,$$

where

$$\begin{aligned} f_c^+(\theta) &= (g + h_z)\ a_+ \\ f_c^-(\theta) &= (g - h_z)\ a_-\ . \end{aligned} \tag{A90}$$

Now

$$\sigma(\theta,\phi) = |f_c^+|^2 + |f_c^-|^2\ ,$$

which for an unpolarized incident beam $|a_{+in}| = |a_{-in}|$ becomes

$$\sigma(\theta,\phi) = |g|^2 + |h_z|^2 + 2\ \mathrm{Re}(gh_z^*)$$

$$= [1 + P(\theta)\cos\phi]\ I(\theta)\ . \tag{A91}$$

$I(\theta)$ = beam intensity = $|a_+|^2 + |a_-|^2$ and from (A91)

$$P(\theta) = [2\ \mathrm{Re}(gh_z^*)]/I(\theta)\ . \tag{A92}$$

By direct multiplication it can be verified that $2\mathrm{Re}(gh_z^*) \equiv |g+h_z|^2 - |g-h_z|^2$. But comparison with Eq. (A90) shows that $|g+h_z|$ and $|g-h_z|$ are the intensities of the a_+ and a_- scattered waves for an unpolarized incident wave. Hence, (A92) becomes

$$\boxed{P(\theta) = (|a_+|^2 - |a_-|^2)/(|a_+|^2 + |a_-|^2) = (N\uparrow - N\downarrow)/(N\uparrow + N\downarrow)}\ , \tag{A93}$$

and is called the polarization of the scattered beam where $N\uparrow$, $N\downarrow$ are the number of particles scattered with spins up and down, respectively.

Of course, for more complex cases of spin-spin and spin-orbit interactions one considers the incident and scattered channel spin $\vec{S} = \vec{S}_1 + \vec{S}_2$ rather than the spin of the incident and scattered particles, and $P(\theta)$ is no longer a simple expression relating spin directions of the scattered particles alone. However, $\vec{P}(\theta)$ still has the direction normal to the plane of the scattering and is still properly a vector polarization function (Mo 65).

Double Scattering

It is clearly difficult to measure the spin direction of a particle. As a consequence, if one is to measure polarization it is necessary to relate it to other measurable quantities. A double scattering affords this possibility.

Assume (Wu 62, Wo 56) an unpolarized beam scattered by a target A and the scattered beam to be scattered again by a second scatterer B. The cross section for the first scattering is

$$\sigma(\theta_A) = I(\theta_A)[1 + P_A(\theta_A)\ \hat{n}_A \cdot \hat{\sigma}_{in}] ,$$

where $\hat{n}_A = (\vec{k}_{in} \times \vec{k}_A)/(k^2 \sin\theta_A)$, $\vec{k}_A$ = the wave vector of the first scattering through the angle θ_A, and $\vec{\sigma}_{in}$ = the spin of the incoming channel.

For the second scattering in the absence of interference terms $\hat{n} = \hat{n}_B = (\vec{k}_A \times \vec{k}_B)/(k^2 \sin\theta_B)$ and the incident channel spin is $\vec{\sigma}_A = P_A\ \hat{n}_A$.

In this case

$$\begin{aligned}\sigma(\theta_A,\theta_B,\phi_{AB}) &= I_A(\theta_A)\ I_B(\theta_B)(1 + P_B\ \hat{n}_B \cdot \vec{\sigma}_A)\\ &= I_A(\theta_A)\ I_B(\theta_B)(1 + P_B\ \hat{n}_B \cdot P_A\ \hat{n}_A)\\ &= I_A(\theta_A)\ I_B(\theta_B)(1 + P_A\ P_B \cos\phi_{AB}) ,\end{aligned} \tag{A94}$$

where ϕ_{AB} = angle between scattering planes. Thus, for double scattering

$$\sigma(\phi=0) = I_1(\theta_1)\ I_2(\theta_2)(1 + P_1\ P_2) ,$$

$$\sigma(\phi=\pi) = I_1(\theta_1)\ I_2(\theta_2)(1 - P_1\ P_2) ,$$

and

$$P_1(\theta_1)\ P_2(\theta_2) = \frac{\sigma(\phi=0) - \sigma(\phi=\pi)}{\sigma(\phi=0) + \sigma(\phi=\pi)} = (L-R)/(L+R) \ ,$$

where L,R are the number of particles scattered to equal left and right angles (θ_2), respectively, in the second scattering. The quantity $P_1P_2 \cos\phi$ is commonly called the asymmetry and designated by the letter e, so that for left-right scattering in the same plane

$$\boxed{e = P_1(\theta_1)\ P_2(\theta_2) = (L-R)/(L+R)} \ . \qquad \text{(A95)}$$

Although the above derivation of Eqs. (A94) and (A95) assumes no interference between incident and scattered waves, the expressions can be shown to be exact (Mo 65).

In the case where a second scattering is used to analyze the polarization of the first scattering $P_2(\theta_2)$ is called analyzing power and designated P_A, which for elastic scattering is the polarization which would be produced by the second scattering alone. In the present experiment, $P_1(\theta_1)$ was assumed known and $P_2(\theta_2)$ was unknown except in the case where $^4He(\vec{n},\hat{n})^4He$ scattering was used to determine the $T(d,\vec{n})^4He$ neutron source polarization.

Another double scattering parameter which is convenient and easily defined is the left-right ratio,

$$r = \frac{\sigma(\phi=0)}{\sigma(\phi=\pi)} = L/R = \frac{1+e}{1-e} \ . \qquad \text{(A96)}$$

In summary the expressions for $P(\theta)$ and e derived in this section relate the easily measured quantities L and R via the scattering amplitudes and wave functions to the spin-spin and spin-orbit interaction potentials just as was done with the differential cross section in Section AIV.

VI. DATA CORRECTION FORMULAE

Artificial Asymmetry Corrections

Libert (Li 66) defines for double scattering the quantities k_o, k, e_m, e_r, μ, and ν as follows:

$$\sigma(\theta_1,\theta_2,\phi_{12}) = k_o I(\theta_1)\ I(\theta_2)[1 + kP_1(\theta_1)\ P_2(\theta_2)\ \cos\phi_{12}] \tag{A97}$$

$$e_m = [e_r + \mu e]/[1 + (1-\nu)\ e] \tag{A98}$$

$$e = P_1(\theta_1)\ P_2(\theta_2)\ \cos\phi_{12}$$

$$e_r = \frac{[I(\theta_1)\ I(\theta_2)_L - I(\theta_1)\ I(\theta_2)_R]}{[I(\theta_1)\ I(\theta_2)_L + I(\theta_1)\ I(\theta_2)_R]}$$

$$\mu = \frac{[k_L I(\theta_1)\ I(\theta_2)_L + k_R I(\theta_1)\ I(\theta_2)_R]}{[I(\theta_1)\ I(\theta_2)_L + I(\theta_1)\ I(\theta_2)_R]} \tag{A99}$$

$$\nu = 1 - \frac{[k_L I(\theta_1)\ I(\theta_2)_L - k_R I(\theta_1)\ I(\theta_2)_R]}{[I(\theta_1)\ I(\theta_2)_L + I(\theta_1)\ I(\theta_2)_R]}\ .$$

The k's are experimental factors of which the ideal value is unity. L and R refer to left and right second scattering, respectively, where the first scattering is assumed to be a left scattering through angle θ_1. e_m is the measured asymmetry. e is the asymmetry one wishes to measure, and it is seen from the definitions (A98) that e_r is an artificial asymmetry measured when either polarization $P_1(\theta_1)$ or $P_2(\theta_2)$ is zero.

From (A97-99) the expression to correct for a measured artificial asymmetry e_r can be derived. If the k's are assumed to be unity then $\mu = 1$, $\nu = 1-e_r$, and

$$e_m = (e_r + e)/(1 + e_r\, e)\ .$$

Consequently,

$$e = (e_m - e_r)/(1 - e_r\, e_m) \qquad \text{(A100)}$$

$$\simeq e_m - e_r$$

for small artificial asymmetry e_r.

Detector Efficiency Correction

To obtain the correction for detector efficiencies, two measurements were made at each angle (θ_2) with detectors interchanged. It is easiest to work the left-right ratio r, which is expressed

$$r_m = r_r\, [1 + k_L \cdot \frac{r-1}{r+1}]/[1 - k_R \cdot \frac{r-1}{r+1}]$$

$$\text{(A101)}$$

$$r_r = I(\theta_1)\, I(\theta_2)_L / I(\theta_1)\, I(\theta_2)_R\ .$$

If it is assumed again that the k's = 1, then $r_m = r_r r$, and for the two measurements $r'_m = r'_r r$ and $r''_m = r''_r r$. The data will be corrected for artificial asymmetries by Eq. (A100) so that $e'_r = e''_r = 0$ or $r'_r r''_r = 1$. Then

$$r^2 = (r'_m/r'_r)(r''_m/r''_r) = r'_m\, r''_m \;, \tag{A102}$$

which is the expression for correcting for detector efficiencies. In terms of asymmetries Eq. (A102) is

$$e = \frac{[(1+e'_m)(1+e''_m)]^{\frac{1}{2}} - [(1-e'_m)(1-e''_m)]^{\frac{1}{2}}}{[(1+e'_m)(1+e''_m)]^{\frac{1}{2}} + [(1-e'_m)(1-e''_m)]^{\frac{1}{2}}} \tag{A103}$$

$$\simeq \tfrac{1}{2}(e'_m + e''_m) \text{ if } e'_m \simeq e''_m \;.$$

Multiple Scattering Corrections

A Monte Carlo multiple scattering computer code developed by W. B. Broste, K. R. Crandall, R. B. Perkins, and J. E. Simmons (Br 69) is used at LASL to calculate multiple scattering corrections for n-^{4}He elastic scattering. The program was adapted to calculate corrections to the n-T polarizations at 22.1-MeV incident neutron energy. The n-^{4}He phase shifts (Ho 66) used in the program yield polarizations which at all angles are within a few percent of the $T(\vec{n},\hat{n})T$ neutron polarizations measured in this experiment. The mean free path was adjusted in the code to be equal to the mean free path of a neutron in the liquid tritium scattering sample, and the resulting corrections were applied to the n-T data.

In Table AIII are listed the multiple scattering correction factors by which each of the $T(\vec{n},\hat{n})T$ neutron polarizations for 22.1-MeV incident neutrons in Table V were multiplied.

TABLE AIII

Multiple Scattering Corrections to the 22.1-MeV n-T Polarization Data

$\theta_2$lab (deg)	Multiply $P_2(\theta_2)$ by
40	1.00±0.01
55	1.00±0.01
70	1.00±0.02
80	1.02±0.03
85	1.02±0.04
90	1.02±0.05
95†	1.00±0.20
100	1.16±0.05
105	1.10±0.05
110¼	1.09±0.03
118½	1.06±0.03

†Zero of polarization where multiplicative correction is undefined.

APPENDIX B

Appendix B describes the computer programs FLZEIT and DSCHNIT which were written for analysis of the data obtained in the experiment. Instructions for using the programs are given, and the codes are listed.

I. PROGRAM FLZEIT

Introduction

FLZEIT (meaning flugzeit = time of flight) is a FORTRAN IV, 512-channel data reduction code with several options. The program calculates 1) the number of counts in Channel I = NET(I), 2) the standard deviation = SD(I), 3) SUM(I) = $\sum_{i=1}^{I}$ NET(i), and 4) SUMVAR(I) = $\sum_{i=1}^{I}$ $(SD(i))^2$ according to the following equations:

NET (Channels 001-256)

$$= NL * (C(1) * FØREGRØUND - C(2) * BACKGRØUND + BKGL) \qquad (B1)$$

NET (Channels 257-512)

$$= NR * (C(3) * FØREGRØUND - C(4) * BACKGRØUND + BKGR)$$

where FØREGRØUND = number of counts in Channel I in the foreground run, BACKGRØUND = number of counts in Channel I for the background run; and NL, NR, C(1), C(2), C(3), C(4), BKGL, and BKGR are normalization constants entered on cards or calculated by the program.

$$SD(I) = [NL^2(C(1)^2 * FØREGRØUND + C(2)^2 * BACKGRØUND + BKGL^2)]^{\frac{1}{2}}, \qquad (B2)$$

and similarly for the right side.

In addition, the program will sum any number of pairs of runs (NUMPR) and calculate NET(I), SD(I), SUM(I), and SUMVAR(I) for the accumulated pairs; i.e.,

$$\mathrm{ACNET(I)} = \left(\sum_{j=1}^{\mathrm{NUMPR}} \mathrm{NET(I)}_{\mathrm{Run}\ j} \right) / \mathrm{NUMPR}$$

$$\mathrm{ACSD(I)} = \left[\sum_{j=1}^{\mathrm{NUMPR}} \left(\mathrm{SD(I)}_{\mathrm{Run}\ j}\right)^2 \right]^{\frac{1}{2}} / \mathrm{NUMPR}$$

$$\mathrm{ACSUM(I)} = \left(\sum_{i=1}^{\mathrm{I}} \mathrm{ACNET(i)} \right) / \mathrm{NUMPR}$$

$$\mathrm{ACSUMVAR(I)} = \left[\sum_{i=1}^{\mathrm{I}} (\mathrm{ACSD(i)})^2 \right] / \mathrm{NUMPR}^2 \ .$$

The program structure includes the main block plus five subroutines, LESEN, UMSATZ, LØCHEN, CEES, and MAHLEN. Subroutine LESEN (= read) reads input data from tape and prints out the run headings directly from the input tape as well as information concerning runs found or called for from tape.

The main block performs the calculations and prints out calculated data.

Subroutine UMSATZ (= translation) records the calculated NET(I) values on an output tape (with appropriate headings).

Subroutine LØCHEN (= punch) punches data on cards.

Subroutine CEES calculates normalizing factors C(1), C(2), C(3), and C(4) from the data if desired.

Subroutine MAHLEN (= draw) plots the data.

To abort recording, punching, or plotting, one need simply replace UMSATZ, LØCHEN, or MAHLEN subroutine decks with

```
SUBRØUTINE UMSATZ        SUBRØUTINE LØCHEN        SUBRØUTINE MAHLEN
321 CØNTINUE             421 CØNTINUE             319 CØNTINUE
                     ,                        , or                     ,
RETURN                   RETURN                   RETURN
END                      END                      END
```

respectively.

Main Program Block

Aside from the input data, which is read from tape by subroutine LESEN, a certain amount of information must be entered on cards as follows:

Data Card I

Field	Format	Name	Explanation
1-6	I6	IDAC	If IBLANK = 0 (see next field) IDAC+1 becomes the first run number in the output (printed and recorded on output tape). Subsequent run numbers are stepped by one. Hence, the IDAC field left blank results in the first run no. = 1.
7-12	I6	IBLANK	IBLANK = 0 (or a blank field) causes data on the output tape to be written from the beginning of a tape with the first run no. = IDAC+1. IBLANK > 0 causes the output tape to be searched for an end of file. The run no. is

Data Card I (cont'd)

Field	Format	Name	Explanation
			stepped beyond the last run written on the tape and new data is added to the old tape.
13-18	I6	INDEX	INDEX = 0 (or a blank field) causes the input data tape to be read in the "new" format. INDEX = 1 causes the tape to be read in the "old" format and L and R normalizing constants (ANØRM) to be set equal. (See Subroutine LESEN for formats.)
19-24	I6	NRERUN	NRERUN tells subprogram LESEN how many runs to search the tape backwards before aborting the search. If this field is left blank NRERUN = 10.

Data Card II

Field	Format	Name	Explanation
1-3	I3	NUMPR	NUMPR = no. of pairs of foreground-background data to be accumulated (see Introduction). NUMPR should not be blank or zero. Two cards read with NUMPR = 0 terminate the job.
4-6	I3	JPLØT	JPLØT = 0 (or a blank field) causes the data to be handled as 1-512 channel array on the printout, tape, and plot. JPLØT = 1 causes the data to be handled as 2-256 channel array on the printout, tape, and plot. For channels

Data Card II (cont'd)

Field	Format	Name	Explanation
			257-512, SUM(I) = SUM(I) - SUM(256), SUMVAR(I) = SUMVAR(I) - SUMVAR(256). Channels 1-256 are labeled "LEFT SIDE," channels 257-512 are "RIGHT SIDE," and reassigned channel nos. 1-256.
7-9	I3	IPLØT	IPLØT = 0 (or blank field) causes a linear-linear plot to be made by MAHLEN. IPLØT = 1 causes a linear-log plot to be made.
10-12	I3	ICHAR1	ICHAR1 = decimal notation for character in which the plotting is done. Some useful values are:

Plot character	Decimal Notation
0 through 9	0 through 9
+	16
-	32
· (dot)	42
*	44
□	63

Field	Format	Name	Explanation
13-15	I3	ICHAR2	ICHAR2 = decimal notation used in plotting negative values in the log plot option. For a log plot the x axis = 10 counts. Values are plotted as follows:

NET(I) > 10 ICHAR1

Data Card II (cont'd)

Field	Format	Name	Explanation
			$-10 \leq NET(I) \leq 10$ on axis
			$NET(I) \leq 10$ plotted as ICHAR2 and
			$NET(I) = \lvert NET(I) \rvert$
16-18	I3	ICØN	ICØN > 0 causes the plotted points to be connected by a line.
19-24	6x		
25-80	5A10 1A6	ACCHEAD	This is the heading for the accumulated runs.

Next 4 × NUMPR Cards

Card	Field	Format	Name	Explanation
1.	1-6	I6	IDFG	IDFG is the identification number of the 1st foreground run to be read from input tape.
	7-12	I6	IDBG	IDBG is the number of the background run to be subtracted from the 1st foreground run. Note: If IDBG $\leq$ 0 no background run will be called for and calculations are made on the foreground run only.
	13-14	2x		
	15	I1	INVC	INVC = 0 (or a blank field) causes C(1) through C(4) (see next two cards) to be used as read in. INVC $\geq$ 1 causes C(1) through C(4) to be replaced by 1/C(1) through 1/C(4) before being used in the program.

Next 4 × NUMPR Cards (cont'd)

Card	Field	Format	Name	Explanation
	16-24	9x		
	25-80	5A10 1A6	PRHEAD	This is the heading for a particular pair of runs.
2.	1-12	12.5	FNØRM(1)	Normalization for channels 1-256 (= NL in Introduction). For a blank field NL = 1.
	13-24	12.5	C(1)	Normalization, see Introduction. If C(1) = -0.0 (i.e., blank field) C's are calculated by subroutine CEES.
	25-36	12.5	C(2)	Normalization, see Introduction.
	37-48	12.5	BKGL	Additive constant, see Introduction.
	49-54	I6	LØWL	Lower and Upper channel Nos. (Left and Right) for calculating C(1), C(2), C(3), C(4) from the data (See subroutine CEES.) If IUPL ≤ 0 (i.e., a blank field) the C's become the normalizing factors BNØRM, CNØRM recorded on the input tape (see subroutine LESEN).
	55-60	I6	IUPL	
	61-66	I6	LØWR	
	67-72	I6	IUPR	
3.	1-12	12.5	FNØRM(2)	Normalization for Channels 257-512 (- Nr in Introduction).
	13-24	12.5	C(3)	Normalization, see Introduction.
	25-36	12.5	C(4)	Normalization, see Introduction.
	37-48	12.5	BKGR	Normalization, see Introduction.

Next 4 × NUMPR Cards (cont'd)

Card	Field	Format	Name	Explanation
	49-54	I6	LØCHL1	
	55-60	I6	LØCHL2	Lower (1) and Upper (2) Channel Nos. Left
	61-66	I6	LØCHR1	(L) and Right (R) for cards to be punched.
	67-72	I6	LØCHR2	

If LØCHL2 ≤ 0 (i.e., blank) Channels 1-512 are all punched. (See LØCHEN) If JPLØT = 0, LØCHR1 and LØCHR2 are ignored.

RESTRICTIONS:

LØCHL1 ≥ 1 and

LØCHL2 > LØCHL1 (unless LØCHL2 is a blank field)

LØCHR1 ≥ 257

512 ≥ LØCHR2 > LØCHR1

NOTE: If any field on card 3 is left blank, it is assigned the corresponding value on card 2. Thus, a blank card 3 means that channels 1-512 are all normalized by the same constants.

Card	Field	Format	Name	Explanation
4.	1-6	I6	KBND(1)	
	7-12	I6	KBND(7)	
	13-18	I6	KBND(2)	
	19-24	I6	KBND(8)	Used in determining graphing limits (see
	25-30	I6	KBND(3)	subroutine MAHLEN). If this option is not
	31-36	I6	KBND(9)	used a blank card must be inserted.
	37-42	I6	KBND(4)	
	43-48	I6	KBND(10)	
	49-54	I6	KBND(5)	

Next 4 × NUMPR Cards (cont'd)

Card	Field	Format	Name	Explanation
	55-60	I6	KBND(11)	Used in determining graphing limits (see subroutine MAHLEN). If this option is not used a blank card must be inserted.
	61-66	I6	KBND(6)	
	67-72	I6	KBND(12)	

The above cards 1, 2, 3, and 4 are repeated for each run pair; i.e., there should be 4 × NUMPR number of cards following a given NUMPR (Data Card II) card.

As soon as the calculations have been made NUMPR number of times, the program expects to read another NUMPR (Data Card II). Hence, the sequence of cards starting with Data Card II may be repeated as often as desired. A blank NUMPR card and another blank card following it will terminate the job.

Subroutine LESEN

LESEN = read input tape. This subroutine assumes the data is written on the input tape in one of the following formats (the format is chosen by the value of INDEX on Data Card I):

"New" Format

Record 1

J,NRUN,BNØRM,CNØRM, (HEAD(I), I=1,11)

FØRMAT (I1,I4,2(F9.4,2X), 10A10, A8)

Records 2-6

(SCALAR(I), I=1,65)

FØRMAT (13A10, 6X)

Records 7-38

((ADATA(I), I=J,512,128), J=1,128)

FØRMAT (1X,16F8.0)

"Old" Format

Record 1

J,NRUN, BNORM,(HEAD(I), I=1,11)

FØRMAT (I1,I4,F12.4,2X,10A10,A8)

Record 2

(SCALAR(I), I=1,13)

FØRMAT (13A10)

Records 3-34

((ADATA(I), I=J,512,128), J=1,128)

FØRMAT (1X,16F8.0)

where J = index searched for the beginning of a run, NRUN = run no., BNØRM and CNØRM = normalization factors calculated by the scalers during the runs, HEAD = heading put on the runs, SCALAR (1-65) = scalers read in, ADATA(I) = no. of counts in the I^{th} channel.

This subroutine sets following indices:

Index	Value	Cause and Effect
No Back	1	No background was called for, C(2) = 0.0. Foreground only is used in calculations.
No Data	1	Either the requested foreground or the background run was not found on the tape. No calculations

Index	Value	Cause and Effect
		are made and the program looks for a new run pair.
IRERUN	NRERUN	Tape has searched backwards NRERUN runs for a given requested run. If the run is not found, NØDATA is set.
LØRUN	1	The background has been found. Search now only for the foreground.
MØRUN	1	The foreground has been found. Search now only for the background.
NØRUN	0	Neither run has yet been found. Continue the search until they are found or it is apparent that they cannot be found.
	1	One of the runs requested has been found. Continue the search if a background is called for; otherwise return to the main program.
	2	Both runs have been found. Return to the main program.

Subroutine UMSATZ

UMSATZ = write output tape. The output tape is written in the following format:

Record 1.

IDAC, (PRHEAD(I) OR ACCHEAD(I), I=1,6)

FØRMAT (3H101, 3X, I6, 5A10, A6)

where 101 in the first three columns are indices which can be used for searching the tape later.

Record 2.

a. FØRMAT (14X, 10HBOTH SIDES) or

b. FØRMAT (14X, 14HLEFT SIDE ONLY) or

c. FØRMAT (14X, 15HRIGHT SIDE ONLY)

Records 3 through 18 (or 3 through 34 for both sides)

a. ((NET(I) = ADATA(I), I=J, 512,128), J=1,128) or

b. ((NET(I) = ADATA(I), I=J, 256,64), J=1,64) or

c. ((NET(I) = ADATA(I), I=J, 512,64), J=257,320)

FØRMAT (12X, 16F7.0)

UMSATZ resets IBLANK = 0 to avoid researching the output tape for an end of file the next time UMSATZ is called.

Subroutine MAHLEN

MAHLEN = plotting routine. This routing uses plotting subroutines coded by E. M. Willbanks (Wi 68) for the LASL CDC 6600 computers and 4020 plotter. The routine plots according to the values of IPLØT (linear or log) and JPLØT (512 or 256 channels). The maximum scale on the plots is determined by searching the data (ADATA(I)) for the maximum value (DATMAX) and assigning the next highest 10, 100, 500, or 1000 as the upper graph limit. In the case of accumulated data, IACC is set to 1 by the main program and the upper graph limit is calculated from MAXDAT = maximum of DATMAX for all NUMPR runs.

If the data has spikes which may cause regions of interest to be plotted insignificantly close to the axis, these spikes may be skipped by using the KBND option in the data cards. For example, assume the data has insignificant pileup peaks in channels 5, 20 to 30, 256 and 512. Then the maximum values other than spikes are calculated skipping channel 5, channels 20-30, channel 256, and channel 512; and the graph upper bound becomes more meaningful if KBND values are assigned as follows:

KBND(1) 1

KBND(7) 4

Channel 5 is skipped

KBND(2) 6

KBND(8) 19

Channels 20 through 30 are skipped

KBND(3) 31

KBND(9) 255

Channel 256 is skipped

KBND(4) 257

KBND(10) 511

Search for DATMAX ends at channel 511

KBND(5) Blank

KBND(11) Blank

KBND(6) Blank

KBND(12) Blank

Up to six regions may be skipped in this manner for the calculation of DATMAX. If all KBND's are left blank DATMAX is automatically calculated for channels 1 through 512.

Subroutine CEES

C(1), C(2), C(3), and C(4) are calculated from the data in the following manner:

ANØRM(J) = normalization factors recorded on input tape for J=1,4

1) foreground left 2) background left

3) foreground right 4) background right

$$C(1) = AN\emptyset RM(1)$$

$$C(2) = C(1) \times \left[\left(\sum_{I=L\emptyset WL}^{IUPL} NET(I)_{FG} \right) / \left(\sum_{I=L\emptyset WL}^{IUPL} NET(I)_{BG} \right) \right]$$

$$C(3) = AN\emptyset RM(3)$$

$$C(4) = C(3) \times \left[\left(\sum_{I=L\emptyset WR}^{IUPR} NET(I)_{FG} \right) / \left(\sum_{I=L\emptyset WR}^{IUPR} NET(I)_{BG} \right) \right] \qquad (B3)$$

If IUPL $\leq$ 0 (i.e., blank), then C(J) = ANØRM(J) for 1 $\leq$ J $\leq$ 4.

Subroutine LØCHEN

The output is punched on cards in the following format:

NET(I), IDAC

6F 12.2, I6, 2HBØ (for both detectors)

66 (for detector 66)

60 (for detector 60)

for I = LØCHL1 through I = LØCHL2 (detector 66)

and for I = LØCHR1 through I = LØCHR2 (detector 60)

or I = LØCHL1 through I = LØCHL2 (both detectors).

A listing of the program follows.

```
      PROGRAM FLZEIT (INPUT,OUTPUT,TAPE10=INPUT,TAPE9=OUTPUT,FILM,TAPE12
     1=FILM,TAPE37,TAPE53,PUNCH)
      DIMENSION ACNET(512),ACSUM(512),ACSD(512),ACSVAR(512),ACCHEAD(6),
     1FNORM(2),BSD(512)
      COMMON ADATA(512),BDATA(512),NOBACK,NODATA,IDFG,IDBG,JPLOT,C(4),
     1IPLOT,ICHAR1,ICHAR2,ICON,IDAC,IBLANK,ACH(512),PRHEAD(6),ANORM(4),
     2KBND(12),IACC,MAXDAT,ASD(512),SUM(512),SUMVAR(512)
      REAL MAXDAT
  649 READ (10,650) IDAC,IBLANK,INDEX,NRERUN
  650 FORMAT (4I6)
      INDEX=INDEX+1
      IF (NRERUN.LE.0) NRERUN=10
    2 LAST=0
  203 IACC=0
      MAXDAT=0.0
 2030 READ(10,60)NUMPR,JPLOT,IPLOT,ICHAR1,ICHAR2,ICON,(ACCHEAD(I),I=1,6)
   60 FORMAT (6I3,6X,5A10,A6)
      IF (EOF,10) 1999,200
  200 IF (NUMPR.LE.0.AND.LAST.NE.0) GO TO 1999
      IF (NUMPR) 201,201,2010
  201 LAST=1
      GO TO 2030
 2010 DO 1 I=1,512
      ACNET(I)=0.0
      ACSUM(I)=0.0
      ACSD(I)=0.0
      ACSVAR(I)=0.0
    1 CONTINUE
  202 DO 299 J=1,NUMPR
    3 READ (10,602) IDFG,IDBG,INVC,(PRHEAD(I),I=1,6),FNORM(1),(C(I),I=1,
     12),BKGL,LOWL,IUPL,LOWR,IUPR,FNORM(2),C(3),C(4),BKGR,LOCHL1,LOCHL2,
     2LOCHR1,LOCHR2,(KBND(K),KBND(K+6),K=1,6)
  602 FORMAT (2I6,2X,I1,9X,5A10,A6/4E12.5,4I6/4E12.5,4I6/12I6)
      IF (FNORM(2).EQ.-0.0) FNORM(2)=FNORM(1)
```

```
      DO 5 I=1,2
      IF (FNORM(I).EQ.-0.0) FNORM(I)=1.0
    5 IF (C(I+2).EQ.-0.0) C(I+2)=C(I)
      IF (BKGL.EQ.-0.0) BKGL=0.0
      IF (BKGR.EQ.-0.0) BKGR=BKGL
      NOBACK=0
      NODATA=0
      NOSTOP=0
      IF (INVC-1) 80,6,6
    6 DO 7 I=1,4
    7 IF (C(I).NE.0.0.AND.C(I).NE.-0.0) C(I)=1.0/C(I)
   80 WRITE (9,603)
  603 FORMAT (1H1)
      WRITE (9,604) IOFG,IDBG,(PRHEAD(I),I=1,6)
  604 FORMAT(1X,3HRUN,I5,1X4H-RUN,I6,6X5A10,A6//1X,53HNET(CHS001-256) =
     1NL*(C1*FOREGND - C2*BACKGND + BKGL)/1X,53HNET(CHS257-512) = NR*(C3
     2*FOREGND - C4*BACKGND + BKGR)/)
    8 CALL LESEN (INDEX,NRERUN)
    9 IF (NODATA) 299,10,299
   10 IF (C(1).EQ.-0.0) CALL CEES(LOWL,IUPL,LOWR,IUPR)
      WRITE (9,6041) FNORM(1),C(1),C(2),BKGL,FNORM(2),C(3),C(4),BKGR
 6041 FORMAT (1X,3HNL=,1PE12.4,5X,3HC1=,1PE12.4,5X,3HC2=,1PE12.4,5X,7HBK
     1GL=   ,1PE12.4/1X,3HNR=,1PE12.4,5X,3HC3=,1PE12.4,5X,3HC4=,1PE12.4,
     25X,7HBKGR=   ,1PE12.4)
      IF (NOBACK) 14,11,14
   11 DO 12 I=1,256
      BDATA(I)=(-C(2))*BDATA(I)
   12 BSD(I)=(-C(2))*BDATA(I)
      DO 13 I=257,512
      BDATA(I)=(-C(4))*BDATA(I)
   13 BSD(I)=(-C(4))*BDATA(I)
   14 DO 15 I=1,256
      ADATA(I)=C(1)*ADATA(I)
   15 ASD(I)=C(1)*ADATA(I)
```

```
      DO 16 I=257,512
      ADATA(I)=C(3)*ADATA(I)
   16 ASD(I)=C(3)*ADATA(I)
      IF (NOBACK) 19,17,19
   17 DO 18 I=1,512
      ADATA(I)=ADATA(I)+BDATA(I)
   18 ASD(I)=ASD(I)+BSD(I)
   19 DO 20 I=1,256
      ADATA(I)=FNORM(1)*(ADATA(I)+BKGL)
   20 ASD(I)=(FNORM(1)**2)*(ASD(I)+BKGL**2)
      DO 21 I=257,512
      ADATA(I)=FNORM(2)*(ADATA(I)+BKGR)
   21 ASD(I)=(FNORM(2)**2)*(ASD(I)+BKGR**2)
      SUM(1)=ADATA(1)
      SUMVAR(1)=ASD(1)
      ASD(1)=SQRT(ASD(1))
      ACH(1)=1.0
      DO 22 I=2,512
      SUM(I)=SUM(I-1)+ADATA(I)
      SUMVAR(I)=SUMVAR(I-1)+ASD(I)
      ASD(I)=SQRT(ASD(I))
   22 ACH(I)=I
      DO 220 I=1,512
      ACNET(I)=ACNET(I)+ADATA(I)
      ACSUM(I)=ACSUM(I)+SUM(I)
      ACSD(I)=SQRT((ASD(I)**2)+(ACSD(I)**2))
  220 ACSVAR(I)=ACSVAR(I)+SUMVAR(I)
      IF (JPLOT) 221,221,23
   23 DO 24 I=257,512
      SUM(I)=SUM(I)-SUM(256)
   24 SUMVAR(I)=SUMVAR(I)-SUMVAR(256)
  221 CALL UMSATZ
      WRITE (9,611)
      IDAC=IDAC+1
```

```
      WRITE (9,6040) IDAC
 6040 FORMAT (1X,I6,18H=RUN NO. IN OUTPUT)
      IF (JPLOT) 25,25,225
  225 WRITE (9,605)
  605 FORMAT (1X,16HDETECTOR 66 ONLY/)
      WRITE (9,606)
  606 FORMAT (2X,2HCH,4X,3HNET,2X,2HSD,5X,3HSUM,1X,6HSUMVAR,3(4X,2HCH,4X
     1,3HNET,2X,2HSD,5X,3HSUM,1X,6HSUMVAR))
      WRITE (9,607) (((ACH(I),ADATA(I),ASD(I),SUM(I),SUMVAR(I)),I=J,256,
     164),J=1,64)
  607 FORMAT(1X,F3.0,F7.1,F4.0,F8.1,F7.0,3(3X,F3.0,F7.1,F4.0,F8.1,F7.0))
      WRITE (9,611)
  611 FORMAT (// )
      IDAC=IDAC+1
      WRITE (9,6040) IDAC
      WRITE (9,612)
  612 FORMAT (1X,16HDETECTOR 60 ONLY/)
      WRITE (9,606)
      WRITE (9,607) (((ACH(I-256),ADATA(I),ASD(I),SUM(I),SUMVAR(I)),I=J,
     1512,64),J=257,320)
      GO TO 26
   25 WRITE (9,613)
  613 FORMAT (* CHANNELS 0 THRU 512, BOTH DETECTORS*)
      WRITE (9,606)
      WRITE (9,607) (((ACH(I),ADATA(I),ASD(I),SUM(I),SUMVAR(I)),I=J,512,
     1128),J=1,128)
   26 CALL MAHLEN
      CALL LOCHEN(LOCHL1,LOCHL2,LOCHR1,LOCHR2)
  299 CONTINUE
      IF (NUMPR.LE.1) GO TO 2
   30 DO 31 I=1,512
      ADATA(I)=ACNET(I)/NUMPR
      ASD(I)=ACSD(I)/NUMPR
      SUM(I)=ACSUM(I)/NUMPR
```

```
 31 SUMVAR(I)=ACSVAR(I)/(NUMPR**2)
    DO 310 I=1,6
310 PRHEAD(I)=ACCHEAD(I)
    IACC=)
    WRITE (9,611)
    IF (JPLOT) 331,331,32
 32 DO 33 I=257,512
    SUM(I)=SUM(I)-SUM(256)
 33 SUMVAR(I)=SUMVAR(I)-SUMVAR(256)
331 CALL UMSATZ
    IDAC=IDAC+1
    WRITE (9,6040) IDAC
    WRITE (9,614) NUMPR,(PRHEAD(I),I=1,6)
614 FORMAT (1X,I3,22H ABOVE FG AND BG PAIRS,5A10,A6)
    IF (JPLOT) 34,34,332
332 WRITE (9,605)
    WRITE (9,606)
    WRITE (9,607) (((ACH(I),ADATA(I),ASD(I),SUM(I),SUMVAR(I)),I=J,256,
   164),J=1,64)
    WRITE (9,611)
    IDAC=IDAC+1
    WRITE (9,6040) IDAC
    WRITE (9,614) NUMPR,(PRHEAD(I),I=1,6)
    WRITE (9,612)
    WRITE (9,606)
    WRITE (9,607) (((ACH(I-256),ADATA(I),ASD(I),SUM(I),SUMVAR(I)),I=J,
   1512,64),J=257,320)
    GO TO 35
 34 WRITE (9,613)
    WRITE (9,607) (((ACH(I),ADATA(I),ASD(I),SUM(I),SUMVAR(I)),I=J,512,
   1128),J=1,128)
 35 CALL MAHLEN
    CALL LOCHEN(LOCHL1,LOCHL2,LOCHR1,LOCHR2)
 37 GO TO 2
1999 STOP
2000 END
```

```
      SUBROUTINE LESEN (INDEX,NRERUN)
      DIMENSION HEAD(11),SCALAR(65)
      COMMON ADATA(512),BDATA(512),NOBACK,NODATA,IDFG,IDBG,JPLOT,C(4),
     1IPLOT,ICHAR1,ICHAR2,ICON,IDAC,IBLANK,ACH(512),PRHEAD(6),ANORM(4)
      NOBACK=0
      NODATA=0
      IRERUN=0
      LORUN=0
      MORUN=0
      NORUN=0
      IF (IDBG) 101,101,106
  101 LORUN=1
      NORUN=NORUN+1
      WRITE (9,511)
      WRITE (9,505)
  505 FORMAT ('  NO BACKGROUND WAS CALLED FOR, C2=-0.0(BLANK)')
  500 FORMAT (I1)
      NOBACK=NOBACK+1
  106 READ (37,500) JSPLAT
      IF (ENDFILE 37)118,1060
 1060 IF (JSPLAT-1) 106,107,107
  107 BACKSPACE 37
      GO TO (108,109),INDEX
  108 READ (37,501) NRUN,BNORM,CNORM,(HEAD(I),I=1,11)
  501 FORMAT (1X,I4,2(F9.4,2X),10A10,A8)
      GO TO 1090
  109 READ (37,502) NRUN,BNORM,(HEAD(I),I=1,11)
  502 FORMAT (1X,I4,F12.4,2X,10A10,A8)
      CNORM=BNORM
 1090 IF (MORUN) 111,110,111
  110 IF (NRUN-IDFG) 111,113,1100
 1100 IF (IRERUN-NRERUN) 1101,124,124
 1101 IRERUN=IRERUN+1
      DO 1102 J=1,40
 1102 BACKSPACE 37
```

```
      GO TO 106
  113 NORUN=NORUN+1
      ANORM(1)=BNORM
      ANORM(3)=CNORM
      MORUN=1
      GO TO 114
  111 IF (LORUN) 106,112,106
  112 IF (NRUN-IDBG) 106,115,1110
 1110 IF (IRERUN-NRERUN) 1111,126,126
 1111 IRERUN=IRERUN+1
      DO 1112 J=1,40
 1112 BACKSPACE 37
      GO TO 106
  115 NORUN=NORUN+1
      ANORM(2)=BNORM
      ANORM(4)=CNORM
      LORUN=1
      GO TO 116
  118 NODATA=NODATA+1
      REWIND 37
      WRITE (9,511)
      WRITE (9,512)
  512 FORMAT (*  TAPE RAN TO EOF WITHOUT FINDING RUNS*)
      GO TO 199
  126 WRITE (9,504)
  504 FORMAT (//1X,45HTHIS BACKGROUND RUN WAS NOT FOUND ON THE TAPE)
      GO TO 125
  124 WRITE (9,507)
  507 FORMAT (//1X,45HTHIS FOREGROUND RUN WAS NOT FOUND ON THE TAPE)
  125 NODATA=NODATA+1
      GO TO 199
  114 GO TO (1142,1140),INDEX
 1142 READ (37,508) (SCALAR(I),I=1,65)
  508 FORMAT (13A10,6X)
```

```
      GO TO 140
 1140 READ (37,5080) (SCALAR(I),I=1,13)
 5080 FORMAT (13A10)
      DO 1141 I=14,65
 1141 SCALAR(I)=0.0
  140 READ (37,509) ((ADATA(I),I=J,512,128),J=1,128)
  509 FORMAT (1X,16F8.0)
      WRITE (9,511)
  511 FORMAT (//)
      WRITE (9,501) NRUN,BNORM,CNORM,(HEAD(I),I=1,11)
      WRITE (9,508) (SCALAR(I),I=1,65)
      GO TO 129
  116 GO TO (1162,1160),INDEX
 1162 READ (37,508) (SCALAR(I),I=1,65)
      GO TO 160
 1160 READ (37,5080) (SCALAR(I),I=1,13)
      DO 1161 I=14,65
 1161 SCALAR(I)=0.0
  160 READ (37,509) ((BDATA(I),I=J,512,128),J=1,128)
      WRITE (9,511)
      WRITE (9,501) NRUN,BNORM,CNORM,(HEAD(I),I=1,11)
      WRITE (9,508) (SCALAR(I),I=1,65)
  129 IF (NORUN.LT.2) GO TO 106
  199 RETURN
      END
```

```
      SUBROUTINE CEES(LOWL,IUPL,LOWR,IUPR)
      DIMENSION CALC(4)
      COMMON ADATA(512),BDATA(512),NOBACK,NODATA,IDFG,IDBG,JPLOT,C(4),
     1IPLOT,ICHAR1,ICHAR2,ICON,IDAC,IBLANK,ACH(512),PRHEAD(6),ANORM(4)
      DO 801 I=1,4
  801 CALC(I)=0.0
      IF (IUPL) 805,805,807
  805 DO 806 K=1,4
  806 C(K)=ANORM(K)
      GO TO 808
  807 DO 802 J=LOWL,IUPL
      CALC(1)=CALC(1)+ADATA(J)
  802 CALC(2)=CALC(2)+BDATA(J)
      DO 803 J=LOWR,IUPR
      CALC(3)=CALC(3)+ADATA(J)
  803 CALC(4)=CALC(4)+BDATA(J)
      C(1)=ANORM(1)
      C(2)=C(1)*(CALC(1)/CALC(2))
      C(3)=ANORM(3)
      C(4)=C(3)*(CALC(3)/CALC(4))
  808 WRITE (9,804) LOWL,IUPL,CALC(1),LOWR,IUPR,CALC(3),LOWL,IUPL,CALC(2
     1),LOWR,IUPR,CALC(4)
  804 FORMAT(/1X,26HSUM OF FOREGROUND CHANNELS,I6,6H  THRU,I6,10H  EQUAL
     1S  ,1PE12.4/1X,26HSUM OF FOREGROUND CHANNELS,I6,6H  THRU,I6,10H  E
     2QUALS  ,1PE12.4/1X,26HSUM OF BACKGROUND CHANNELS,I6,6H  THRU,I6,10
     3H  EQUALS  ,1PE12.4/1X,26HSUM OF BACKGROUND CHANNELS,I6,6H  THRU,I
     46,10H  EQUALS  ,1PE12.4//1X,65HC(I) WERE CALCULATED FROM ANORM(I)
     5AND/OR NORMALIZING ON THE DATA)
      RETURN
      END
```

```
      SUBROUTINE UMSAT7
      COMMON ADATA(512),BDATA(512),NOBACK,NODATA,IDFG,IDBG,JPLOT,C(4),
     1IPLOT,ICHAR1,ICHAR2,ICON,IDAC,IBLANK,ACH(512),PRHEAD(6),ANORM(4)
      IF (IBLANK) 3002,3002,3000
 3000 READ (53,719)
  719 FORMAT (I1)
      IF (ENDFILE53) 3001,3000
 3001 DO 3003 I=1,35
      BACKSPACE 53
 3003 CONTINUE
 3030 READ (53,700) ISPLAT,IDAC
  700 FORMAT (2X,I1,3X,I6)
      IF (ISPLAT) 3030,3030,3031
 3031 READ (53,719)
      IF (ENDFILE53) 3032,3031
 3032 IDAC=IDAC+1
 3002 IDAC=IDAC+1
      BACKSPACE 53
      IF (JPLOT) 301,301,302
  301 WRITE (53,701) IDAC,(PRHEAD(I),I=1,6)
  701 FORMAT (3H101,3X,I6,5A10,A6)
       WRITE (53,7010)
 7010 FORMAT (*                    BOTH DETECTORS*)
      WRITE (53,702) ((ADATA(I),I=J,512,128),J=1,128)
  702 FORMAT (12X,16F7.0)
      GO TO 320
  302 WRITE (53,701) IDAC,(PRHEAD(I),I=1,6)
      WRITE (53,703)
  703 FORMAT(*                    DETECTOR 66 ONLY*)
      WRITE (53,702) ((ADATA(I),I=J,256,64),J=1,64)
      KDAC=IDAC+1
      WRITE (53,701) KDAC,(PRHEAD(I),I=1,6)
      WRITE (53,704)
  704 FORMAT (*                    DETECTOR 60 ONLY*)
```

```
      WRITE (53,702) ((ADATA(I),I=J,512,64),J=257,320)
  320 WRITE (53,732)
  732 FORMAT (12X,46HTHIS IS THE LAST RECORD BEFORE EOF WAS WRITTEN)
      ENDFILE 53
      IBLANK=0
      IDAC=IDAC-1
      RETURN
      END



      SUBROUTINE MAHLEN
      DIMENSION CDATA(256),FDATA(512),DDATA(512),HDATA(256),GDATA(256)
      COMMON ADATA(512),BDATA(512),NOBACK,NODATA,IDFG,IDBG,JPLOT,C(4),
     1IPLOT,ICHAR1,ICHAR2,ICON,IDAC,IBLANK,ACH(512),PRHEAD(6),ANORM(4),
     2KBND(12),IACC,MAXDAT,ASD(512),SUM(512),SUMVAR(512)
      DATA ATITLE/10HBOTH SIDES/,BTITLE/10HDETECT   66/,CTITLE/10HDETECT
     1 60/
 5600 FORMAT(I5)
      DO 53 I=1,256
   53 CDATA(I)=ADATA(I+256)
      IF (IACC-1) 5094,5095,5095
 5094 DATMAX=0.0
      IF (KBND(7).LE.0) GO TO 5098
      DO 5097 K=1,6
      LOBND=KBND(K)
      MOBND=KBND(K+6)
      IF (MOBND.LE.0) GO TO 5093
      DO 5096 I=LOBND,MOBND
      DATMAX=AMAX1(DATMAX,ADATA(I))
 5096 CONTINUE
 5097 CONTINUE
      GO TO 5093
 5098 DO 51 I=1,512
```

```
   51 DATMAX=AMAX1(DATMAX,ADATA(I))
 5093 MAXDAT=AMAX1(MAXDAT,DATMAX)
      GO TO 5099
 5095 DATMAX=MAXDAT
 5099 IF (DATMAX-100.0) 5100,5100,5101
 5100 DATMAX=(DATMAX/10.0)+1.0
      YBNDT=10.0*AINT(DATMAX)
      YBNDB=-10.0
      NY=(YBNDT-YBNDB)/10.0
      GO TO 531
 5101 IF (DATMAX-1000.0) 5102,5102,5103
 5102 DATMAX=(DATMAX/100.0)+1.0
      YBNDT=100.0*AINT(DATMAX)
      YBNDB=-100.0
      NY=(YBNDT-YBNDB)/100.0
      GO TO 531
 5103 IF (DATMAX-5000.0) 5104,5104,5105
 5104 DATMAX=(DATMAX/500.0)+1.0
      YBNDT=500.0*AINT(DATMAX)
      YBNDB=-500.0
      NY=(YBNDT-YBNDB)/500.0
      GO TO 531
 5105 IF (DATMAX-10000.0) 5106,5106,5107
 5106 DATMAX=(DATMAX/1000.0)+1.0
      YBNDT=1000.0*AINT(DATMAX)
      YBNDB=-1000.0
      NY=(YBNDT-YBNDB)/1000.0
      GO TO 531
 5107 DATMAX=(DATMAX/10000.0)+1.0
      YBNDT=10000.0*AINT(DATMAX)
      YBNDB=-10000.0
      NY=10
  531 XL=0.0
      XR1=260.0
```

```
      XR2=570.0
      IF (IPLOT) 55,55,70
   55 IF (JPLOT) 56,56,57
   56 ENCODE(5,5600,TITLE)IDAC
      CALL TSP(120,10,10,TITLE)
      CALL TSP (208,10,56,PRHEAD)
      CALL TSP(120,30,10,ATITLE)
      CALL DGA (120,980,50,910,XL,XR2,YBNDT,YBNDB)
      CALL DLNLN(26,NY)
      CALL SLLIN(NY,01)
      CALL SBLIN (13,00)
      CALL PLOT (512,ACH,1,ADATA,1,ICHAR1,ICON)
      GO TO 90
   57 KDAC=IDAC-1
      ENCODE(5,5600,TITLE)KDAC
      CALL TSP(120,10,10,TITLE)
      CALL TSP (208,10,56,PRHEAD)
      CALL TSP(120,30,10,BTITLE)
      CALL DGA (120,980,50,910,XL,XR1,YBNDT,YBNDB)
      CALL DLNLN(26,NY)
      CALL SLLIN(NY,01)
      CALL SBLIN (13,00)
      CALL PLOT (256,ACH,1,ADATA,1,ICHAR1,ICON)
      CALL ADV(1)
      ENCODE(5,5600,TITLE)IDAC
      CALL TSP(120,10,10,TITLE)
      CALL TSP (208,10,56,PRHEAD)
      CALL TSP(120,30,10,CTITLE)
      CALL DGA (120,980,50,910,XL,XR1,YBNDT,YBNDB)
      CALL DLNLN(26,NY)
      CALL SLLIN(NY,01)
      CALL SBLIN (13,00)
      CALL PLOT (256,ACH,1,CDATA,1,ICHAR1,ICON)
      GO TO 90
```

```
 70 BNDT=ABS(YBNDT)
    BNDT=ALOG10(BNDT)
    BNDB=1.0
    DO 800 I=1,512
    FDATA(I)=1.0
    DDATA(I)=1.0
    IF (ADATA(I)-10.0) 72,72,71
 71 DDATA(I)=ABS(ADATA(I))
    DDATA(I)=ALOG10(DDATA(I))
    GO TO 800
 72 IF (ADATA(I)+10.0) 73,800,800
 73 FDATA(I)=ABS(ADATA(I))
    FDATA(I)=ALOG10(FDATA(I))
800 CONTINUE
731 DO 732 I=1,256
    GDATA(I)=DDATA(I+256)
732 HDATA(I)=FDATA(I+256)
 74 IF (JPLOT) 75,75,76
 75 ENCODE(5,5600,TITLE)IDAC
    CALL TSP(120,10,10,TITLE)
    CALL TSP (208,10,56,PRHEAD)
    CALL TSP(120,30,10,ATITLE)
    CALL DGA (120,980,50,910,XL,XR2,BNDT,BNDB)
    CALL DLNLG(26)
    CALL SBLIN (13,00)
    CALL SLLOG
    CALL PLOT (512,ACH,1,DDATA,1,ICHAR1,ICON)
    CALL PLOT (512,ACH,1,FDATA,1,ICHAR2,ICON)
    GO TO 90
 76 KDAC=IDAC-1
    ENCODE(5,5600,TITLE)KDAC
    CALL TSP(120,10,10,TITLE)
    CALL TSP (208,10,56,PRHEAD)
    CALL TSP(120,30,10,BTITLE)
```

```
      CALL DGA (120.980.50.910.XL.XR1.BNDT.BNDB)
      CALL DLNLG(26)
      CALL SBLIN (13.00)
      CALL SLLOG
      CALL PLOT (256.ACH.1.DDATA.1.ICHAR1.ICON)
      CALL PLOT (256.ACH.1.FDATA.1.ICHAR2.ICON)
      CALL ADV(1)
      ENCODF(5.5600.TITLE)IDAC
      CALL TSP(120.10.10.TITLE)
      CALL TSP (208.10.56.PRHEAD)
      CALL TSP(120.30.10.CTITLE)
      CALL DGA (120.980.50.910.XL.XR1.BNDT.BNDB)
      CALL DLNLG(26)
      CALL SBLIN (13.00)
      CALL SLLOG
      CALL PLOT (256.ACH.1.GDATA.1.ICHAR1.ICON)
      CALL PLOT (256.ACH.1.HDATA.1.ICHAR1.ICON)
   90 CALL ADV(1)
   91 RETURN
      END


      SUBROUTINF LOCHEN(LOCHL1.LOCHL2.LOCHR1.LOCHR2)
      COMMON ADATA(512).BDATA(512).NOBACK.NODATA.IDFG.IDBG.JPLOT.C(4).
     1IPLOT.ICHAR1.ICHAR2.ICON.IDAC.IBLANK.ACH(512).PRHEAD(6).ANORM(4).
     2KBND(12).IACC.MAXDAT.ASD(512).SUM(512).SUMVAR(512)
      IF (JPLOT) 4001.4001.4002
 4001 IF (LOCHL2) 4040.4040.401
 4040 LOCHL1=1
      LOCHL2=512
  401 N=LOCHL1
      M=N+5
 4100 PUNCH 4010.(ADATA(I).I=N.M).IDAC
```

```
4010 FORMAT (6F12.2,I6,2H80)
     IF ((N+5)-LOCHL2) 4011,420,420
4011 N=N+6
     M=N+5
     GO TO 4100
4002 IF (LOCHL2) 4041,4041,402
4041 LOCHL1=1
     LOCHL2=256
     LOCHR1=257
     LOCHR2=512
 402 KDAC=IDAC-1
     N=LOCHL1
     M=N+5
4300 PUNCH 4014,(ADATA(I),I=N,M),KDAC
4014 FORMAT (6F12.2,I6,2H66)
     IF ((N+5)-LOCHL2) 4015,403,403
4015 N=N+6
     M=N+5
     GO TO 4300
 403 N=LOCHR1
     M=N+5
4500 PUNCH 4018,(ADATA(I),I=N,M),IDAC
4018 FORMAT (6F12.2,I6,2H60)
     IF ((N+5)-LOCHR2) 4019,420,420
4019 N=N+6
     M=N+5
     GO TO 4500
 420 RETURN
     END
```

II. PROGRAM DSCHNIT

DSCHNIT (meaning Durchschnitt = average) is a FORTRAN IV program which numerically integrates separate numerator and denominator functions by the trapezoidal rule and gives their ratio. The trapezoidal rule states

$$\int_a^b f(x)\ dx = f(a)\,\frac{\Delta x}{2} + f(a + \Delta x)\ \Delta x + f(a + 2\Delta x)\ \Delta x$$

$$+ \ldots + f(b - \Delta x)\ \Delta x + f(b)\,\frac{\Delta x}{2}\ . \tag{B4}$$

In particular, define

$$\text{AITGR} = \int_A^o \text{YNUN}(x)\ dx + \int_o^B \text{YNUP}(x)\ dx \tag{B5}$$

$$\text{BITGR} = \int_A^o \text{YDEN}(x)\ dx + \int_o^B \text{YDEP}(x)\ dx\ ; \tag{B6}$$

then the result of the program calculation is

$$\text{DSNIT} = \frac{\text{AITGR}}{\text{BITGR}}\ . \tag{B7}$$

All function statements at the beginning of the program listing were necessary for the particular calculation of this work only and may be replaced by any other YNUN(x), YNUP(x), YDEN(x), and YDEP(x) statements which one desires to integrate. For this experiment

$$\text{YNUN}(\phi) = \phi\cdot\text{YDEN}(\phi) = \sigma_1(\phi)\left\{1-\exp[-2n\sigma_2(\phi)(R^2-d^2\phi^2)^{\frac{1}{2}}]\right\}\phi\ , \tag{B8}$$

YNUP(ϕ) = YNUN(ϕ), and YDEP(ϕ) = YDEN(ϕ), where $\sigma_1(\phi)$, $\sigma_2(\phi)$, d, and n are cross sections, target sample distance, and scattering sample density as explained in Chapter IV, Section II.

Two data cards are necessary to run the program. The first contains integration limits, the number of intervals for the first integration, and the accuracy required of numerator and denominator. The second data card lists the parameters necessary for the particular functions to be integrated; hence, the READ (10,2000) statement must be changed when new functions are substituted. Also all WRITE statements except WRITE (9,6000) refer to the functions used by the program and must be revised with the functions.

Data Card Formats

Data Card I

Field	Format	Name	Explanation
1-12	I12	N	N = No. of intervals for the first integration. If the integration does not yield the required accuracy, the second integration is performed with 2N intervals, then 3N, 4N, etc. (If this field is left blank, N = 10.)
13-24	E12.4	A	Lower integration limit.
25-36	E12.4	B	Upper integration limit.
37-48	E12.4	SETNUM	Maximum fractional error of the numerator = $\lvert$(AITGR(2) - AITGR(1))/AITGR(2)$\rvert$. The program compares succeeding integrations and

Data Card I (cont'd)

Field	Format	Name	Explanation
			repeats the integration process until the errors are within this limit.
49-60	E12.4	SETDEN	Maximum fractional error of the denominator. (If this field is left blank, SETDEN = SETNUM.)
61-72	I12	NØDEN	NØDEN.GE.1 sets the denominator = 1.0. This option is provided in order that the program may be used to evaluate single integrals.

Data Card II

Field	Format	Name	Explanation
1-12	E12.4	d	Source to sample distance
13-24	E12.4	n=ATØMS	Scattering center density in molecules/cm^3.
25-36	E12.4	SIGMAA	Total cross section σ_2 of the scattering sample at an energy corresponding to ϕ = A.
37-48	E12.4	SIGMAB	Total cross section σ_2 of the scattering sample at an energy corresponding to ϕ = B.

The program continues to read new parameters and reintegrate the functions until it reads SETNUM.LE.0.0; thus a blank data card I terminates the job.

A listing of the program follows.

```
      PROGRAM DSCHNIT (INPUT,OUTPUT,TAPE10=INPUT,TAPE9=OUTPUT)
      SIGMAN(X)=((SIGMAB-SIGMAA)*(X-A)/(B-A))+SIGMAA
      P(X)=1.0-((2.71828)**(-2.0*ATOMS*SIGMAN(X)*SQRT(ABS(((1.79426)-
     2((ABS(X))**2.0)*(D**2.0)))))
      SIGMAS(X)=-1.1422*X+0.44
      SIGMAT(X)=-0.4569*X+0.44
      YDEN(X)=SIGMAS(X)*P(X)
      YNUN(X)=YDEN(X)*X
      YDEP(X)=SIGMAT(X)*P(X)
      YNUP(X)=YDEP(X)*X
    7 READ(10,1000)N,A,B,SETNUM,SETDEN,NODEN
      IF(SETNUM.LE.0.0) GO TO 50
   71 READ(10,2000)D,ATOMS,SIGMAA,SIGMAB
 1000 FORMAT (I12,4F12.4,I12)
 2000 FORMAT(4F12.4)
      IF(N.LE.0)N=10
      IF(SETDEN.LE.0.0)SETDEN=SETNUM
      ADIFF=10.0*SETNUM
      AITGP=0.0
      BITGP=0.0
      AENOS=YNUN(A)+YNUP(B)
      BENOS=YDEN(A)+YDEP(B)
      J=1
    8 AITGR=0.0
      IF(ADIFF.LE.SETNUM)GO TO 19
      L=J*N
      ADELX=(B-A)/L
      K=L-1
      DO 10 I=1,K
      DELX=I*ADELX
      XVALUE=A+DELX
      Y=YNUN(XVALUE)
      IF(XVALUE.GT.0.0)Y=YNUP(XVALUE)
   10 AITGR=AITGR+Y*ADELX
```

```
      AITGR=AITGR+AENDS*ADELX/2.0
      ADIFF=ABS((AITGR-AITGP)/AITGR)
      AITGP=AITGR
      J=J+1
      GO TO 8
   19 IF(NODEN.GE.1)GO TO 39
      J=1
   20 BITGR=0.0
      M=J*N
      BDELX=(B-A)/M
      K=M-1
      DO 30 I=1,K
      DELX=I*BDELX
      XVALUE=A+DELX
      Y=YDEN(XVALUE)
      IF(XVALUE.GT.0.0)Y=YDEP(XVALUE)
   30 BITGR=BITGR+Y*BDELX
      BITGR=BITGR+BENDS*BDELX/2.0
      BDIFF=ABS((BITGR-BITGP)/BITGR)
      BITGP=BITGR
      IF(BDIFF.LE.SETDEN)GO TO 40
      J=J+1
      GO TO 20
   39 BITGP=1.0
   40 DSNIT=AITGP/BITGP
      WRITE(9,4000)
 4000 FORMAT(1H1,1X,88HDENOMINATOR FUNCTION = SIGMA(SOURCE) * (1-E **-(2N*
     2SIGMA(SCATTERING)*SQRT(R**2-D**2+X**2))/1X,37HNUMERATOR FUNCTION I
     3S DENOMINATOR * X//)
      WRITE(9,5000)ATOMS,D
 5000 FORMAT(1X,13HATOM DENSITY=,1PE12.4/1X,16HSAMPLE DISTANCE=,E12.4//)
      WRITE(9,6000)AITGP,L,ADELX,BITGP,M,BDELX,A,B,DSNIT,ADIFF,BDIFF
```

```
6000 FORMAT(1X,5H NUM=,1PE12.4,12X,2HL=,I7,12X,6HADELX=,1PE12.4/1X,5H D
    2EN=,1PE12.4,12X,2HM=,I7,12X,6HBDELX=,1PE12.4//1X,2HA=,1PE12.4,12X,
    32HB=,1PE12.4//1X,16HDSNIT=NUM/DEN = ,1PE12.4//1X,9HNUMERROR=,1PE12
    4.4,12X,9HDENERROR=,1PE12.4)
     WRITE(9,7000)SIGMAA,SIGMAB
7000 FORMAT(2E12.4)
     GO TO 7
  50  STOP
  51 END
```

REFERENCES

(Ba 57) S. J. Bame, Jr. and J. E. Perry, Jr., Phys. Rev. 107, 1616 (1957).

(Ba 66) H. H. Barschall, Proceedings of the 2nd International Symposium on Polarization Phenomena of Nucleons, P. Huber and H. Schopper, eds. (Birkhäuser Verlag, Basel, 1966) p. 393.

(Bo 61) P. H. Bowen, J. P. Scanlon, G. H. Stafford, J. J. Thresher, and P. E. Hodgson, Nucl. Phys. 22, 640 (1961).

(Br 69) W. B. Broste and J. E. Simmons, private communication (1969).

(Bü 69) F. W. Büsser, H. Dubenkropp, F. Niebergall, and K. Sinram, Nucl. Phys. A129, 666 (1969).

(Co 63) E. U. Condon and G. H. Shortley, The Theory of Atomic Spectra (Cambridge University Press, Cambridge, 1963) Chap. III, p. 56.

(Cr 61) L. Cranberg, R. A. Fernald, F. S. Hahn, and E. F. Shrader, Nucl. Inst. Meth. 12, 335 (1961).

(Cz 64) J. B. Czirr, D. R. Nygren, and C. D. Zafiratos, Nucl. Inst. Meth. 31, 226 (1964).

(Da 61) W. Daehnick and R. Sherr, Rev. Sci. Instr. 32, 666 (1961).

(Di 68) D. R. Dixon, private communication (1968).

(Do 69) D. C. Dodder, private communication (1969).

(Ga 66) T. Gardiner and J. Levin, IEEE Trans. on Nucl. Sci. NS13, 151 (1966).

(He 59) R. G. Herb, Handbuch der Physik, S. Flügge, ed. (Springer Verlag, Berlin, 1959) Vol. XLIV, p. 64.

(Ho 66) B. Hoop, Jr. and H. H. Barschall, Nucl. Phys. 83, 65 (1966).

(Ho 67) J. C. Hopkins, H. Condé, D. M. Drake, P. W. Keaton, J. D. Seagrave, R. K. Smith, W. E. Stein, and A. R. Sattler, Nuclear Data for Reactors (International Atomic Energy Agency, Vienna, 1967) Vol. I, p. 419.

(Ja 45) E. Jahnke and F. Emde, Tables of Functions with Formulae and Curves, 4th Ed. (Dover Publications, New York, 1945) pp. 128, 131, 143, 146.

(Ke 63) M. G. Kendall and A. Stuart, The Advanced Theory of Statistics, 2nd Ed. (Charles Griffen and Co., London, 1963) Vol. 1, p. 157.

(Ke 69a) P. W. Keaton, private communication (1969).

(Ke 69b) E. C. Kerr and R. H. Sherman, private communication (1969).

(Le 68) J. S. Levin, private communication (1968).

(Le 69) J. S. Levin, M. P. Kellogg, R. B. Perkins, and E. T. Ritter, Conference on Computer Systems in Experimental Nuclear Physics, Skytop, Pa., March 1969 (Proceedings to be published).

(Li 66) J. Libert, Nucl. Instr. Meth. 41, 348 (1966).

(Ma 66) J. J. Malanify, J. E. Simmons, R. B. Perkins, and R. L. Walter, Phys. Rev. 146, 632 (1966).

(Mo 65) N. F. Mott and H. S. W. Massey, The Theory of Atomic Collisions, 3rd Ed. (Clarendon Press, Oxford, 1965) p. 279.

(Mo 68) R. H. Moore and R. K. Zeigler, "The Solution of the General Least Squares Problem with Special Reference to High-Speed Computers," Los Alamos Scientific Laboratory Report LA-2367 (1960).

(Pe 61) R. B. Perkins and J. E. Simmons, Phys. Rev. 124, 1153 (1961).

(Pr 62) M. A. Preston, Physics of the Nucleus (Addison-Wesley Publishing Co., Inc., Reading, Mass., 1962) p. 474.

(Re 66) W. B. Reid and R. H. Hummel, Can. Nucl. Tech. 5, No. 1, 36 (Jan-Feb 1966).

(Sc 55) L. I. Schiff, Quantum Mechanics, 2nd Ed. (McGraw-Hill Book Co., Inc., New York, 1955) p. 74, 233.

(Se 60) J. D. Seagrave, L. Cranberg, and J. S. Simmons, Phys. Rev. 119, 1981 (1960).

(Se 67) J. D. Seagrave, Few Body Problems, Light Nuclei, and Nuclear Interactions, Proceedings of the Symposium held in Brela, Yugoslavia, June 26-July 5, 1967 (Gordon and Breach, New York, 1969) Vol. 2, p. 787.

(Se 69) J. D. Seagrave, "The Elastic Channel in Nucleon-Deuteron Scattering," Proceedings of the Conference on the Three-Body Problem, Birmingham, England, July 1969 (to be published).

(Sh 59) C. W. Sherwin, Introduction to Quantum Mechanics (Holt, Rinehart, and Winston, New York, 1959) Appendix 5, p. 353.

(St 64) L. Stewart, "n-^{4}He Scattering," Los Alamos Scientific Laboratory Preliminary Report (1964) unpublished.

(St 65) L. Stewart, "Evaluated Neutron Cross Sections for Tritium," Los Alamos Scientific Laboratory Report LA-3270 (1965).

(St 68) L. Stewart, "Evaluated Neutron Cross Sections for Deuterium," Los Alamos Scientific Laboratory Report LA-3271 (1968).

(Ti 68) W. F. Tivol, "Proton-^{3}He Polarization in the Range from 10 to 20 MeV," Ph.D. Thesis, University of California, Berkeley (April 1968).

(To 66) T. A. Tombrello, Phys. Rev. 143, 772 (1966).

(Va 46) R. J. Van de Graaff, J. G. Trump, and W. W. Buechner, Rpts. on Prog. in Phys. XI, 1 (1946-47).

(Wh 50) E. T. Whittaker and G. N. Watson, Modern Analysis, 4th Ed. (University Press, Cambridge, 1950) Chap. XV, p. 302.

(Wi 68) E. M. Willbanks, private communication (1968).

(Wo 54) L. Wolfenstein, Phys. Rev. 96, 1654 (1954).

(Wo 56) L. Wolfenstein, Ann. Rev. of Nucl. Sci. 6, 43 (1956).

(Wu 62) Ta-You Wu and T. Ohmura, Quantum Theory of Scattering (Prentice-Hall, Inc., Englewood Cliffs, N.J., 1962) pp. 129, 134, 152.